CALIFORNIA INSTITUTE OF TECHNOLOGY

EARTHQUAKE ENGINEERING RESEARCH LABORATORY

DEFENSIVE DESIGN OF CONCRETE GRAVITY DAMS

by

John F. Hall
Michael J. Dowling
Bahaa El–Aidi

Report No. EERL 91–02

A Report on Research Supported by a Grant from the
United States National Science Foundation

Pasadena, California

1991

This investigation was sponsored by grant(s) from the National Science Foundation under the supervision of John F. Hall. Any opinions, findings, conclusions or recommendations expressed in this publication are those of the authors and do not necessarily reflect the views of the National Science Foundation.

Defensive Design of Concrete Gravity Dams

John F. Hall
Michael J. Dowling
Bahaa El-Aidi

Report No. 91-02

Abstract

Failure of a concrete gravity dam during an earthquake could occur as a sliding instability along an earthquake-induced crack, possibly assisted by uplift pressures from water flowing into the crack. Reliable assessment of the likelihood of such an event is thought to be difficult, and this suggests a need for designs which are less prone to cracking and uncertain behavior than are typical existing designs. Several schemes for reducing the potential for cracking during earthquake loading are investigated by finite element simulations: use of a sliding plane at the base of the dam, modification of the cross-sectional shape, use of a joint in the upper part of the dam, prestressing, and hydrodynamic isolation. The sliding plane, modified cross-section, and upper joint may only be applicable to new construction, while prestressing and hydrodynamic isolation could also be used to upgrade existing dams. While all of the schemes show potential, modification of the cross-sectional shape is probably the most practical considering acceptability, cost and effectiveness.

Table of Contents

Chapter 1. Introduction

Previous research on the earthquake behavior of concrete gravity dams has been directed mostly to assessing typical, existing dams. Linearly elastic analyses show that tensile stresses in the neck region of a gravity dam produced by earthquake shaking of even moderate intensity can be large enough to cause cracking (1). Such cracking is a concern because of the possibility that a potential failure mechanism will be created, for example, one involving sliding along a crack sloping downward in the downstream direction. Water exerting uplift pressure in a crack would assist sliding by decreasing the effective frictional resistance.

Concern about the role of cracking in the seismic safety of gravity dams has resulted in a number of attempts at nonlinear analysis (2–10). However, none of these developments have reached the stage of being able to accurately represent effects of cracking on the earthquake stability of a gravity dam. Further, recent small-scale experiments (11) indicate that the path a crack takes may be sensitive to details of the dam geometry, inhomogeneity in the concrete, ground motion, etc. and, thus, emphasize the difficulty of carrying out reliable nonlinear analyses. In addition, these experiments showed that a rough crack dilates during sliding, and this would facilitate water flow into the crack from the reservoir. These findings suggest the need to develop modified designs which are less prone to cracking during earthquakes.

This report investigates methods for improving the seismic resistance of concrete gravity dams, with applications to upgrading existing dams and designing new dams. Most existing gravity dams employ a similar cross-sectional shape which is optimal for eliminating tensile stress under static loading, but which may not be optimal for earthquake loading. After the earthquake response of a dam with typical profile is defined in Chapter 2, the responses of dams with cross-sectional shapes modified for improved seismic resistance are examined in Chapter 3. Prestressing and pre-formed joints are investigated in Chapter 4. Prestressing across potential cracking surfaces can reduce the amount and extent of cracking. A pre-formed joint, if properly constructed, may be able to eliminate earthquake-induced cracking altogether and thus confine the nonlinear behavior of the type associated

with cracking to the plane of the joint itself, a more tractable situation to analyze. A technique to reduce the dynamic component of the water pressure acting on the dam during an earthquake is investigated in Chapter 5. This technique is referred to as hydrodynamic isolation.

All analyses in this report are based on either the original profile of a 400 foot high monolith of Pine Flat Dam (Figure 1) or on modifications. The method of analysis is similar to that described in reference 9 and details are given below.

Dam: Young's modulus of concrete = 4×10^6 psi; Poisson's ratio of concrete = 0.2; unit weight of concrete = 155 pcf; damping = 5% of critical at 2.5 Hz (stiffness proportional). The frequency 2.5 Hz is the fundamental frequency of the dam with full reservoir. A mass proportional component of damping is omitted to eliminate any artificial restraint to sliding and overturning.

Dam foundation: 635 ft by 317 ft rigid rectangular plate on a three-dimensional half space; shear modulus of half space = 4.5×10^6 psi; Poisson's ratio of half space = 0.33; shear wave speed of half space = 11,602 ft/sec; internal hysteretic damping ratio of half space = 2%.

Water: depth = 380 feet (referred to as full condition); compression wave speed = 4720 ft/sec; unit weight = 62.4 lb/ft^3; wave reflection coefficient at reservoir floor = 0.87; small amplitude surface waves included; cavitation included; approximate transmitting boundary located at 770 ft upstream. A small amount of stiffness proportional damping is added to the water (1% of critical at 3.1 Hz). Some analyses use an empty reservoir.

Ground motion: 1.5 × El Centro 1940 S00E for horizontal direction (Figure 2a); 1.5 × El Centro 1940 vertical for vertical direction (Figure 2b). With this amplitude scaling, the peak accelerations become .52g horizontal and .32g vertical. Some analyses are run using a suite of ground motions constructed by varying the time scale of the ground motion by factors ranging from 0.5 to 1.5 in increments of 0.1.

Time integration scheme: The Bossak α method (12) is employed with $\alpha_\beta = -0.2$, $\gamma = 0.7$ and $\beta = 0.36$.

Cracking in the dam is not allowed but pre-formed joints may be present in the body of the dam or at the base of the dam. Such joints are represented by the smeared crack technique within a single row of finite elements using a tensile strength of zero and a coefficient of friction of 0.75 (9). The joint at the base of the dam represents the dam-foundation interface and is either fully bonded (neither opening nor sliding allowed), keyed (opening allowed but no sliding), or unkeyed (opening and sliding allowed).

Allowing opening at the dam-foundation interface as for the keyed and unkeyed bases eliminates the stress concentrations which occur at the heel and the toe. High tensile stresses at the interface resulting from such a stress concentration would initiate a crack which could propagate along the interface and destroy any bond between the dam and the foundation. For this reason, representing the interface with the treatment used for the keyed or unkeyed base may be more appropriate, which one depending on actual conditions of a particular dam.

Water pressure inside a joint, which could assist joint opening and sliding, is neglected. Water causing uplift could be present as internal water in the dam and foundation, and it could flow into the joint from the reservoir during opening at the upstream end of the joint. Entry from the reservoir is assumed to be prevented by a silt layer for the case of a base joint and by a built-in water seal for the case of an upper joint. Neglect of uplift from the internal hydrostatic pressure can be justified if enough drains are present to reduce the pressure to small values. Even if significant uplift pressure exists prior to the earthquake, the low permeability of concrete could restrict the seepage of water into the joint enough so that negligible uplift occurs during opening as well as during sliding that is accompanied by dilation. In practice, neglecting uplift may or may not be appropriate, and assumptions should be based on actual conditions.

Damping in the mathematical model comes from material damping in the dam, material and radiation damping in the foundation, material damping in the water, pressure wave absorption along the reservoir floor, and radiation in the reservoir. The overall level

of damping which results from these sources as quantified earlier is significantly greater than the damping usually observed during forced vibration field testing of actual gravity dams (13), and so a case could be made that the damping used here is too high and that the computed stresses are too low. Also, the material damping in the dam used here is somewhat higher than that used by the authors in a previous study (3% for the dam in reference 9 compared to 5% here), and so the stresses computed here are correspondingly lower. In addition, the stiffness proportional damping used for the dam as well as some algorithmic damping from the time integration scheme strongly damp high frequency deformations. Stress levels presented in this report should be interpreted with these considerations in mind. The results of various analyses are meant to be judged in relation to one another. The most appropriate level of damping and method to incorporate damping are still open questions.

Chapter 2. Response of Pine Flat Dam

In this chapter, the earthquake response of the unmodified Pine Flat Dam is defined in order to provide a reference to which the results of later chapters can be compared. Analyses are made for both empty and full reservoir cases as well as for the bonded, keyed and unkeyed conditions at the dam-foundation interface.

Figure 3 shows the finite element meshes of the dam and water. Time history responses and maximum tensile stress contours for an earthquake time scale of one are presented in Figures 4 to 9 as follows:

Figure 4: empty reservoir, bonded base
Figure 5: full reservoir, bonded base
Figure 6: empty reservoir, keyed base
Figure 7: full reservoir, keyed base
Figure 8: empty reservoir, unkeyed base
Figure 9: full reservoir, unkeyed base.

Parts a, b and c of each figure follow a standard format which is used throughout this report. Six time histories are presented in part a: horizontal displacement of the crest, water pressure adjacent to the dam at a depth of 66 ft, sliding displacement of the upper joint (not applicable here), opening of the upper joint at the upstream end (not applicable here), sliding displacement of the base joint (applicable here for the unkeyed base), and opening of the base joint at the upstream end (applicable here for the keyed and unkeyed bases). Joint opening and sliding displacements are computed as differences in nodal displacements across the row of elements containing the joint and therefore include a small elastic component. The crest and joint sliding displacements are positive in the upstream direction. Part b shows the contact histories of the upper joint (not applicable here) and the base joint (applicable here for the keyed and unkeyed bases). In part b, each finite element through which a joint passes is represented by five horizontal lines which break in the time dimension to indicate opening. A denser pattern of unbroken lines is used in part b to indicate the absence of a joint. Contours of maximum principal tensile stress

are shown in part c where the numbers indicate hundreds of psi, and stress vector plots are presented in part d to indicate the orientation of the maximum principal tensile stress. Some peak responses are listed in Table 1.

The dam response as a function of the earthquake time scale in the range 0.5 to 1.5 is shown in Figures 10 (empty reservoir) and 11 (full reservoir). The time scale is the factor by which the earthquake is compressed (if $< 1.$) or expanded (if $> 1.$) in time. By varying the time scale of the earthquake, a more complete picture of the effect of some parameter can be obtained. The quantities plotted are the maximum principal tensile stresses that occur on the dam faces, one each for the upstream and downstream faces, except that the tensile stresses at the stress concentration points at the heel and toe of the dam which occur with the bonded base are disregarded. Thus, all stresses plotted in Figures 10 and 11 come from locations in the neck region.

If the reservoir is empty, the ground motions employed are not enough to cause significant opening and sliding at the base of the dam even when opening and/or sliding are allowed as for the keyed and unkeyed conditions (small opening and/or sliding in Figures 6a and 8a). For this reason, the dam response is not strongly affected by the base condition when the reservoir is empty (Figure 10). Such is not the case when the reservoir is full (significant opening and/or sliding in Figures 7a and 9a). Larger stresses occur for the case of keyed base with full reservoir than with the unkeyed base, especially at the downstream face, while stresses with the bonded base have intermediate values (Figure 11). Apparently, the sliding plane at the base of the dam partially isolates the dam from the horizontal component of ground motion and thereby reduces the earthquake induced stresses. The peak stresses for the case of the unkeyed base with full reservoir are similar in magnitude, or even lower, to those occurring when the reservior is empty. When sliding is not allowed (bonded or keyed base), the presence of water increases the stresses induced in the dam by the earthquake (comparing Figures 10 and 11). These results show that base condition is an important parameter in the earthquake response of a concrete gravity dam.

The large reduction in stresses which occur when the dam is able to slide on its foundation suggests the use of an unkeyed foundation surface as a defensive design measure

against earthquakes. Careful study would have to be made to ensure that the sliding not be excessive and to limit the flow of water into the interface so as not to generate significant uplift forces. For the present analysis with unkeyed base, full reservoir and an earthquake time scale of 1.0, the base sliding amounts to 8.0 inches downstream and the opening at the upstream end of the interface reaches 0.37 in (Figure 9a). This opening is much smaller than the 2.4 in opening which occurs with the keyed base and full reservoir (Figure 7a). Providing a key to prevent sliding increases the dam-foundation interface opening as well as the stresses in the dam. The benefits of allowing the dam to slide on its foundation have been noted in a previous study (14).

It should also be repeated from Chapter 1 that the foundation representation uses a rigid rectangular plate on a 3-d half-space. Although approximately accounting for 3-d effects, this representation restricts the foundation surface at the base of the dam to remain plane. It would be desirable to remove this restriction in any serious study of using an unkeyed foundation surface as a defensive design measure against earthquakes.

Chapter 3. Dams with Modified Profiles

Most existing gravity dams employ a similar cross-sectional shape which is optimal for eliminating tensile stresses under static loading, but which is not optimal for earthquake loading. During an earthquake the motion of the upper region of a concrete gravity dam of typical profile is considerably amplified, and this can result in large dynamic tensile stresses in the neck region, as seen in Chapter 2. To investigate whether these stresses can be reduced by reshaping the dam cross section, two modified profiles are examined here. One is a simple shape with flat upstream and downstream faces (geometry and finite element mesh in Figure 12), and the other is the same as Pine Flat Dam except that part of the crest has been replaced by a light-weight structure (geometry and finite element mesh in Figure 13). Analyses are made with the keyed and unkeyed base conditions and with full reservoir.

Time history and stress contour results at a time scale of one are presented in Figures 14 to 17 as follows:

Figure 14: straight-sided dam, keyed base

Figure 15: straight-sided dam, unkeyed base

Figure 16: light-weight crest dam, keyed base

Figure 17: light-weight crest dam, unkeyed base.

The responses of the straight-sided dam and the light-weight crest dam are similar, and, compared to the respone of Pine Flat Dam in Chapter 2, as summarized in Table 1, exhibit significantly smaller peak tensile stresses and slightly smaller amounts of bottom joint opening and sliding.

The reductions noted in Table 1 are still apparent from results obtained by varying the time scale of the earthquake from 0.5 to 1.5. This is shown in Figure 18 (keyed base) and Figure 19 (unkeyed base) for the maximum principal tensile stresses on the upstream and downstream faces. The average stress reduction for the modified dams compared to Pine Flat Dam is about 30% to 40%, whether the base is keyed or unkeyed. Also, the effect of base condition on the modified dams is similar to that for Pine Flat Dam; that is, lower

stresses occur when the base is allowed to slide (the unkeyed condition) and the reduction of the higher stresses on the downstream face is especially significant. As a result, the tensile stress levels for the modified dams with unkeyed base are low.

Determination of an optimum cross-sectional shape for a concrete gravity dam must consider cost as well as performance. The volume of the straight-sided dam exceeds that of Pine Flat Dam by 6% while the volume of the light-weight crest dam is less than that of Pine Flat Dam by 1%. However, the savings in concrete volume for the light-weight crest dam would be offset by other costs associated with building the light-weight crest. Both of the modified dams would probably cost more to construct than Pine Flat Dam, but the additional expenditure would be more than justified by the better earthquake performance of the modified dams. The benefits of a dam with a light-weight crest have been noted in a previous study (15).

Chapter 4. Joints and Prestressing

Cracking in a concrete gravity dam during an earthquake is a concern because of the possibility that a potential failure mechanism will be created. One example would be a sliding failure along a crack which had propagated through the dam with a downward slope in the downstream direction. Given the difficulty in trying to predict the paths of earthquake-induced cracks in actual dams, the probability of occurrence of such an event would be hard to assess. Therefore, there may be some merit in placing a joint in a concrete gravity dam, say, in the neck region where the dynamic tensile stresses are highest, if the joint could be given a favorable profile regarding stability and if the presence of this joint reduced the earthquake-induced tensile stresses enough to prevent cracks from forming. The analysis of such a structure is much more tractable than one for which propagating cracks occur, and, therefore, the results would be more reliable.

The penetration of reservoir water into a crack which opens on the upstream face of a concrete gravity dam during earthquake shaking would cause uplift and thereby assist any failure process. Although little is known about the possible extent and effect of such an occurrence, sliding along a rough crack surface dilates the crack and would facilitate water penetration (11). However, if a pre-formed joint is present and effective in preventing the formation of cracks, sealing the joint at the upstream face of the dam would eliminate the water penetration problem. This could be an important advantage of using such a joint.

The use of prestressing in concrete gravity dams could serve two roles related to cracking. First, it increases the initial compressive stresses so that the tensile stresses reached during an earthquake are reduced. With enough prestress, no cracks would form; however, this may take a large amount of steel. Another role of prestressing relates to crack control rather than crack prevention. That is, even if a crack does occur in a region which has been prestressed, it would likely propagate less and undergo less opening and sliding because of the prestress.

To investigate the effects of joints and prestressing on the earthquake response of concrete gravity dams, four problems have been analyzed. All employ the Pine Flat Dam

cross-section with full reservoir and an earthquake time scale of one. Geometries and finite element meshes appear in Figures 20 to 23. The four problems are:

Horizontal joint without prestress (Figure 20). The horizontal joint is located a distance 71′10″ below the crest.

Stepped joint without prestress (Figure 21). The joint is formed by two horizontal planes connected by a 3 foot high step in the middle. The top plane is located a distance 70′2″ below the crest.

Inclined joint without prestress (Figure 22). The joint slopes up in the downstream direction and intersects the upstream and downstream faces at distances 85′4″ and 69′5″ below the crest, respectively.

Horizontal joint with prestress (Figure 23). This problem is similar to the first one, but with prestress added, and it is designed to investigate the effect of prestress on crack control. Two groups of cables, each with cross-sectional area of 3 in^2 and each stressed to carry an effective tension of 80 ksi, are used to prestress the neck region. The groups are anchored at their ends where all load transfer takes place. Since the width of the two-dimensional cross section analyzed is one foot, the group spacing in the direction of the dam axis is also one foot. The total prestressing force of 480 kips per foot along the dam axis exceeds the weight of concrete above the joint which equals 386 kips per foot along the dam axis.

Time history and stress contour results at a time scale of one are presented in Figures 24 to 31 as follows:

Figure 24: horizontal joint without prestressing, keyed base

Figure 25: horizontal joint without prestressing, unkeyed base

Figure 26: stepped joint without prestressing, keyed base

Figure 27: stepped joint without prestressing, unkeyed base

Figure 28: inclined joint without prestressing, keyed base

Figure 29: inclined joint without prestressing, unkeyed base

Figure 30: horizontal joint with prestressing, keyed base

Figure 31: horizontal joint with prestressing, unkeyed base.

Examination of the stress distributions from parts c of the figures shows that the peak tensile stresses are significantly reduced, compared to the results without neck joints from Chapter 2, except in the region immediately adjacent to the joint. In this region, very large tensions occur; also, it is doubtful that the mesh fineness is sufficient to capture these stresses accurately. For the horizontal joint without prestressing, large horizontal tensions occur near the ends of the joint (Figures 24d and 25d). Such large tensions have been observed in a previous numerical study (9), and are believed to arise from high shear forces transferred across the joint when the contact reduces to a small area during joint opening. Other large tensions occur at the corners of the stepped joint (Figures 26d and 27d) where there are stress concentrations. The inclined joint (Figures 28d and 29d) and the horizontal joint with prestressing (Figures 30d and 31d) suffer least from the high local tensions. The results indicate that it would be prudent to provide some reinforcement adjacent to the joint because of the potential for crack initiation there. Such reinforcement would be parallel to the joint to be in line with the stress vectors from parts d of the figures, and it would cover a zone 5 feet to 10 feet wide on each side.

Highlights of the analyses are summarized in Table 1. The peak tensile stresses listed are from the body of the dam away from the region adjacent to the joint which would not have the benefit of the joint reinforcement listed above. Insertion of a joint produces significant reductions in these stresses compared to those of the unjointed dam, and, for the cases without prestress, the stresses are about the same whether the base condition is keyed or unkeyed, unlike the situation for the unjointed dam with full reservoir. Joint

sliding is largest with the horizontal joint without prestress, nearly 2 feet in the downstream direction. The step nearly eliminates joint sliding but at the expense of larger joint opening which reaches 11 inches for the keyed base. Sealing to prevent water penetration into the joint for such an opening would require some ingenuity. Of the unprestressed joints, the inclined one has the smallest openings and intermediate values of sliding.

Prestressing significantly reduces the opening and sliding of the horizontal joint, and this suggests that prestressing may be an effective means for crack control. The prestressing forces increase by a maximum of 37% (keyed base on downstream side of joint, see extra time histories in Figures 30a and 31a) during the earthquake, and this can be accounted for in the design. However, the sliding displacement on the horizontal joint, although small when prestressing is used, may be enough to break the steel cables, and, for this reason, reliance on prestressing may be unwise. Some further investigation of this point is needed before prestressing can be recommended.

The best of the schemes examined regarding earthquake performance may be the inclined joint. However, this joint may be harder to construct than the horizontal and stepped joints. Any of the joints, including a prestressed one, should have some reinforcement parallel to the joint to control cracking in the region immediately adjacent to the joint.

Chapter 5. Hydrodynamic Isolation

The presence of water affects the response of a dam to an earthquake through extra water pressure loads which act on the dam. These pressures are generated by accelerations of the dam and by accelerations of the floor and sides of the reservoir. As shown in Chapter 2, the presence of water generally increases the earthquake response of a concrete gravity dam that is restrained from sliding at its base. Since gravity dams are often keyed in at the base, there is merit in investigating the feasibility of reducing the dynamic component of the water pressure, i.e., isolating the dam from this part of the pressure. This can be accomplished by placing enough of a very soft material into the reservoir near the upstream face of the dam. The static water pressure would not be effected.

A number of possible ways exist to introduce the soft material. Gas-filled balloons suspended in the reservoir and bubble injection into the reservoir may not be practical because of the large gas volume required to accomplish the isolation (16). The method examined here involves placing the soft material directly against the upstream face of the dam. The compressibility of the soft material is taken to be that of a gas which is better than could ever be achieved for real materials. In addition, a perfect gas is assumed. With the further assumption that volume changes occur only by one-dimensional straining in the horizontal direction, the absolute pressure in the soft material at some depth d below the water surface is given by

$$p(d,t) = \frac{(\gamma_w d + p_a) W_o(d)}{W(d,t)}$$

where t = time; γ_w = unit weight of water; p_a = atmospheric pressure; $W_o(d)$ and $W(d,t)$ = horizontal dimension (thickness) of soft material at depth d under static water pressure conditions and at time t, respectively. With its shearing resistance neglected, the soft material can thus be treated as a continuous distribution of nonlinear horizontal springs, and it is so represented here by finite elements with stiffness in the horizontal degrees of freedom only. The bulk tangent stiffness equals the current absolute pressure of the gas.

The soft material is applied to the upstream face of Pine Flat Dam with a thickness of 4 feet down to a water depth of 45 feet from which point the thickness varies linearly

to zero at a depth of 120 feet. With this profile, the upstream edge of the soft material is nearly vertical. The finite element mesh is shown in Figure 32. Since the soft material is assumed to be softer than would be possible and since a substantial volume is used, the results obtained should overestimate what can be practically accomplished.

Results of the analyses for the dam with hydrodynamic isolation appear in Figure 33 for the keyed base and time scale of one. As seen in part a of the figure, the pressures in the soft material still have considerable dynamic variation, although the frequency content of the pressure response has been significantly altered by the soft material (compare to Figure 7a for the unisolated dam). Maximum principal tensile stresses are reduced only slightly by the isolation (compare to Figure 7c). The performance of hydrodynamic isolation is generally better at other earthquake time scales (Figure 34), and, on average over the range of earthquake time scale from 0.5 to 1.5, the effect of hydrodynamic isolation is to reduce the maximum principal tensile stress by about 20%.

The other curve in Figure 34 represents the case of perfect isolation; that is, during the analysis the water pressure distribution over the entire upstream face was set equal to the static distribution. The further effect of completely eliminating the dynamic component of the water pressure varies with the earthquake time scale, although, on average, it is beneficial. The results with perfect isolation represent the limit of what could be achieved through hydrodynamic isolation.

Chapter 6. Summary

1. Base condition is an important parameter in the earthquake response of a concrete gravity dam. Compared to the case where the dam is fully bonded to its foundation, lift-off at the dam base without sliding (keyed condition) produces higher stresses while sliding (unkeyed condition) can significantly reduce stresses. These findings warrant some further investigation into the desirability of constructing new gravity dams on special bases to allow sliding. The effect of water uplift pressures under the dam to assist lift-off and sliding, which was neglected here with some justification, should be fully investigated.

2. Earthquake induced tensile stresses in gravity dams of typical profile, such as Pine Flat Dam, can be reduced on the order of 30% to 40% by thickening the neck region or by replacing the solid crest by a light-weight structure. The geometry of the dam with the thickened neck investigated here had a simple profile of straight upstream and downstream sides and requires 6% more concrete volume than the Pine Flat Dam profile. In a seismic region, this extra expense for a new dam would be justified by the better seismic performance. High costs to reshape an existing dam may confine this technique to use in new construction.

3. Placing a water-sealed joint in the neck region of a gravity dam of the typical profile effectively reduces earthquake-induced tensile stresses except in the region adjacent to the joint where some local reinforcement would be needed to control cracking. Keying such a joint eliminates sliding but may cause large opening. An inclined joint sloping at an angle of 19° upward in the downstream direction behaved favorably for the problem studied. Difficulties in placing a reinforced joint in an existing dam may confine this technique to use in new construction.

4. The use of prestressing to prevent earthquake-induced cracking in the neck region of a typical concrete gravity dam during strong shaking requires a lot of steel and probably would be impractical. However, an amount of steel below that needed to prevent cracking could still effectively improve the stability of a gravity dam during

an earthquake through crack control after cracks form. In the study made here, 6 in^2 of steel area per foot along the dam axis (still quite high) significantly improved the performance of a dam with an initial horizontal joint. Cost-benefit considerations for prestressing new or existing dams for the purpose of seismic crack control remain to be evaluated. One concern which deserves further study relates to possible damage to the prestressing steel incurred at crack planes during relative sliding between the concrete masses on opposite sides of the crack.

5. Earthquake-induced tensile stresses can also be reduced by hydrodynamic isolation. Modest reductions on the order of 20% were obtained for the problem studied which used a substantial volume of an ideal soft material which has the properties of a perfect gas. However, the higher stiffness of real materials means that an even greater volume would be needed to achieve the same performance. So, hydrodynamic isolation will probably not prove to be a viable technique for improving the seismic behavior of new and existing gravity dams. However, the technique may find greater benefit for arch dams for which the presence of water on the dynamic response is more important.

6. An immediate recommendation of the studies performed here is that future designs of concrete dams employing the typical thin neck be abandoned for construction in seismic areas in favor of the straight-sided dam or the light-weight crest dam such as considered in Chapter 3.

References

1. Hall, J. F., "Study of the Earthquake Response of Pine Flat Dam," *Earthquake Engineering and Structural Dynamics*, Volume 14, Number 2, March–April 1986.

2. Pal, N., "Nonlinear Earthquake Response of Concrete Gravity Dams," *Report No. EERC 74–14*, Earthquake Enginering Research Center, University of California, Berkeley, December 1974.

3. Agbabian Associates, "Nonlinear Analysis of Norris Dam for Seismic Loads," El Segundo, California, June 1975.

4. Chapuis, J., B. Rebora and T. Zimmermann, "Numerical Approach of Crack Propagation Analysis in Gravity Dams During Earthquakes," *Proceedings of the 15th Congress on Large Dams, Question 57*, International Commission on Large Dams, Lausanne, 1985.

5. Skrikerud, P. E. and H. Bachmann, "Discrete Crack Modelling for Dynamically Loaded Unreinforced Concrete Structures," *Earthquake Enginering and Structural Dynamics*, Volume 14, Number 2, March–April 1986.

6. Mlakar, P. F., "Nonlinear Response of Concrete Gravity Dams to Strong Earthquake-Induced Ground Motion," *Computers and Structures*, Volume 26, Numbers 1–2, 1987.

7. Vargas-Loli, L. M. and G. Fenves, "Nonlinear Earthquake Response of Concrete Gravity Dams," Deparment of Civil Engineering, University of Texas, Austin, December 1987.

8. Droz, Patrice, "Modele numerique du comportement non-lineaire d'ouvrages massifs en beton non arme," *Thesis Number 682*, Department de Genie Civil, Ecole Polytechnique Federale de Lausanne, EPFL, 1987.

9. El-Aidi, B., "Nonlinear Earthquake Response of Concrete Gravity Dam Systems," *Report No. EERL 88–02*, Earthquake Engineering Research Laboratory, California Institute of Technology, Pasadena, 1988.

10. Ayari, M. L. and V. E. Saouma, "A Fracture Mechanics Based Seismic Analysis of Concrete Gravity Dams Using Discrete Cracks," *Engineering Fracture Mechanics*, Volume 35, Number 1/2/3, 1990.

11. Donlon, W. P., "Experimental Investigation of the Nonlinear Seismic Response of Concrete Gravity Dams," *Report No. EERL 89–01*, Earthquake Engineering Research Laboratory, California Institute of Technology, Pasadena, 1988.

12. Hughes, T.J.R., "The Finite Element Method — Linear Static and Dynamic Finite Element Analysis," Prentice-Hall, 1987.

13. Hall, J. F., "The Dynamic and Earthquake Behavior of Concrete Dams: Review of Experimental Behavior and Observational Evidence," *Soil Dynamics and Earthquake Engineering*, Volume 7, Number 2, April 1988.

14. Leger, P. and M. Katsouli, "Seismic Stability of Concrete Gravity Dams," *Earthquake Engineering and Structural Dynamics*, Volume 18, Number 6, August 1989.

15. Thakkar, S. K., A. K. Dinkar and R. P. Mathur, "Dynamic Behavior of Gravity Dam with Light Structural Systems at Top," *Proceedings of the Eighth World Conference on Earthquake Engineering*, Volume 5, San Francisco, 1984.

16. Hall, J. F. and B. El-Aidi, "Hydrodynamic Isolation of Concrete Dams," *Proceedings of the ASCE Structures Congress*, San Francisco, 1989.

Table 1

SUMMARY OF PEAK RESPONSES FOR AN EARTHQUAKE TIME SCALE OF 1.0

Case	Prin. ten. stress up. face	Prin. ten. stress down. face	Base opening up. face	Base sliding disp.	Joint opening up. face	Joint sliding disp.
PF–E–B	370 psi*	610 psi*	—	—	—	—
PF–E–K	480 psi	500 psi	.09 in	—	—	—
PF–E–U	420 psi	540 psi	.07 in	0.6 in (us)	—	—
PF–F–B	460 psi*	700 psi*	—	—	—	—
PF–F–K	490 psi	1060 psi	2.4 in	—	—	—
PF–F–U	450 psi	470 psi	0.4 in	8.0 in (ds)	—	—
SSD–F–K	240 psi	640 psi	2.1 in	—	—	—
SSD–F–U	280 psi	360 psi	0.4 in	7.6 in (ds)	—	—
LWCD–F–K	340 psi	660 psi	1.8 in	—	—	—
LWCD–F–U	280 psi	370 psi	0.3 in	7.9 in (ds)	—	—
PFHJ–F–K	400 psi^{x}	370 psi^{x}	1.3 in	—	5.4 in	20.2 in (ds)
PFHJ–F–U	420 psi^{x}	430 psi^{x}	0.2 in	6.1 in (ds)	2.0 in	23.0 in (ds)
PFSJ–F–K	250 psi^{x}	430 psi^{x}	1.4 in	—	11.0 in	0.8 in (ds)
PFSJ–F–U	220 psi^{x}	360 psi^{x}	0.2 in	6.7 in (ds)	4.6 in	0.7 in (ds)
PFIJ–F–K	410 psi^{x}	450 psi^{x}	0.9 in	—	4.7 in	10.5 in (us)
PFIJ–F–U	290 psi^{x}	350 psi^{x}	0.2 in	5.6 in (ds)	1.9 in	1.5 in (ds)
PFHJP–F–K	250 psi^{x}	670 psi^{x}	2.3 in	—	1.6 in	5.0 in (ds)
PFHJP–F–U	230 psi^{x}	380 psi^{x}	0.2 in	7.2 in (ds)	1.3 in	2.3 in (ds)
PFHI–F–K	400 psi	1040 psi	1.3 in	—	—	—

PF = original Pine Flat Dam, SSD = straight-sided dam, LWCD = light-weight crest dam, PFHJ = Pine Flat Dam with horizontal joint, PFSJ = Pine Flat Dam with stepped joint, PFIJ = Pine Flat Dam with inclined joint, PFHJP = Pine Flat Dam with horizontal joint and prestress, PFHI = Pine Flat Dam with hydrodynamic isolation, E = empty reservoir, F = full reservoir, B = bonded base, K = keyed base, U = unkeyed base, us = toward upstream, ds = toward downstream.

* high stresses at heel and toe disregarded

^{x} high stresses adjacent to joint disregarded

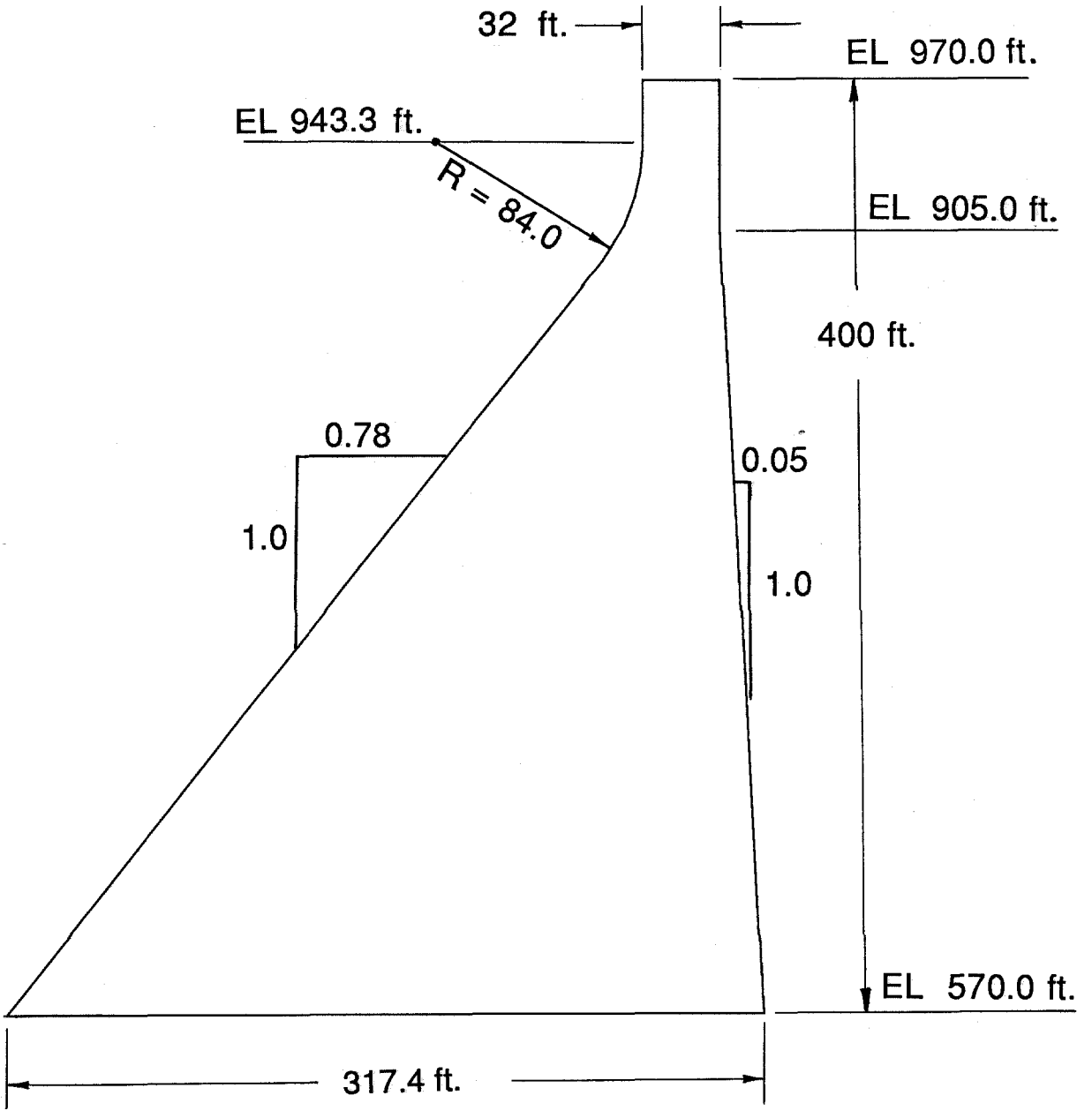

Figure 1. Geometry definition of the 400 foot high monolith of Pine Flat Dam.

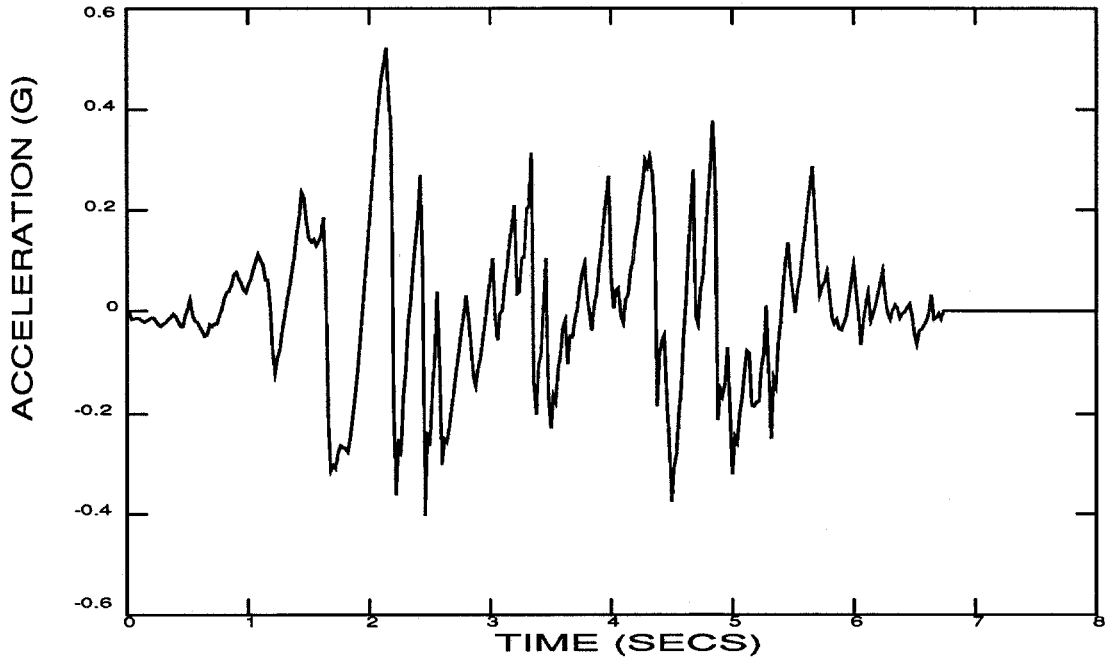

a. S00E component. Used for horizontal ground motion.

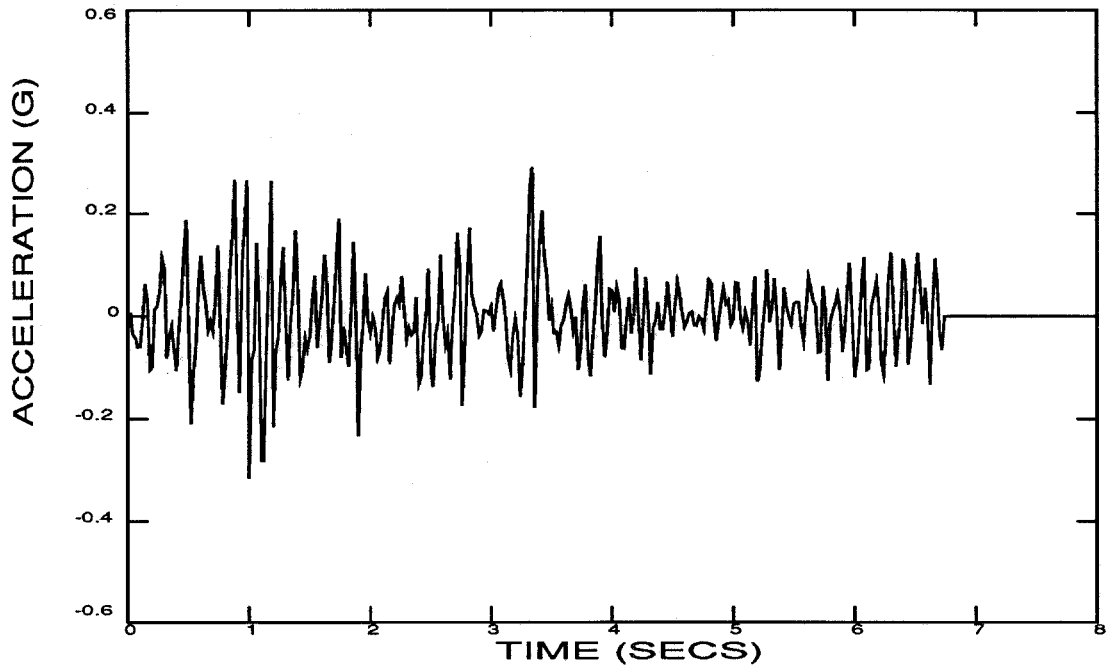

b. Vertical component. Used for vertical ground motion.

Figure 2. El Centro 1940 ground motions scaled amplitude-wise by a factor of 1.5

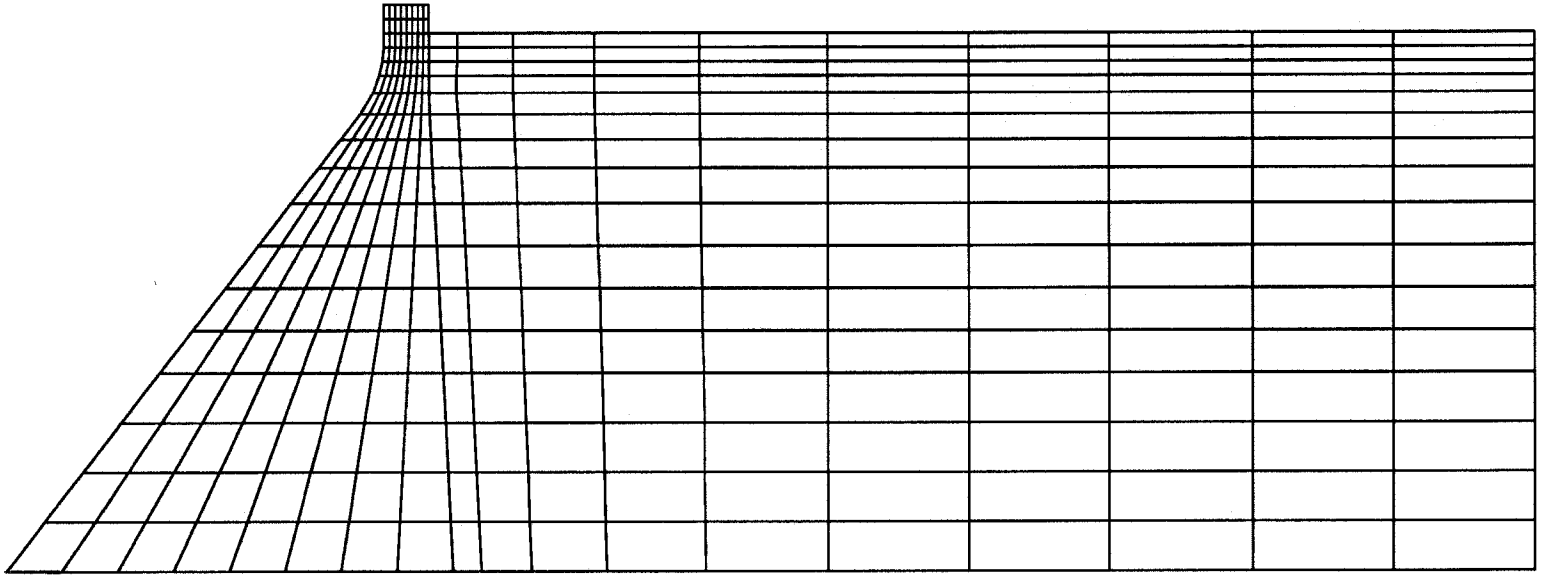

Figure 3. Finite element meshes of Pine Flat Dam and water

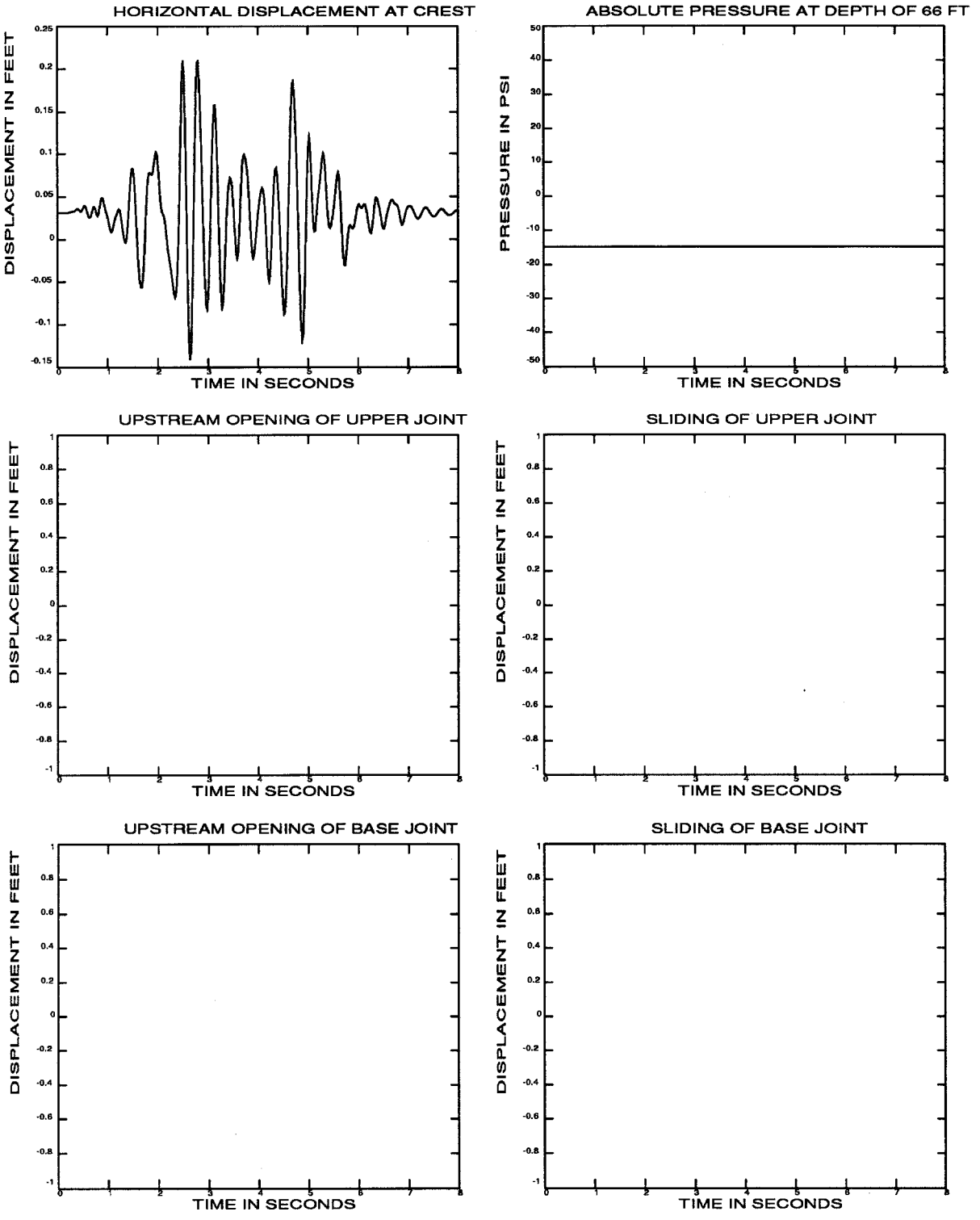

a. Time history responses

Figure 4. Results of earthquake analysis of Pine Flat Dam with empty reservoir and bonded base. The earthquake time scale equals one.

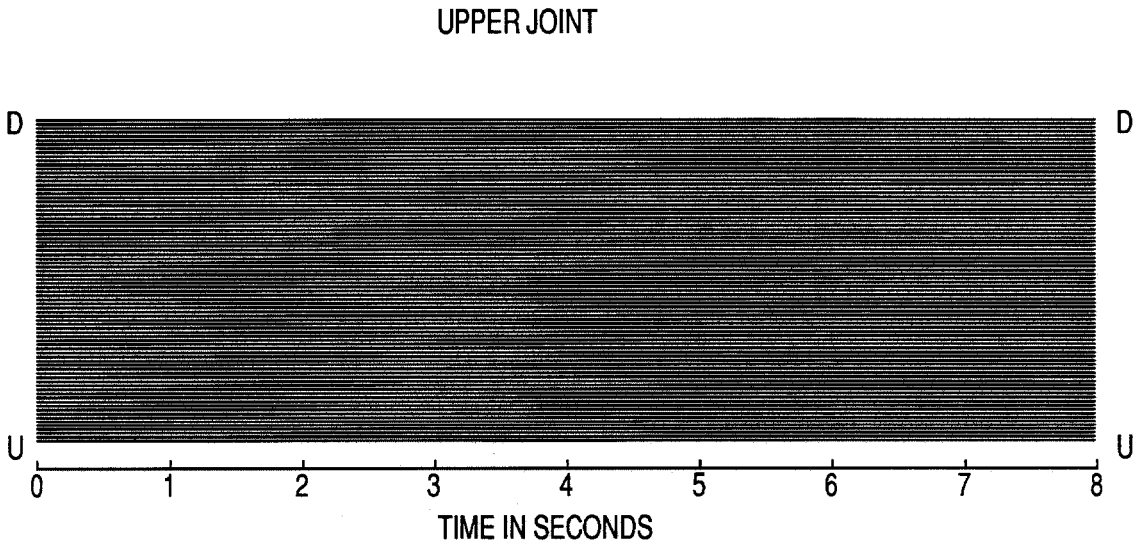

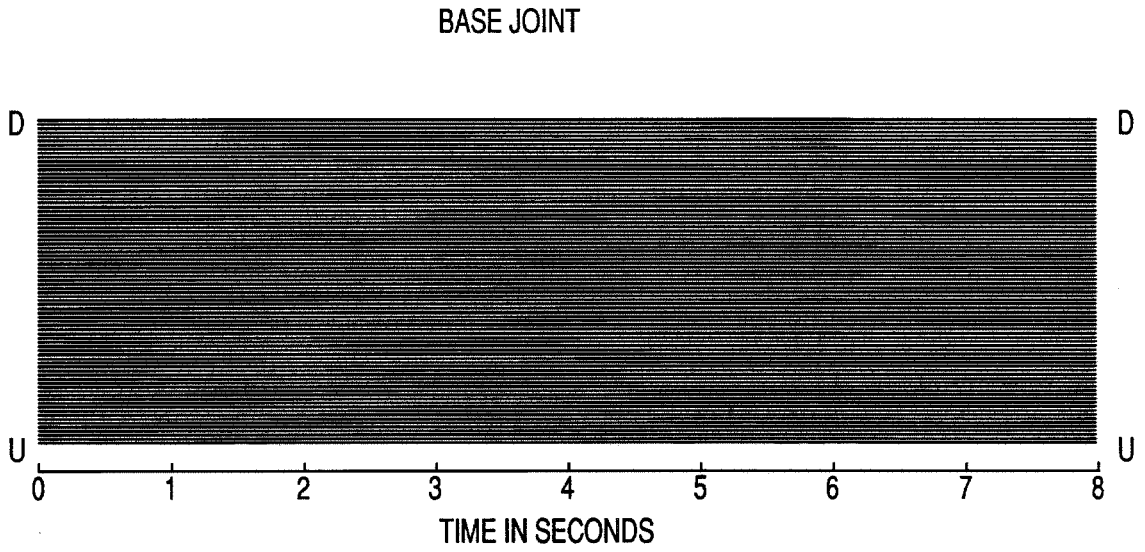

Figure 4b. Contact time histories of joints

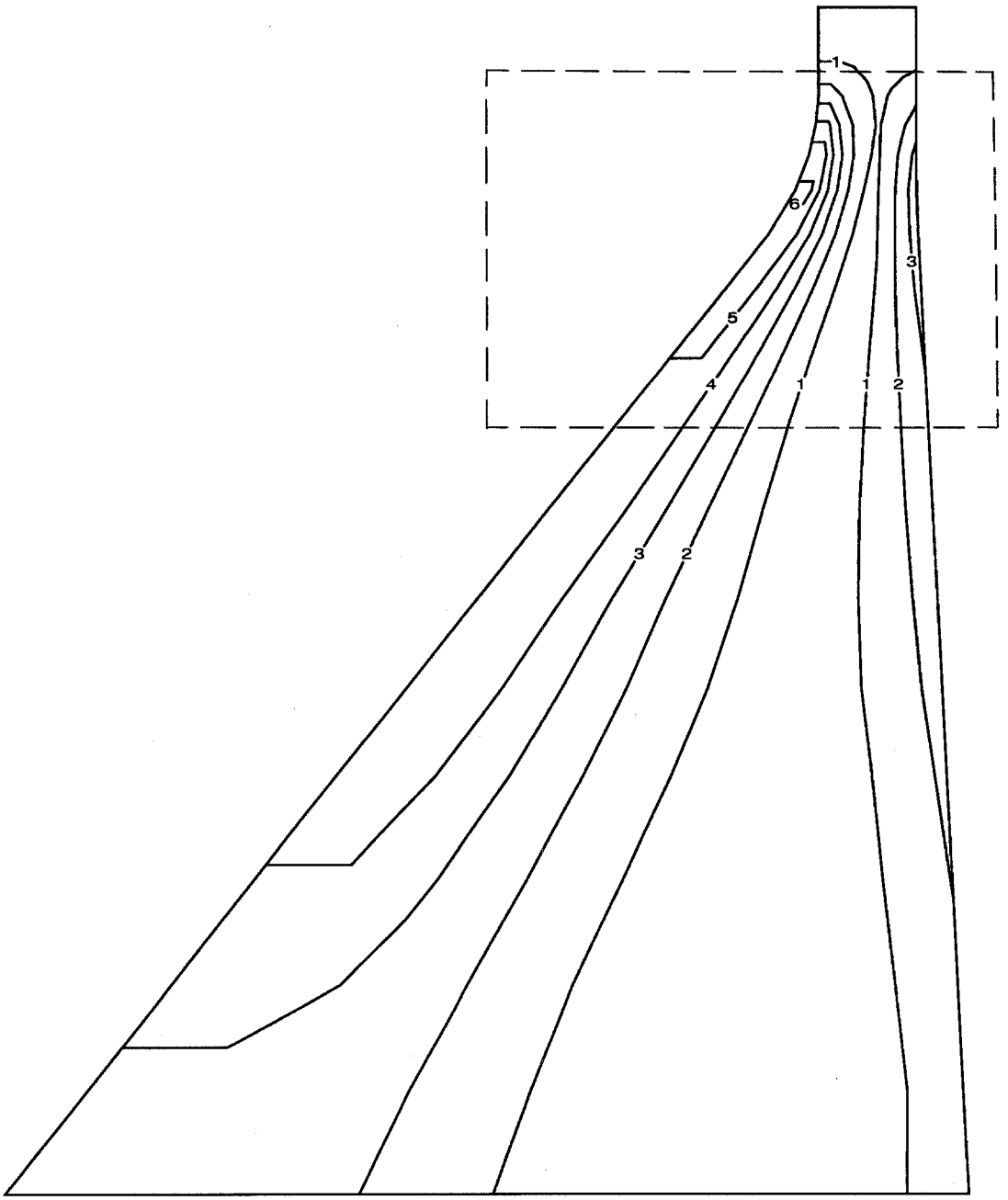

Figure 4c. Contours of maximum principal tensile stress (static plus dynamic). Stress vectors within the boxed region are shown in part d.

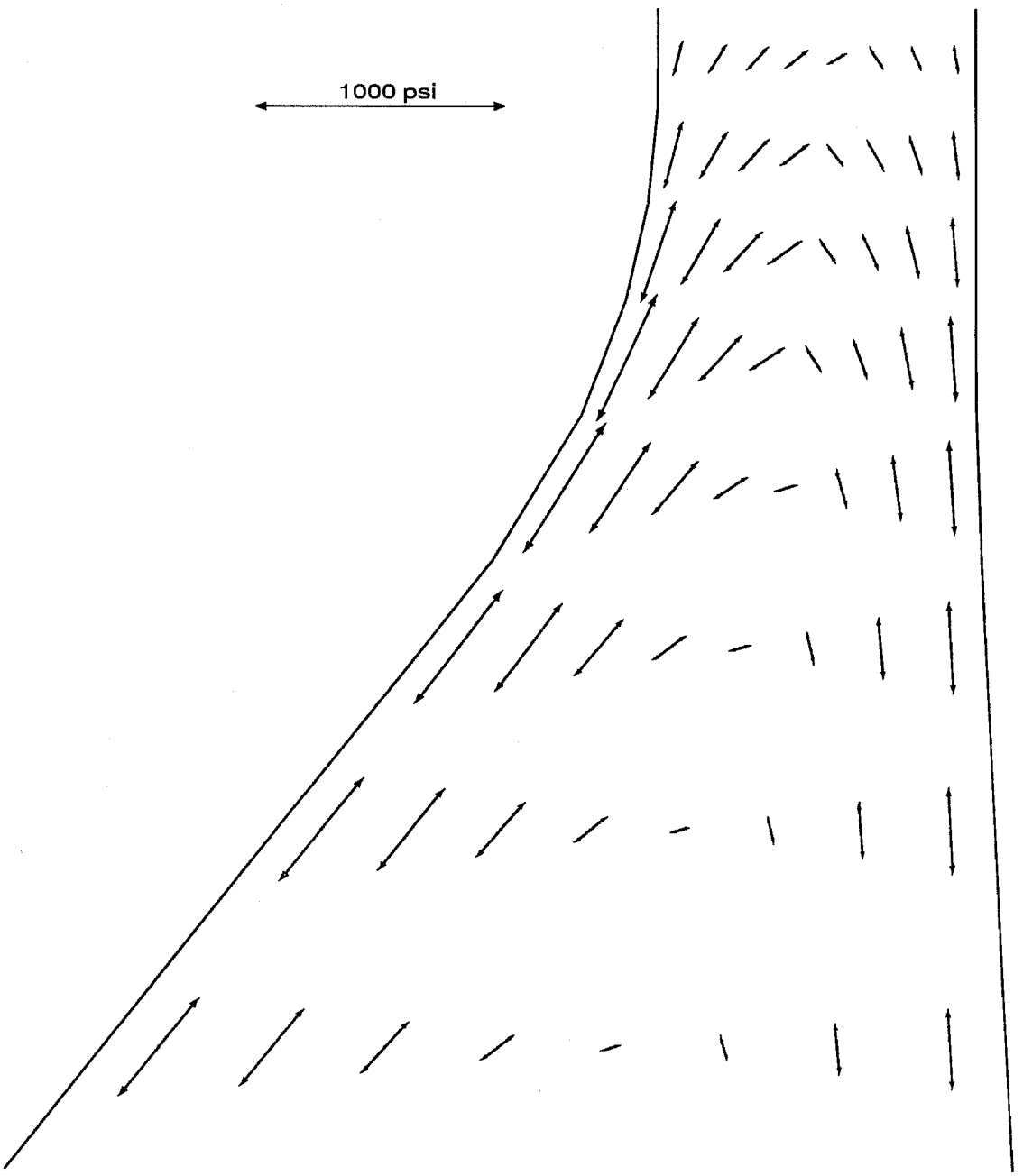

Figure 4d. Vectors of maximum principal tensile stress (static plus dynamic) in the neck region. See part c for region plotted.

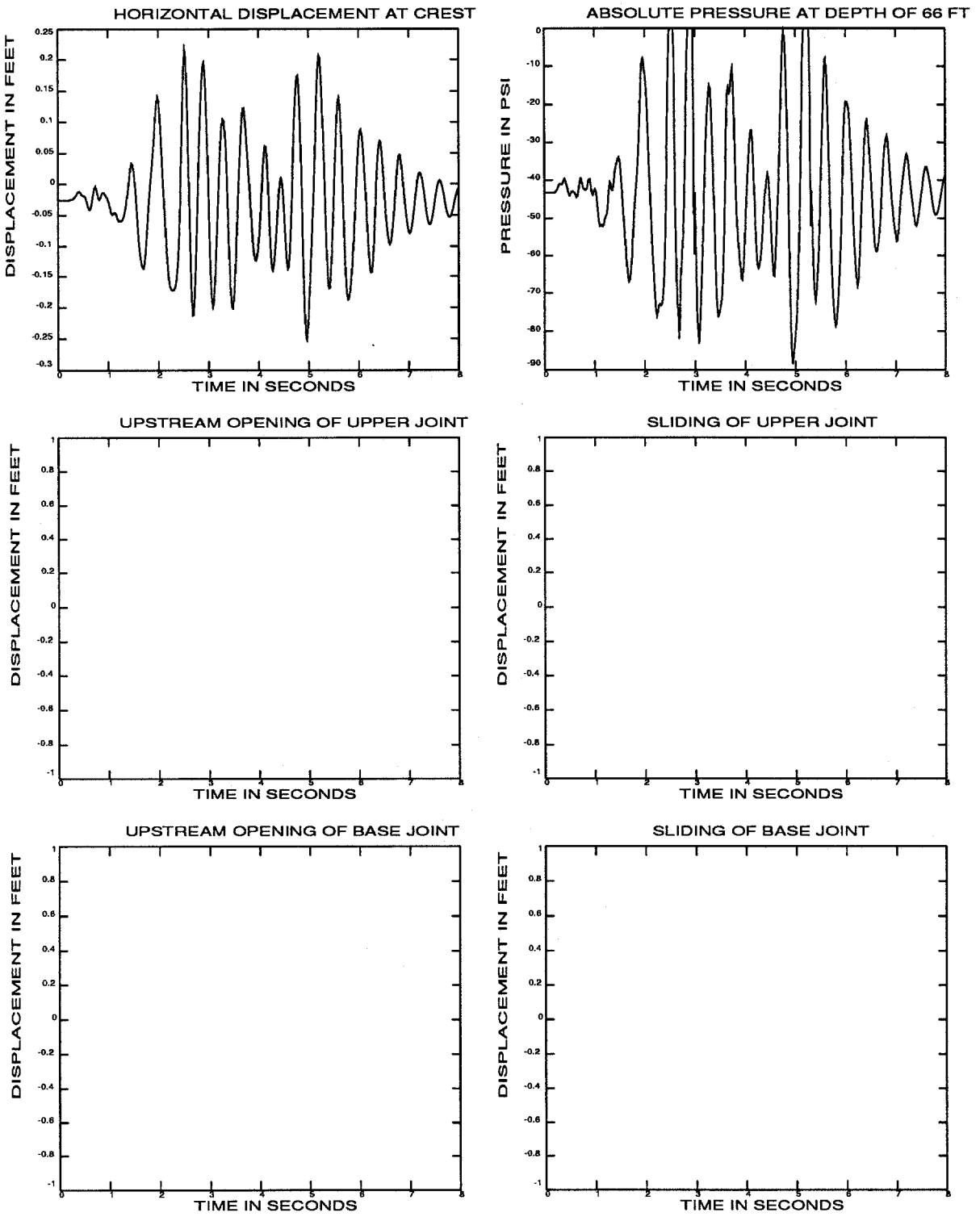

a. Time history reponses

Figure 5. Results of earthquake analysis of Pine Flat Dam with full reservoir and bonded base. The earthquake time scale equals one.

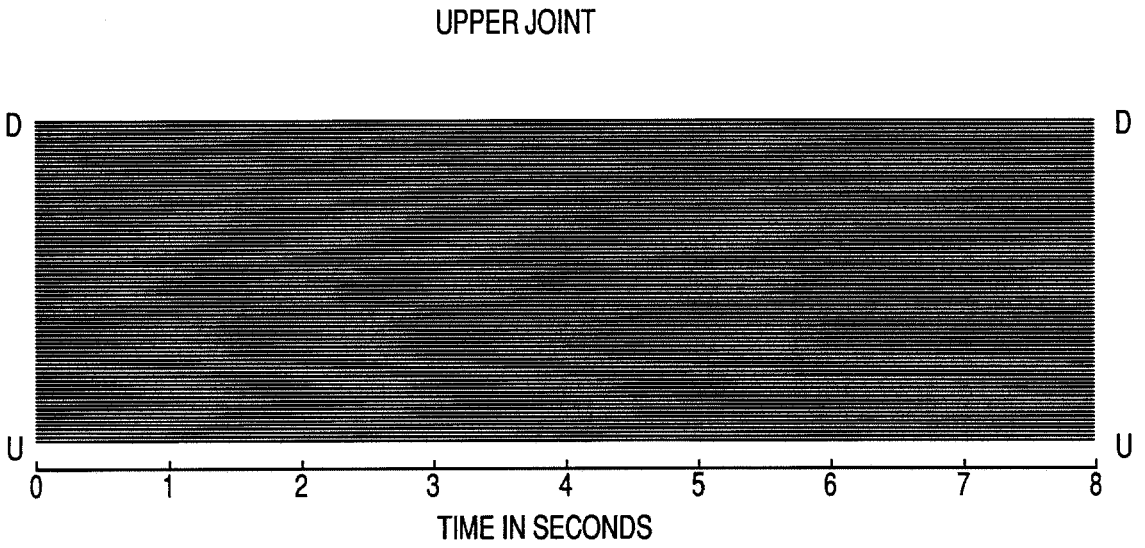

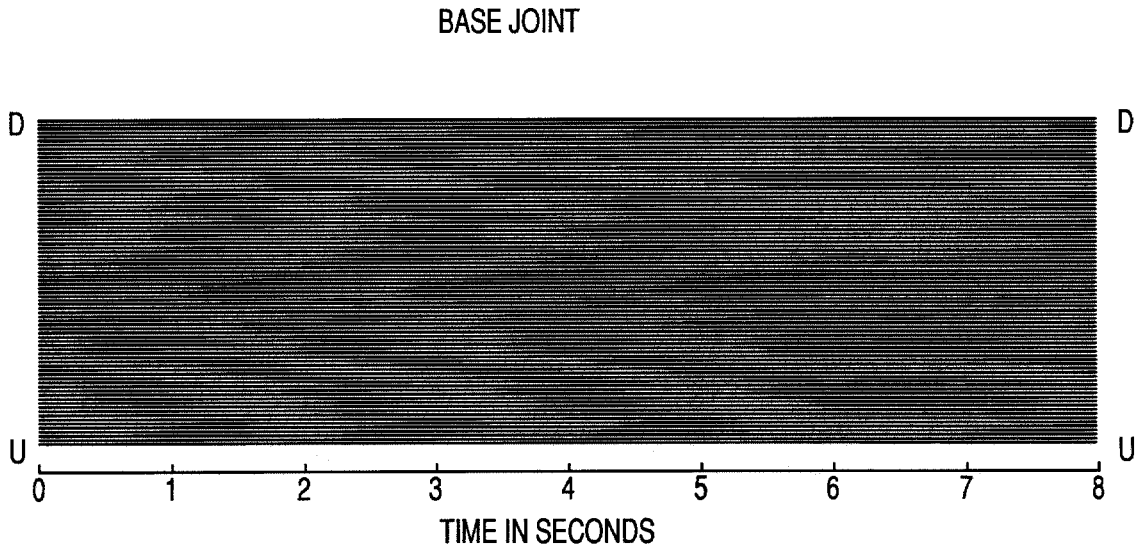

Figure 5b. Contact time histories of joints

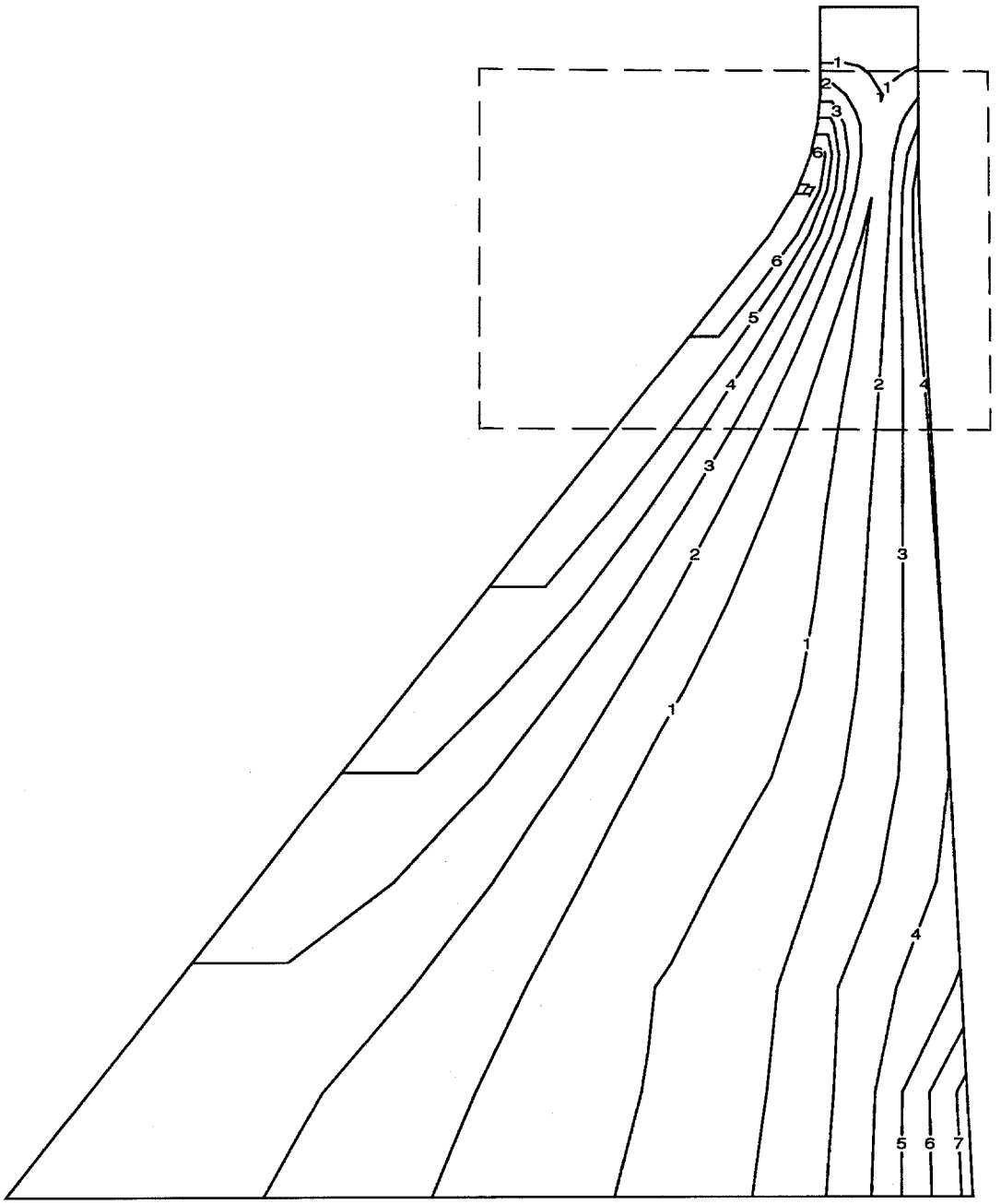

Figure 5c. Contours of maximum principal tensile stress (static plus dynamic). Stress vectors within the boxed region are shown in part d.

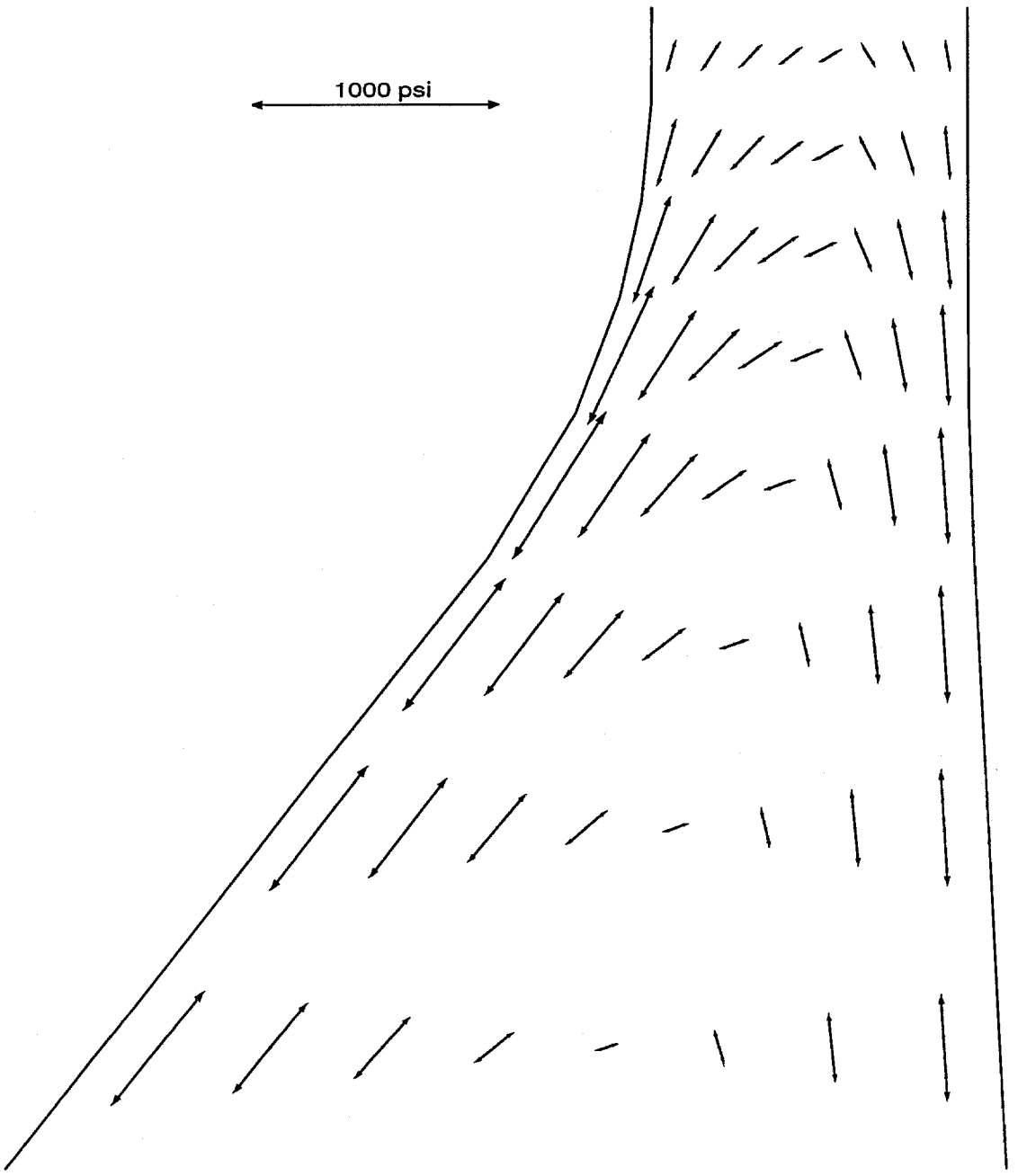

Figure 5d. Vectors of maximum principal tensile stress (static plus dynamic) in the neck region. See part c for region plotted.

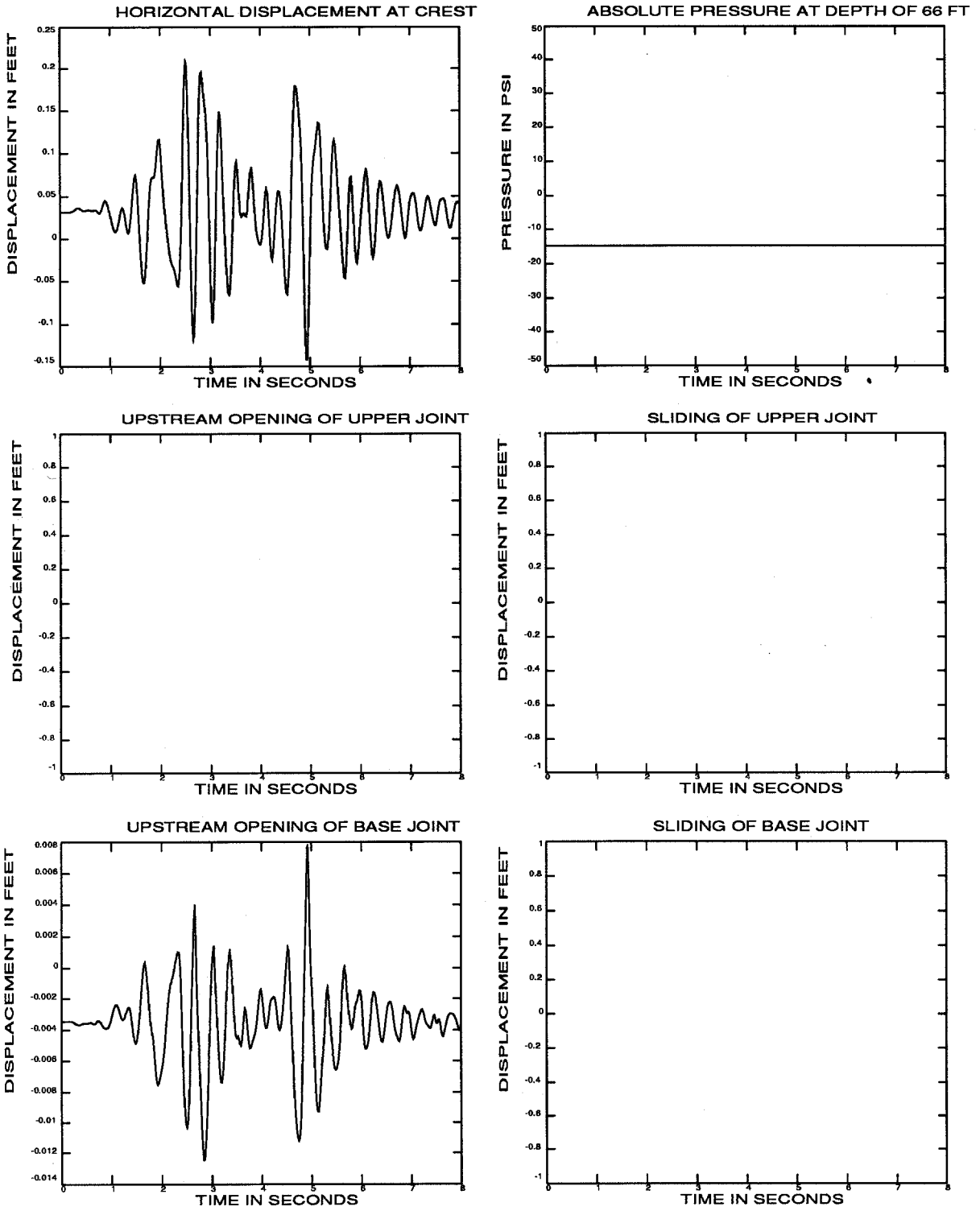

a. Time history reponses

Figure 6. Results of earthquake analysis of Pine Flat Dam with empty reservoir and keyed base. The earthquake time scale equals one.

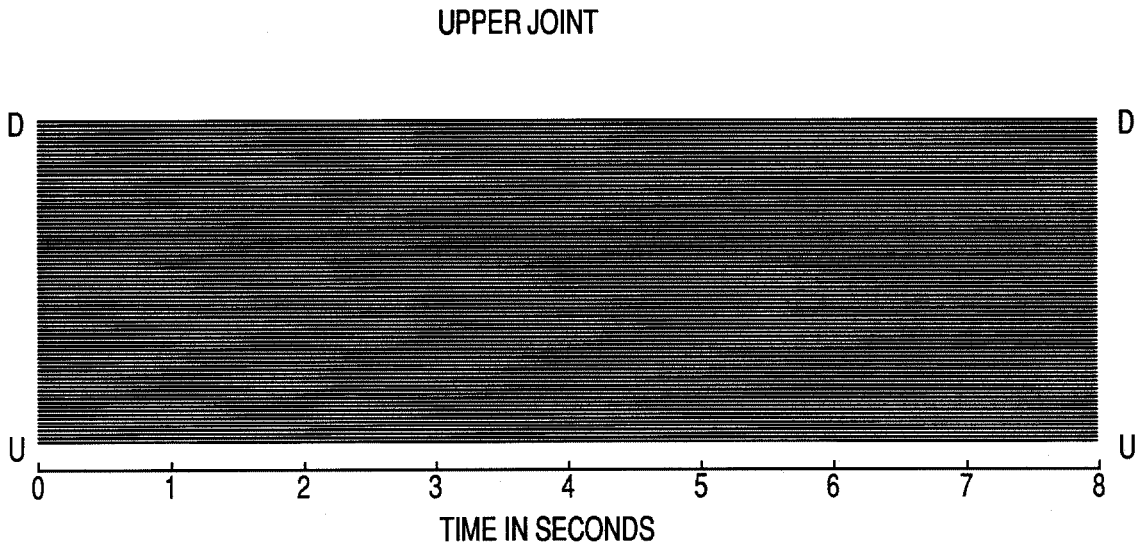

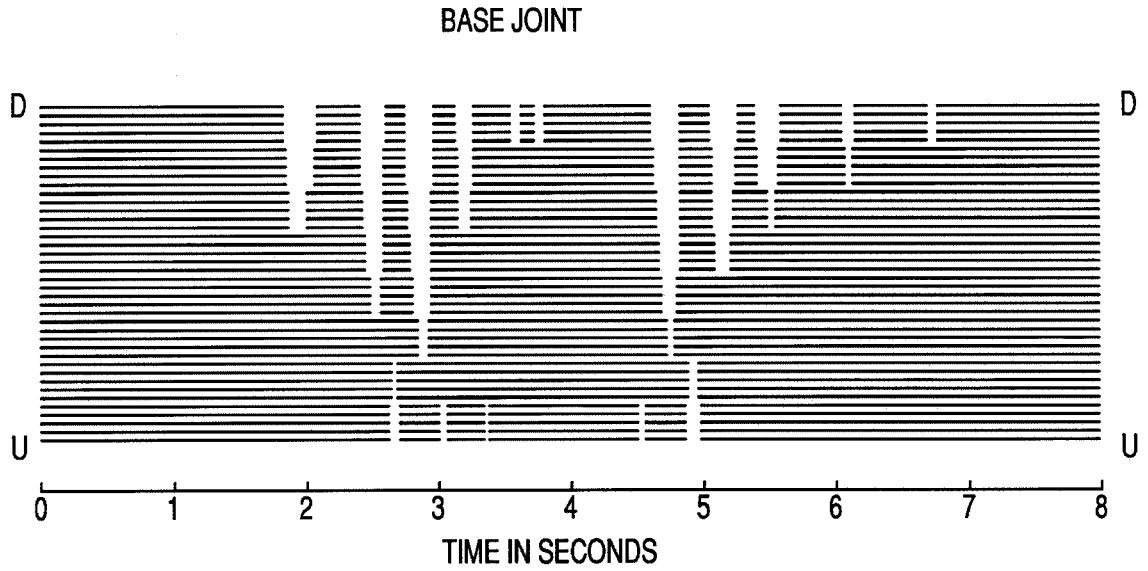

Figure 6b. Contact time histories of joints

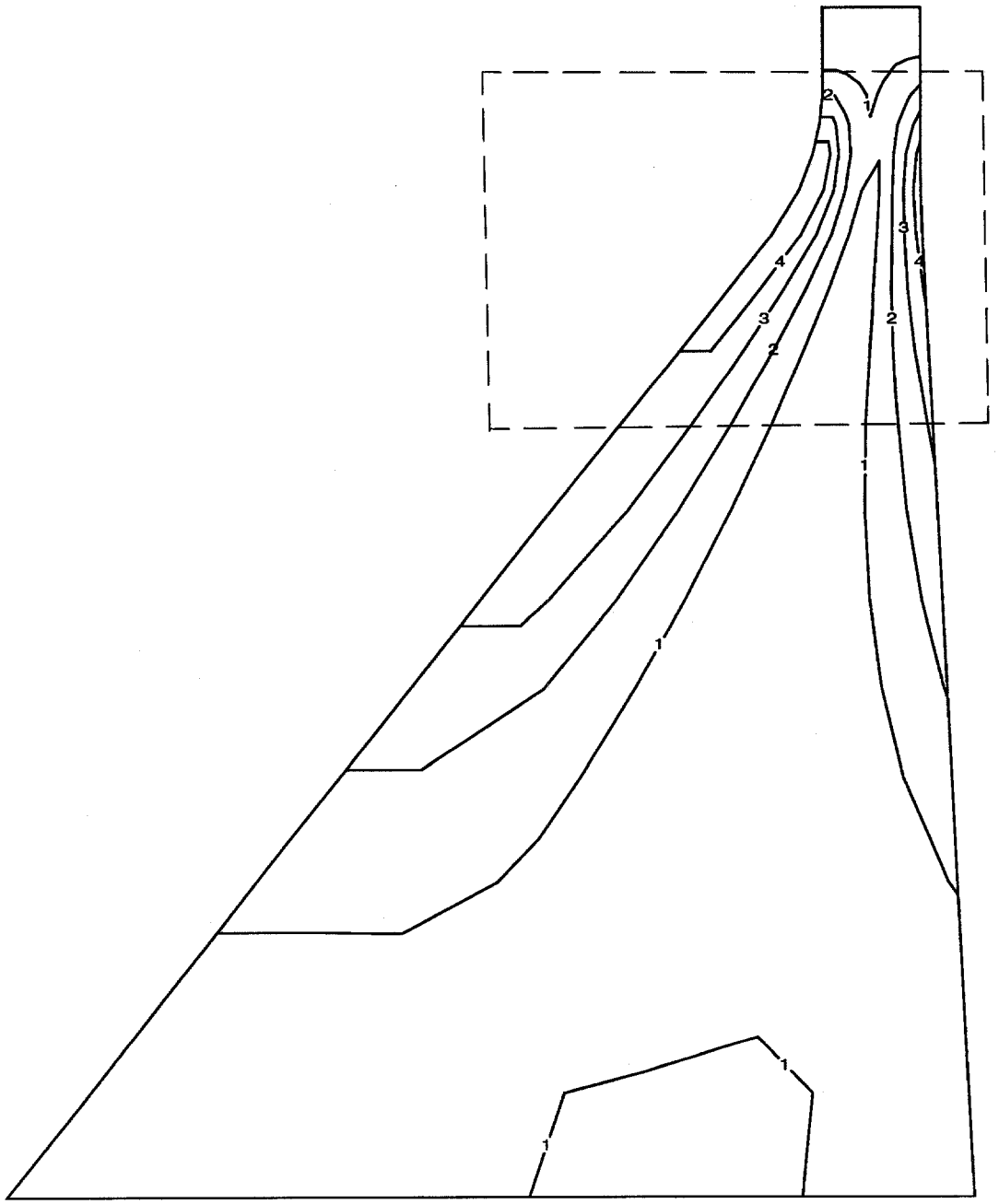

Figure 6c. Contours of maximum principal tensile stress (static plus dynamic). Stress vectors within the boxed region are shown in part d.

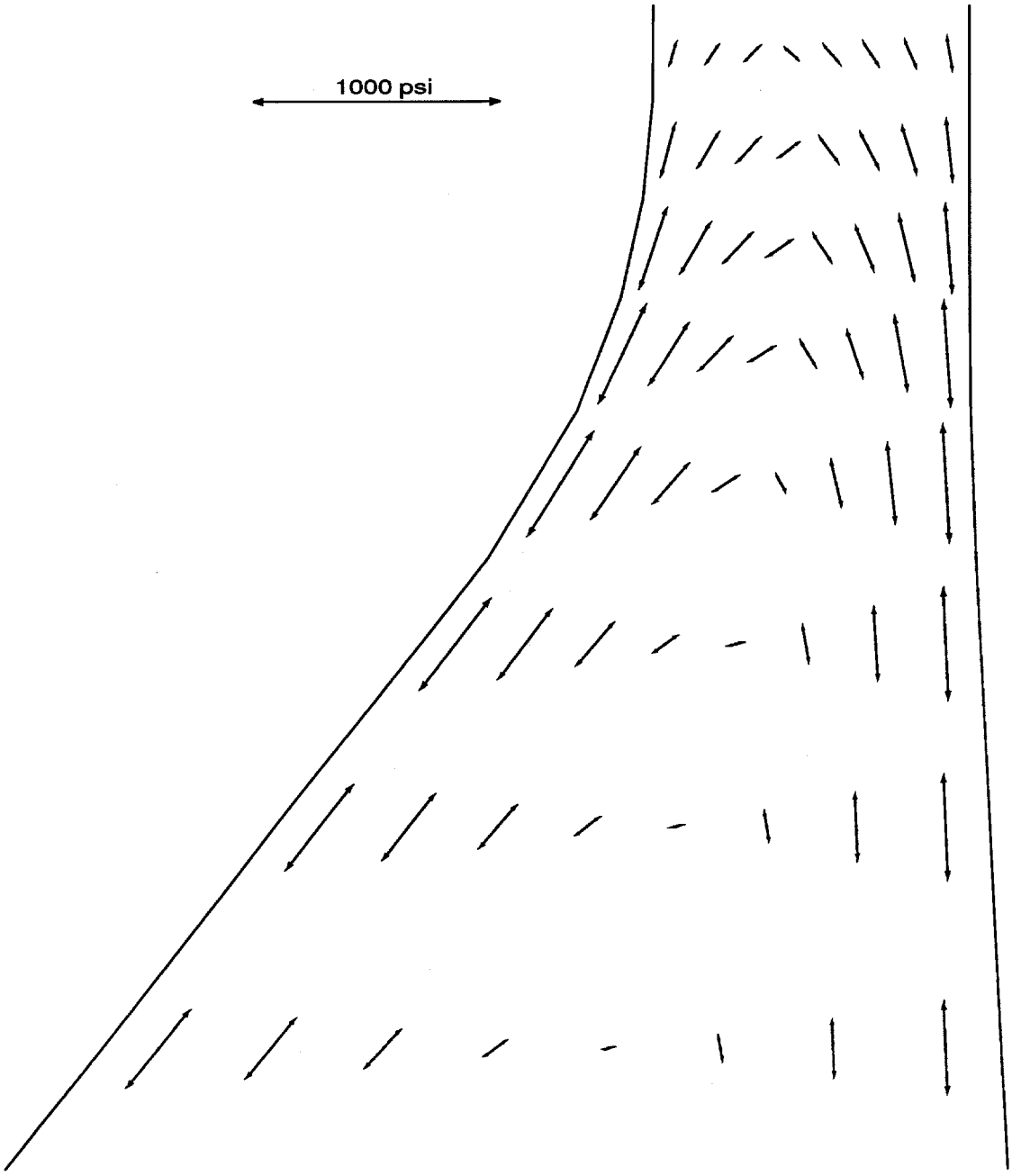

Figure 6d. Vectors of maximum principal tensile stress (static plus dynamic) in the neck region. See part c for region plotted.

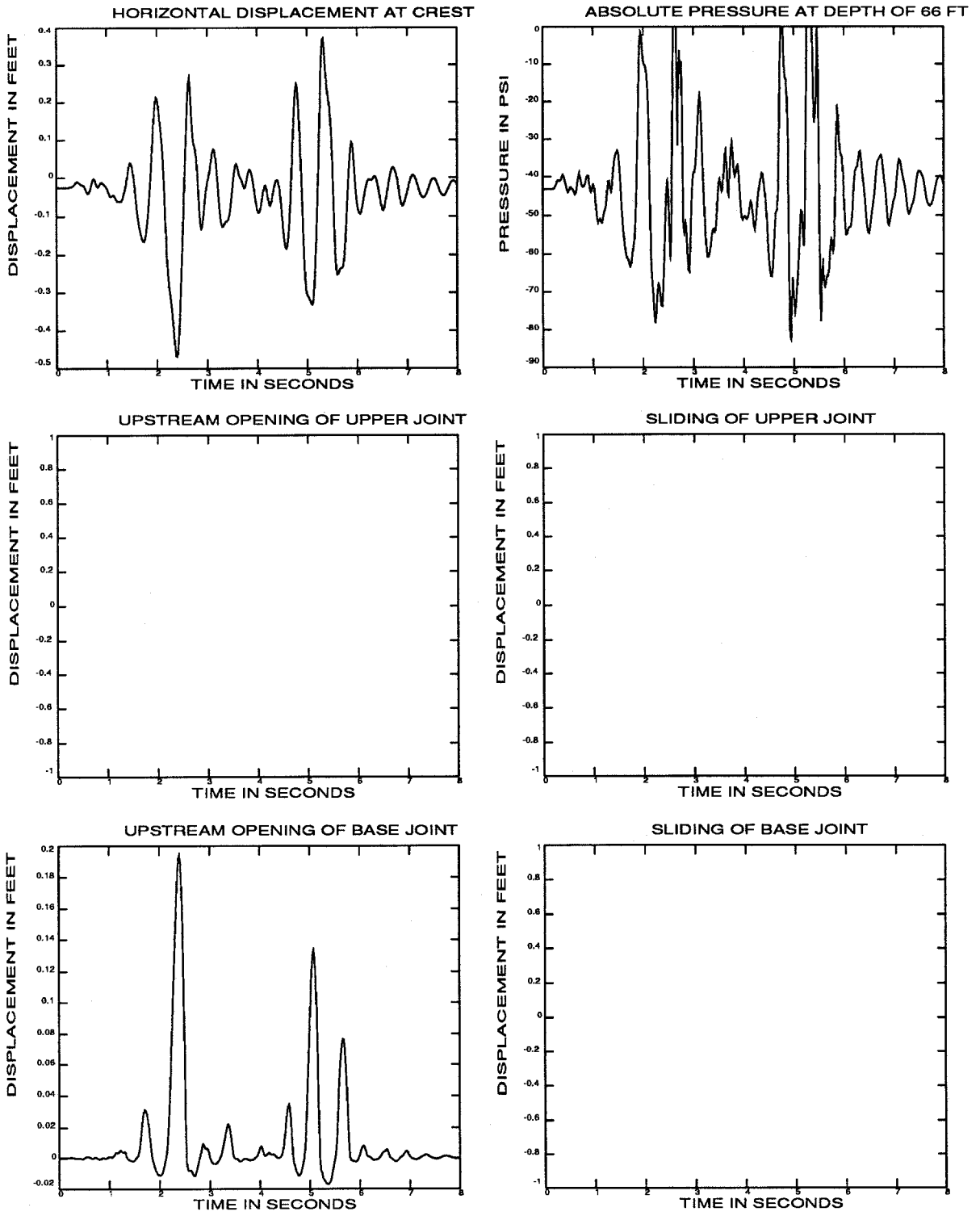

a. Time history reponses

Figure 7. Results of earthquake analysis of Pine Flat Dam with full reservoir and keyed base. The earthquake time scale equals one.

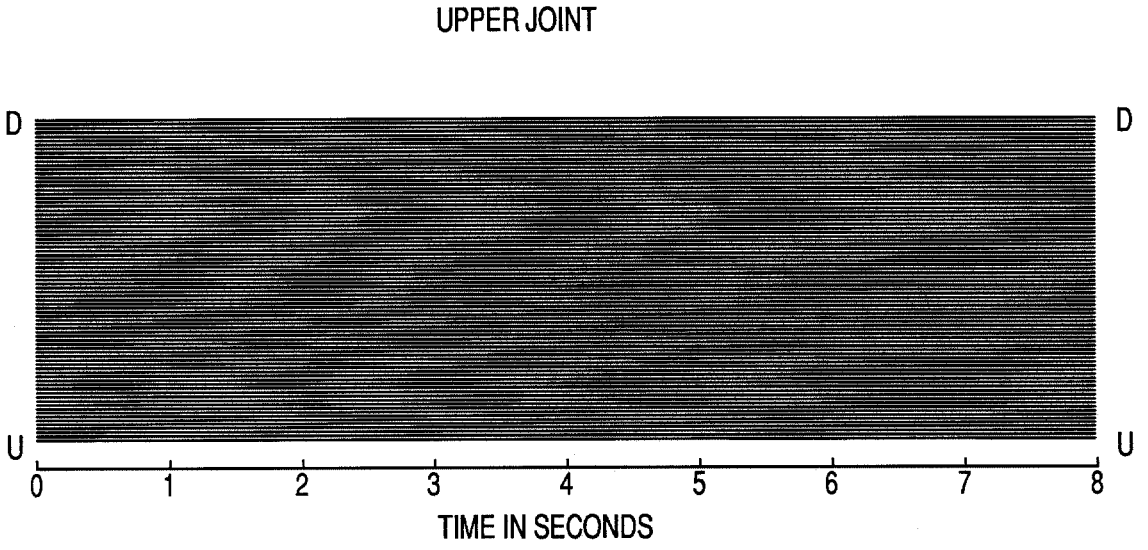

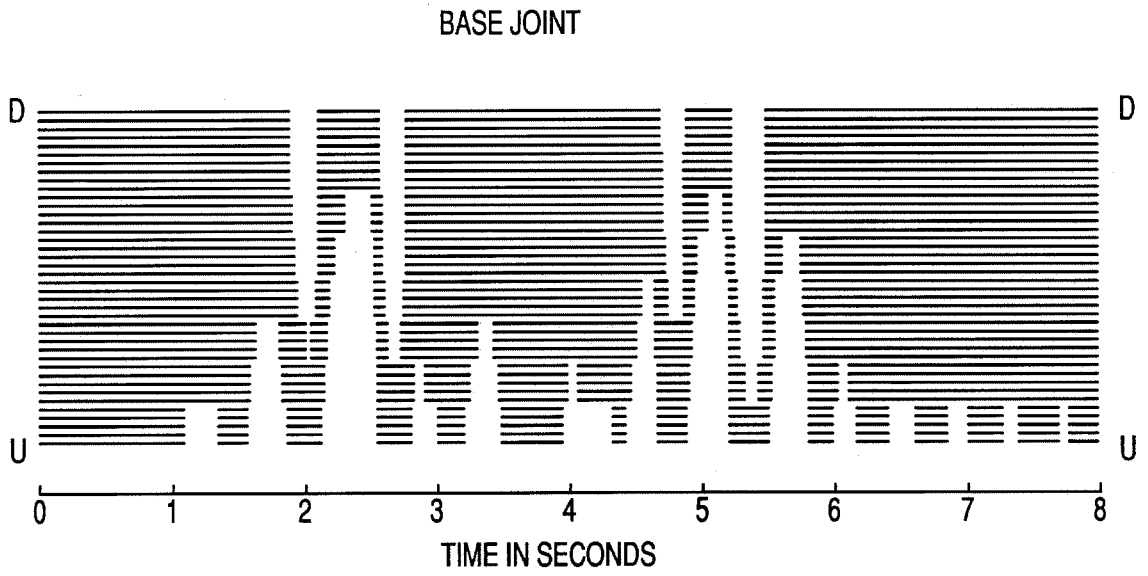

Figure 7b. Contact time histories of joints

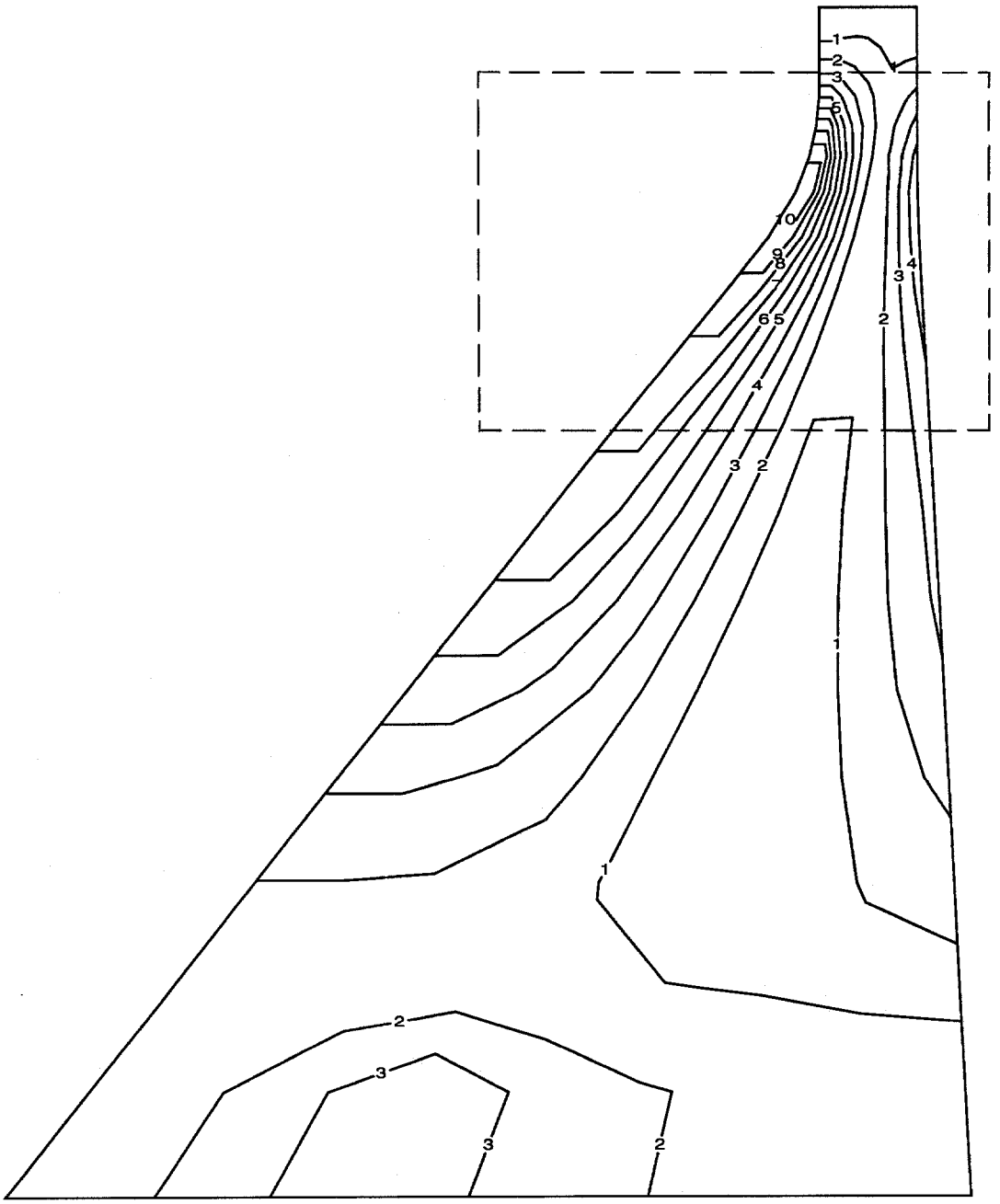

Figure 7c. Contours of maximum principal tensile stress (static plus dynamic). Stress vectors within the boxed region are shown in part d.

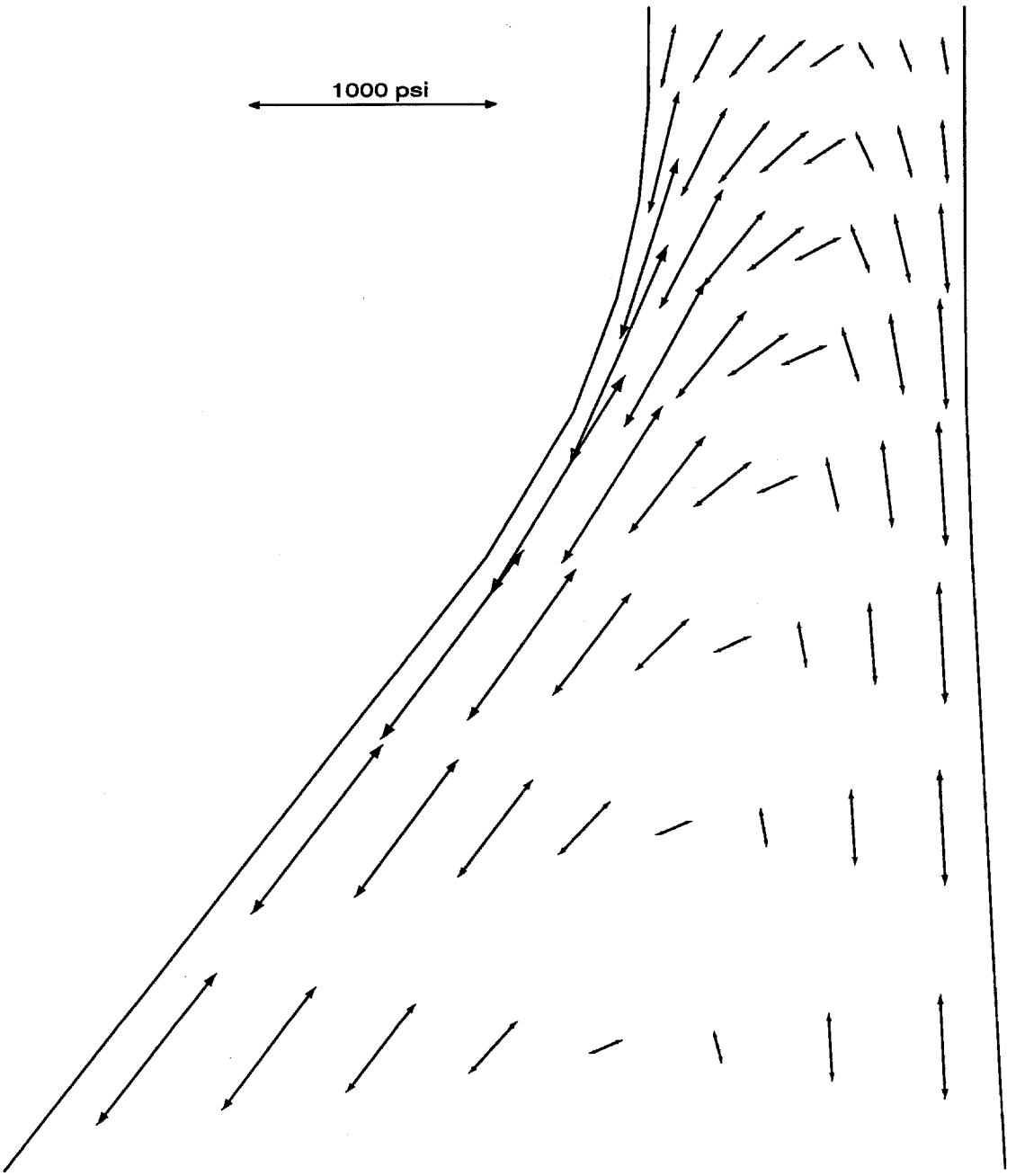

Figure 7d. Vectors of maximum principal tensile stress (static plus dynamic) in the neck region. See part c for region plotted.

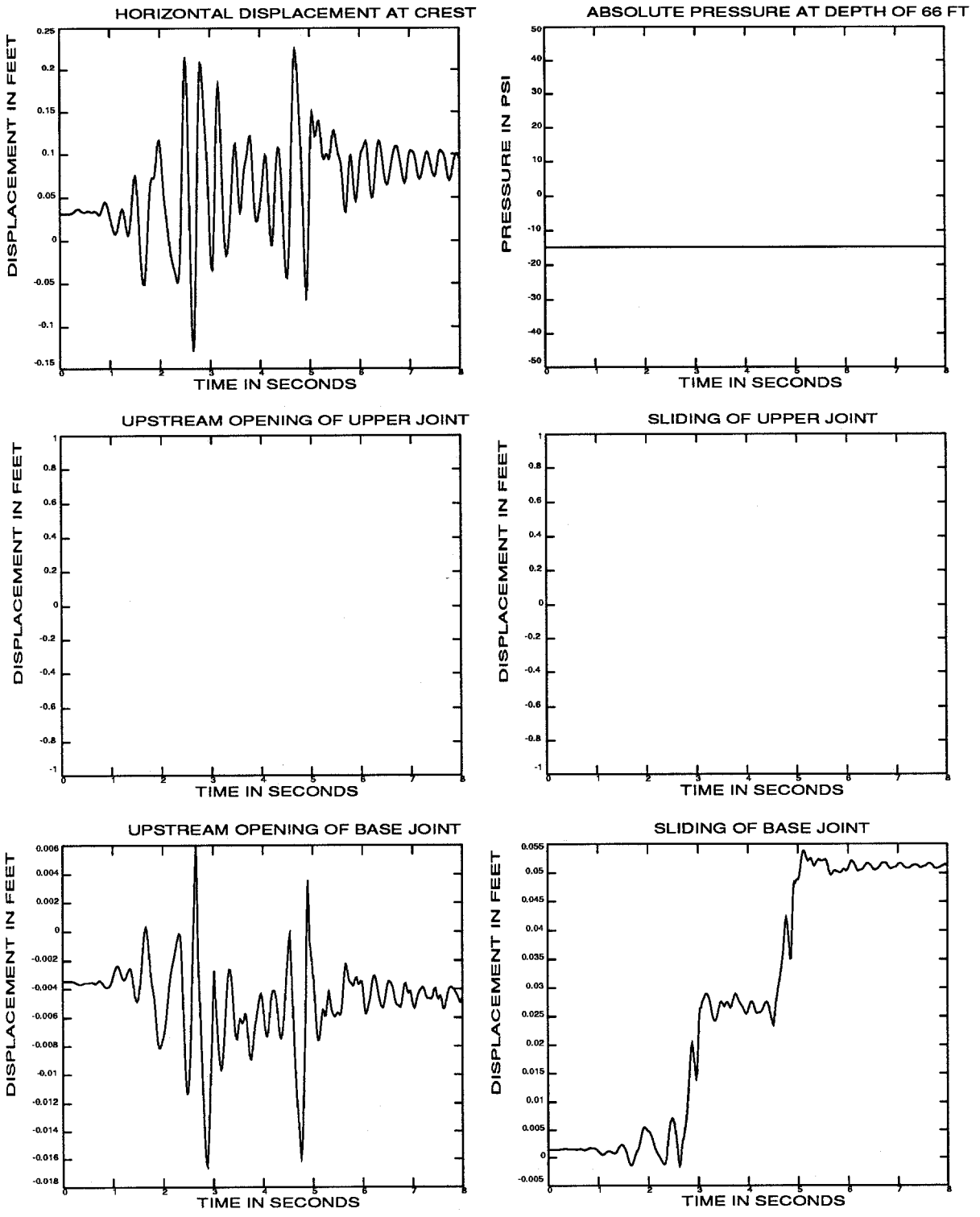

a. Time history reponses

Figure 8. Results of earthquake analysis of Pine Flat Dam with empty reservoir and unkeyed base. The earthquake time scale equals one.

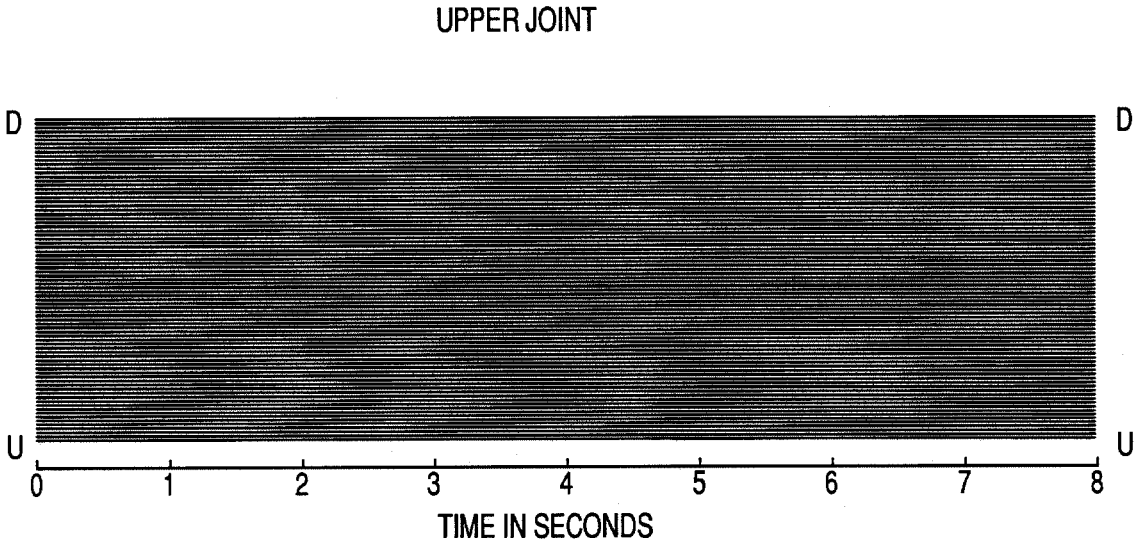

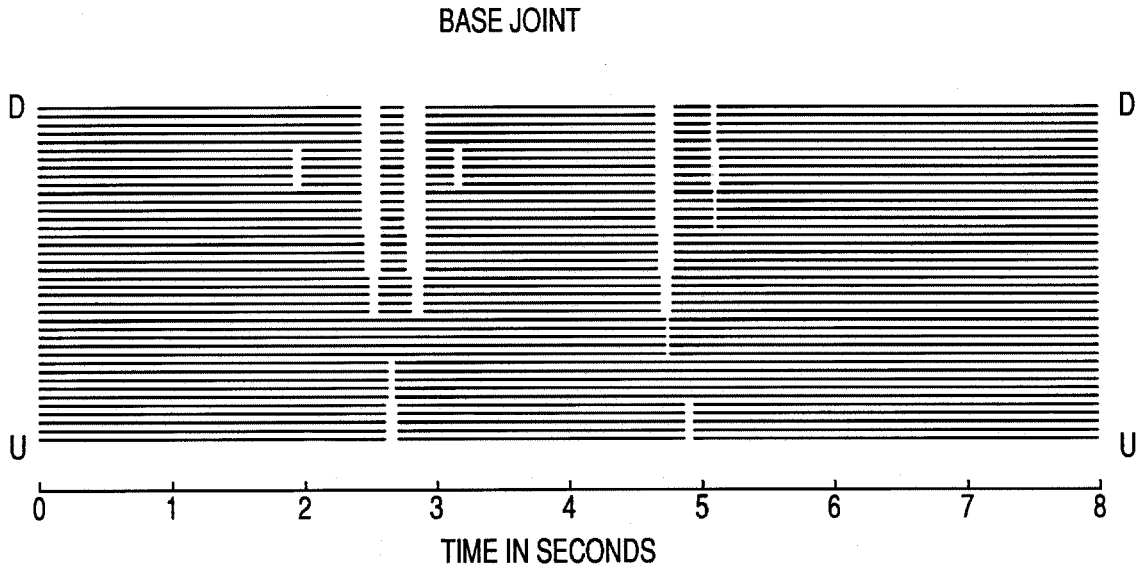

Figure 8b. Contact time histories of joints

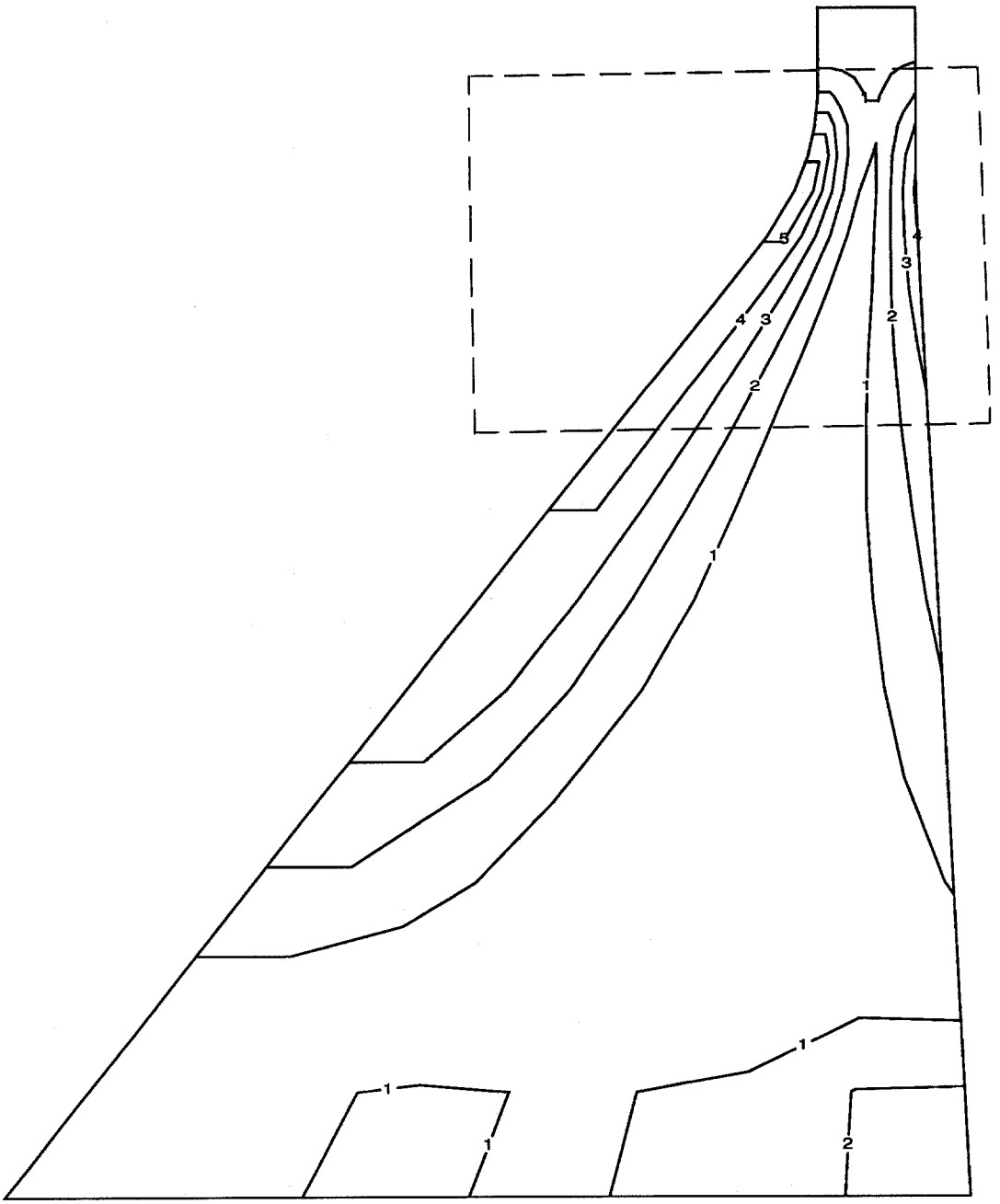

Figure 8c. Contours of maximum principal tensile stress (static plus dynamic). Stress vectors within the boxed region are shown in part d.

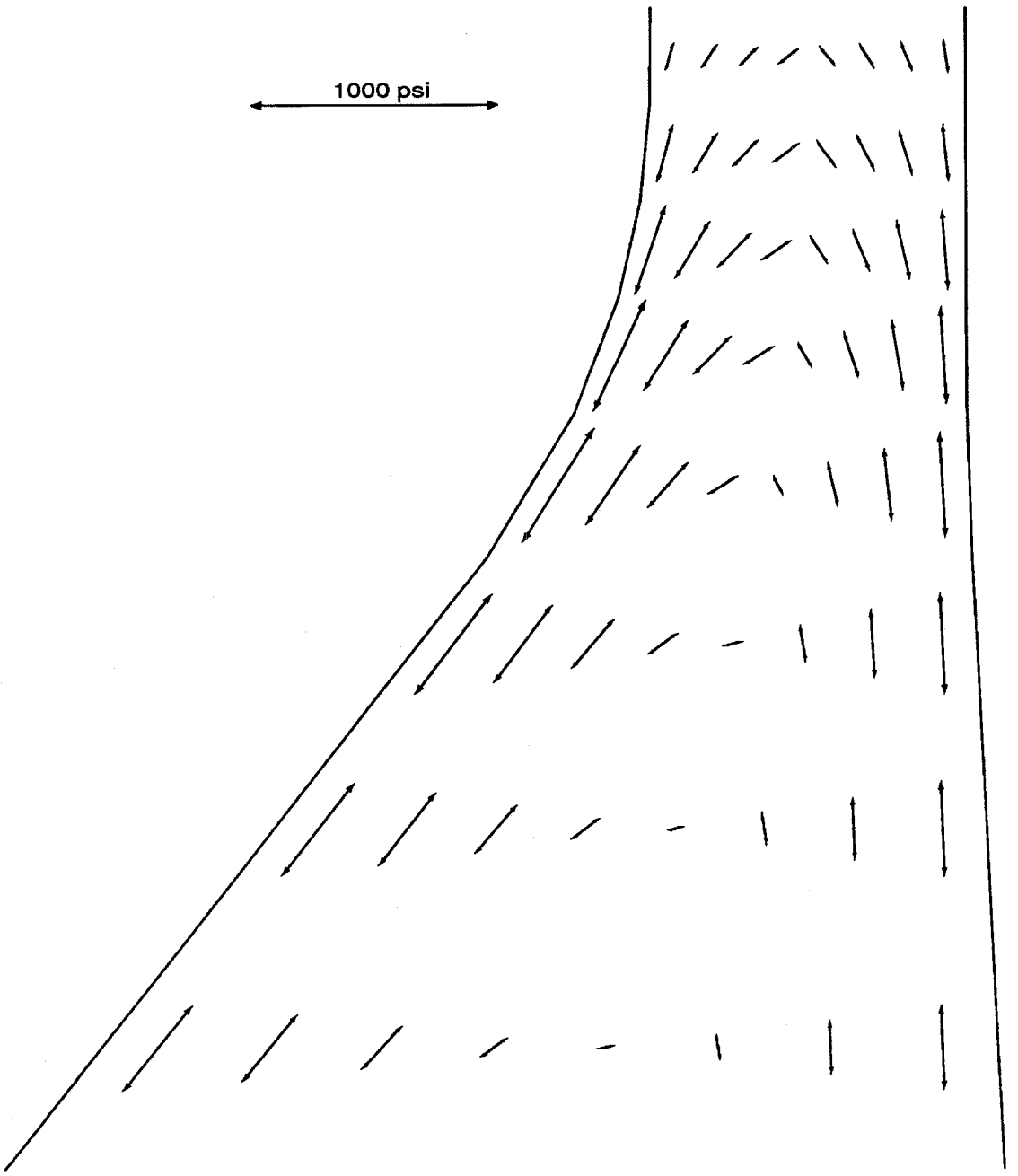

Figure 8d. Vectors of maximum principal tensile stress (static plus dynamic) in the neck region. See part c for region plotted.

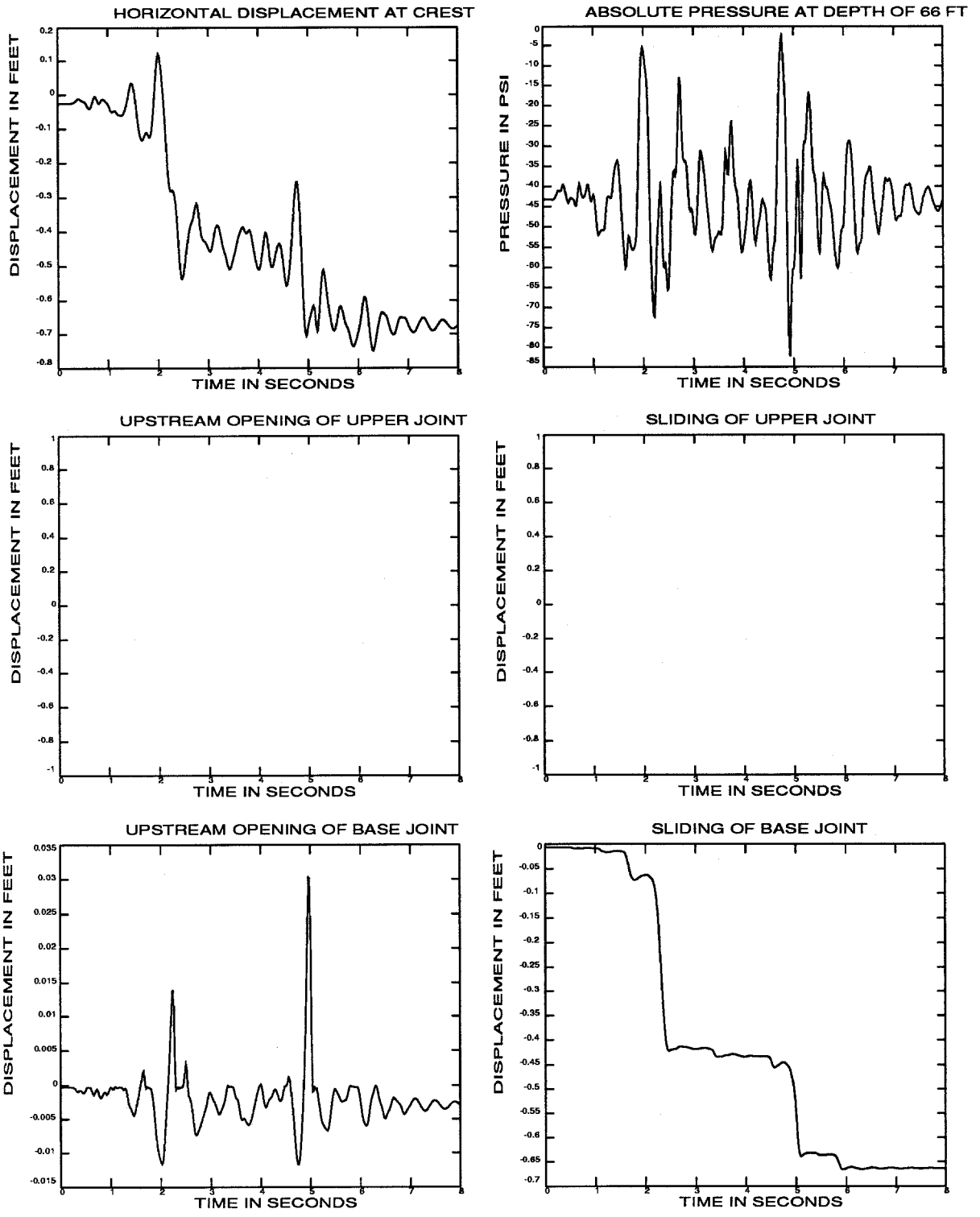

a. Time history reponses

Figure 9. Results of earthquake analysis of Pine Flat Dam with full reservoir and unkeyed base. The earthquake time scale equals one.

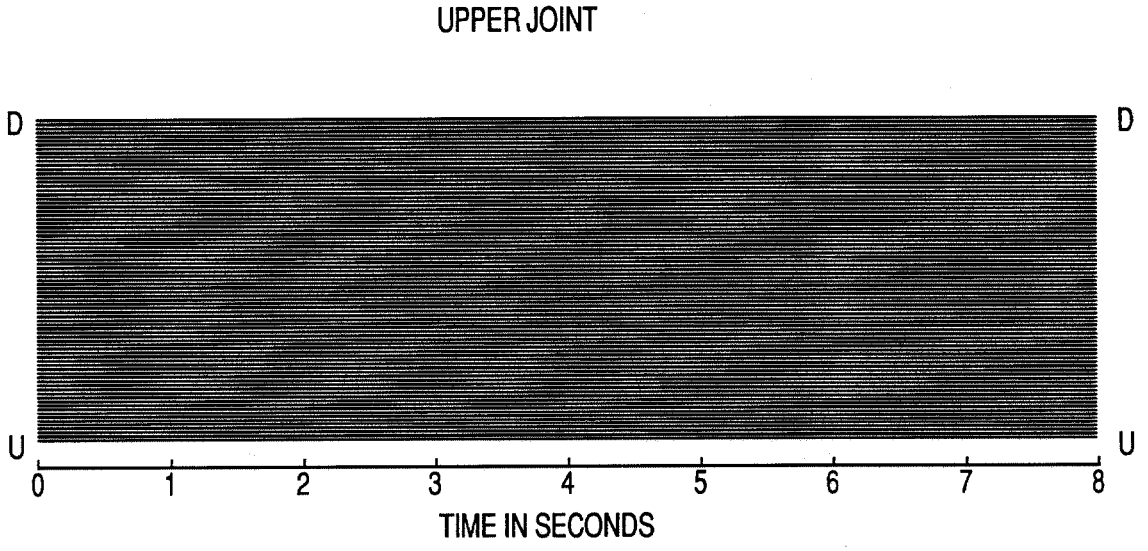

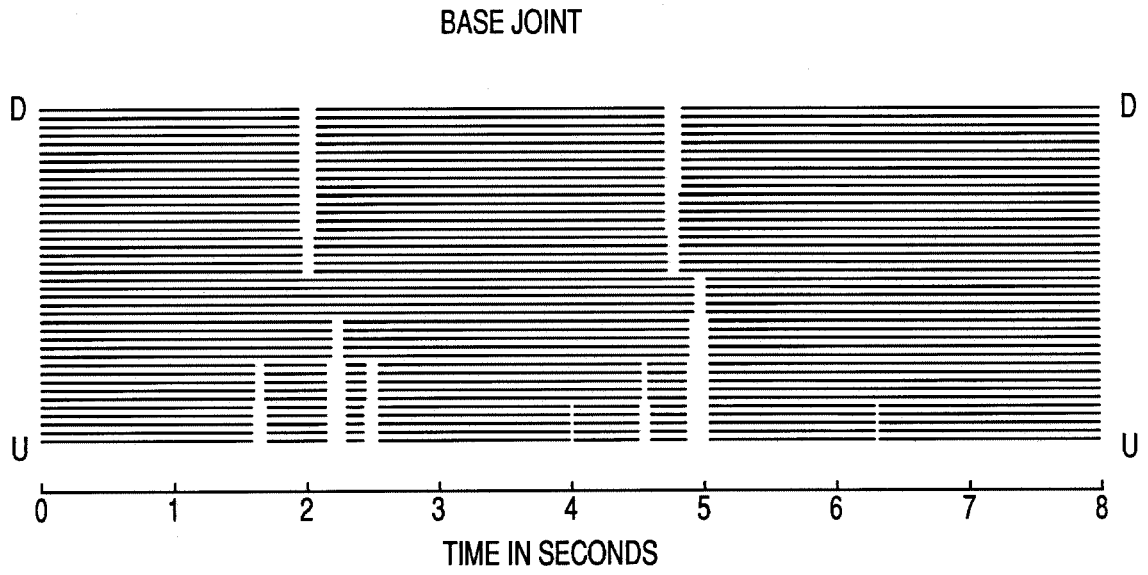

Figure 9b. Contact time histories of joints

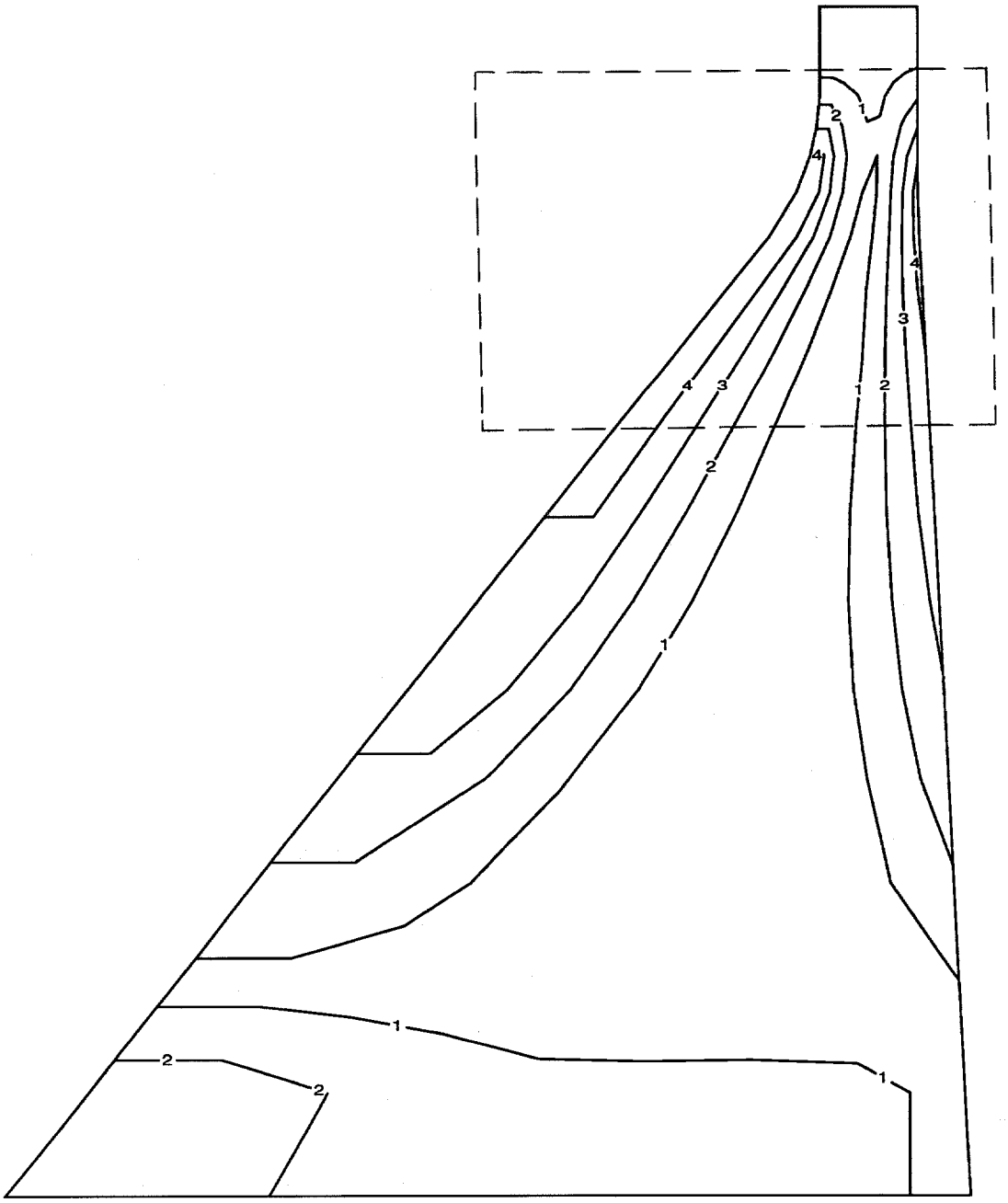

Figure 9c. Contours of maximum principal tensile stress (static plus dynamic). Stress vectors within the boxed region are shown in part d.

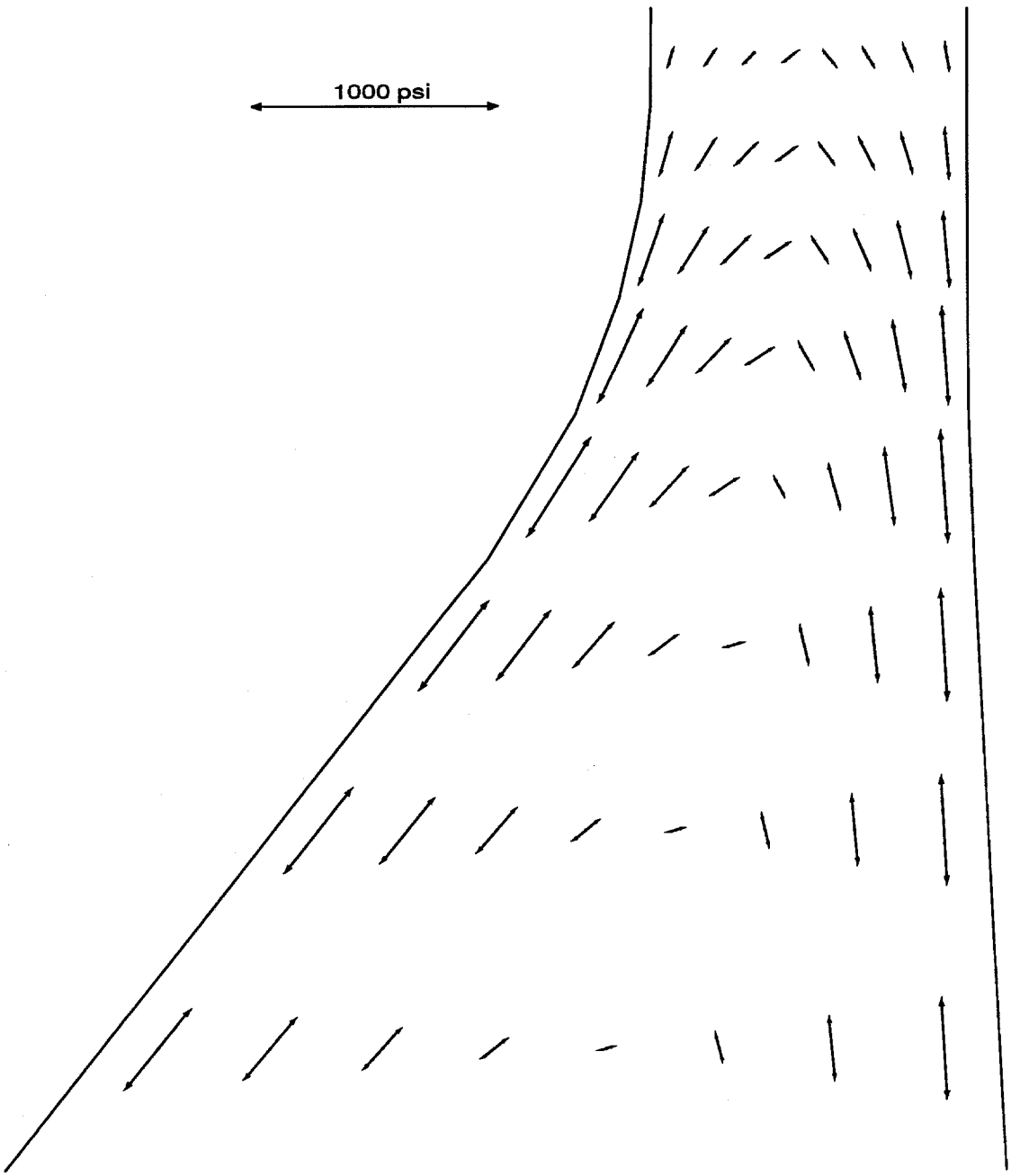

Figure 9d. Vectors of maximum principal tensile stress (static plus dynamic) in the neck region. See part c for region plotted.

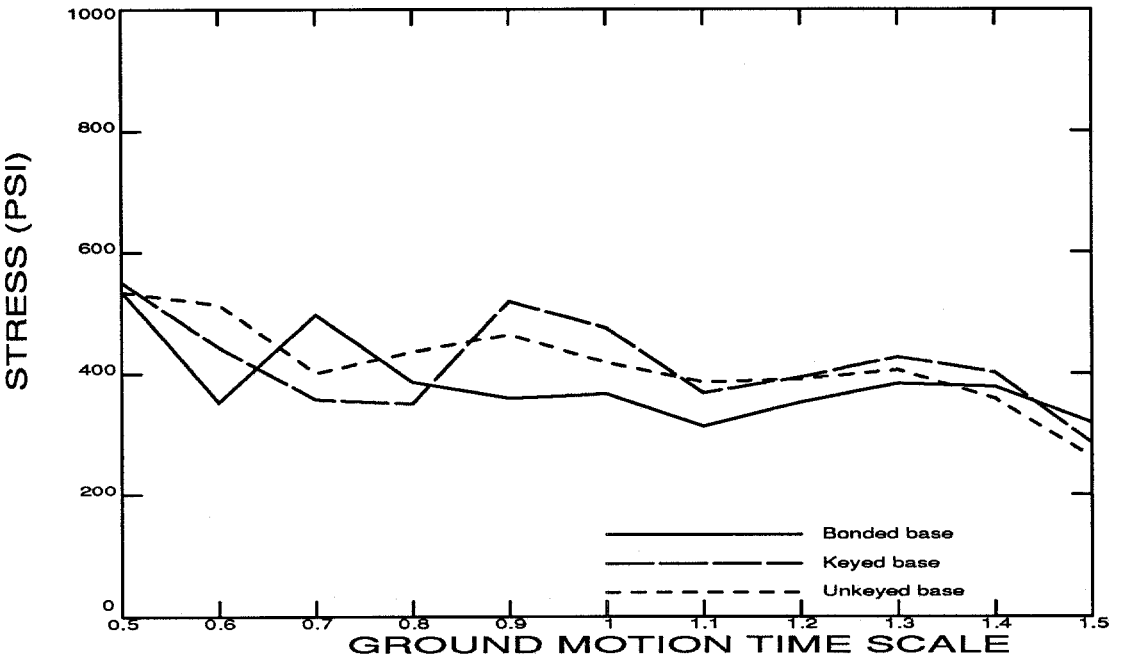

a. Upstream face

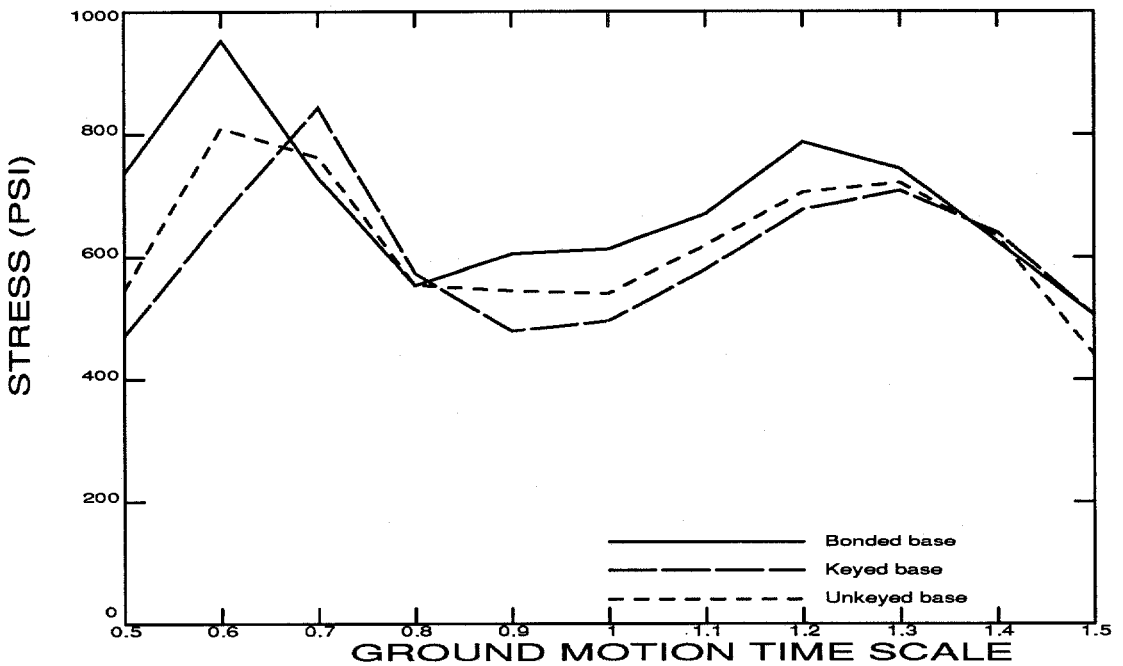

b. Downstream face

Figure 10. Maximum principal tensile stresses (static plus dynamic) as a function of ground motion time scale that occur at the faces of Pine Flat Dam with empty reservoir except that the stresses which occur at the stress concentrations at the base (bonded dam) are not included.

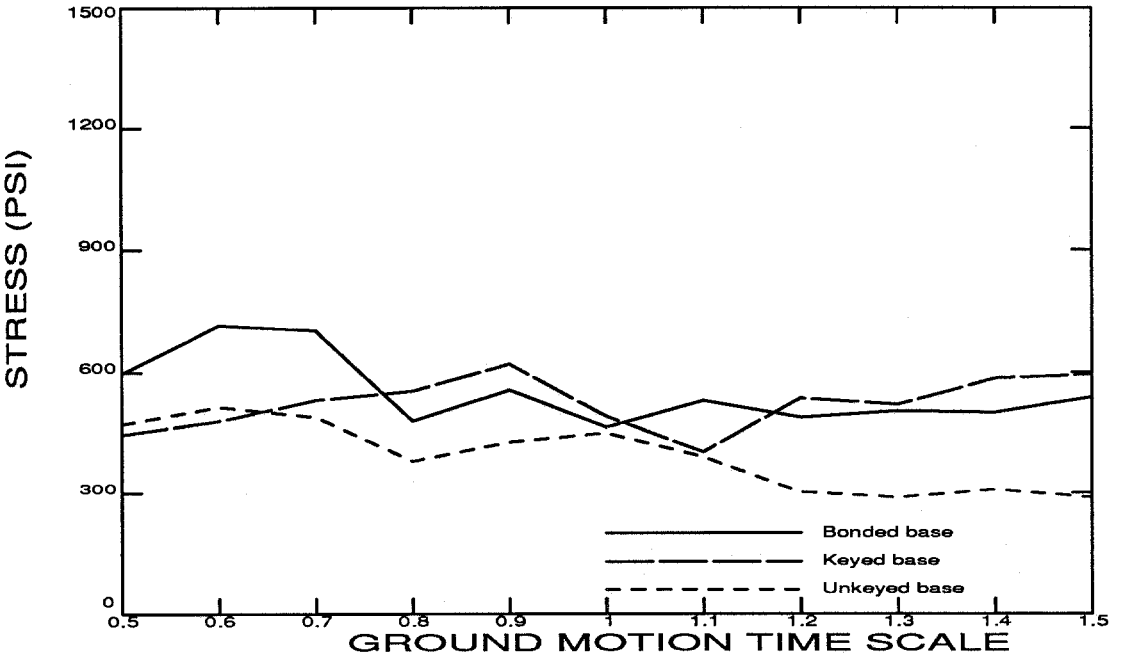

a. Upstream face

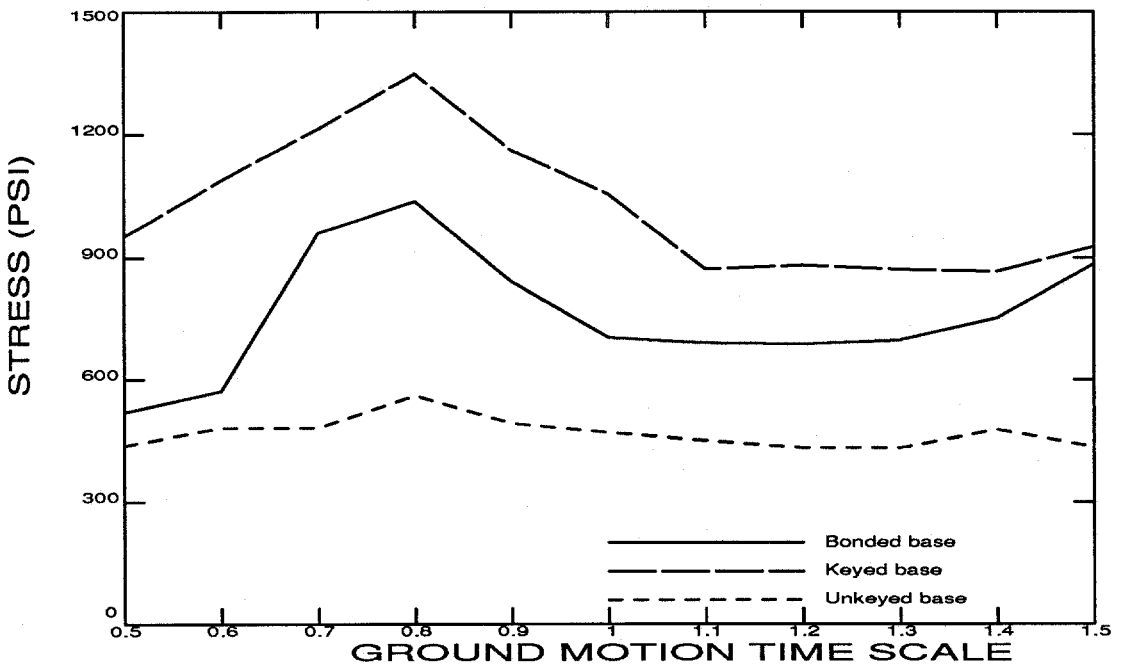

b. Downstream face

Figure 11. Maximum principal tensile stresses (static plus dynamic) as a function of ground motion time scale that occur at the faces of Pine Flat Dam with full reservoir except that the stresses which occur at the stress concentrations at the base (bonded dam) are not included.

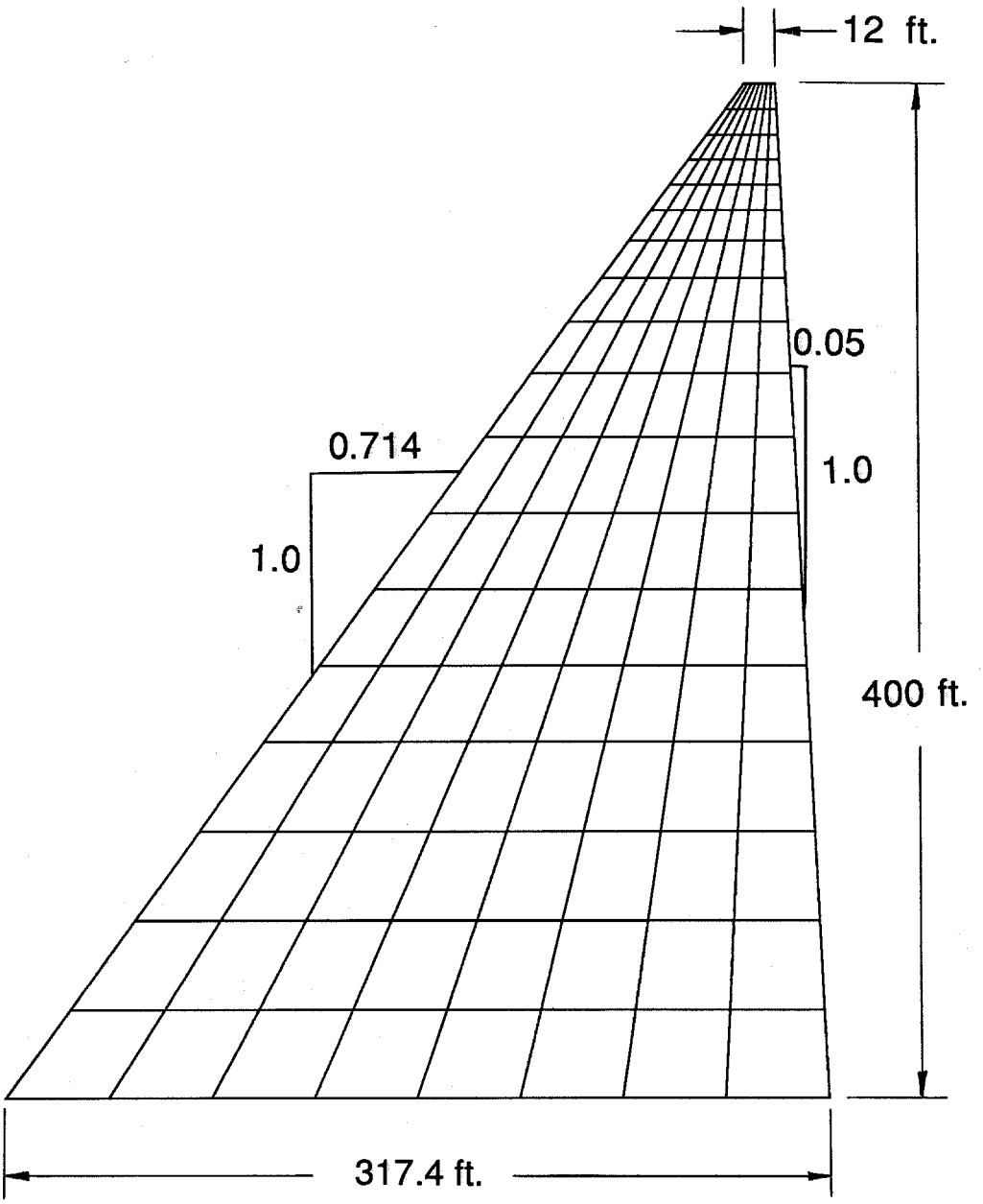

Figure 12. Geometry and finite element mesh for the straight-sided dam.

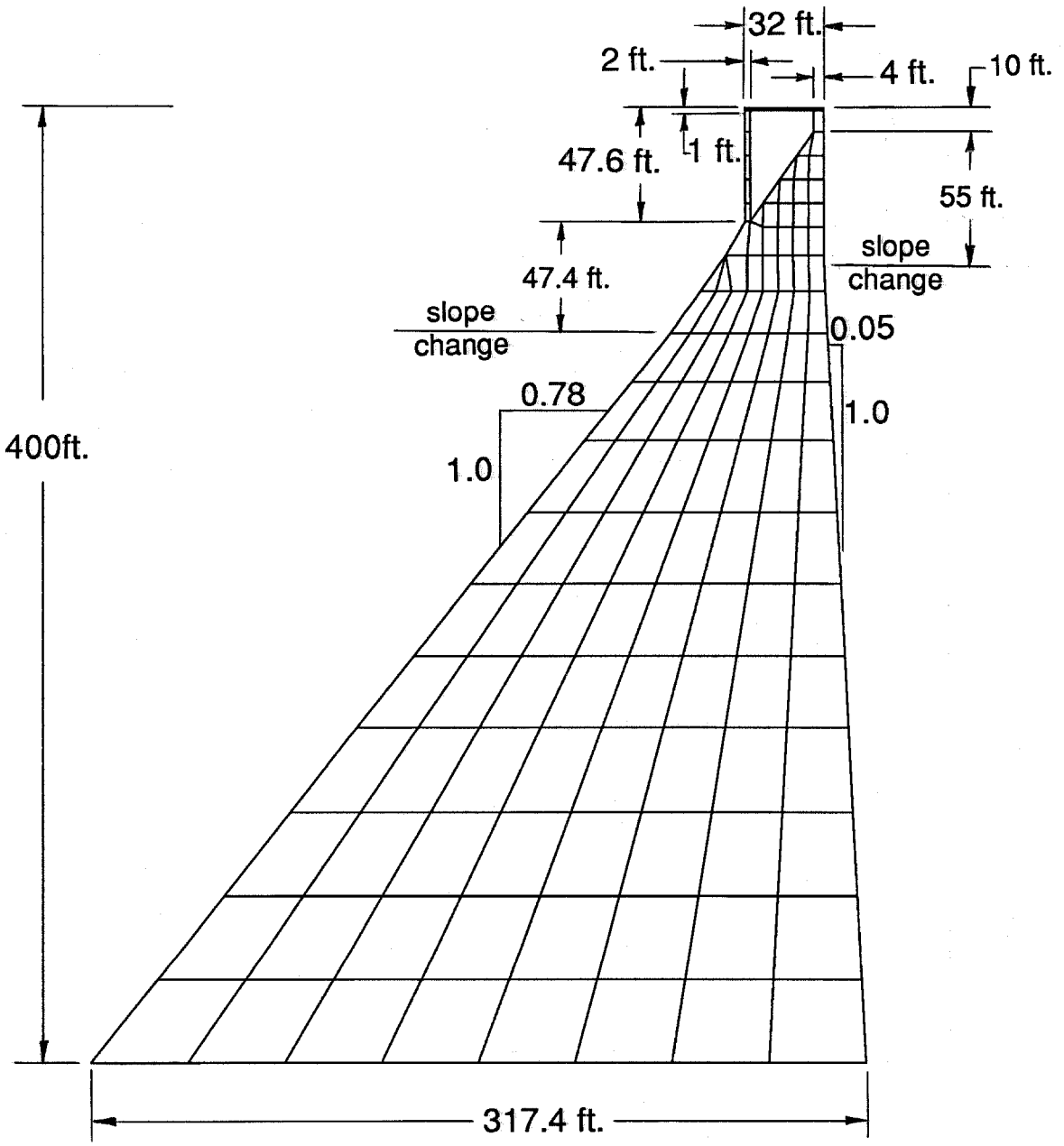

Figure 13. Geometry and finite element mesh for the dam with a light-weight crest. The geometry below the crest section and the profile of the upstream face are similar to the 400 ft high monolith of Pine Flat Dam.

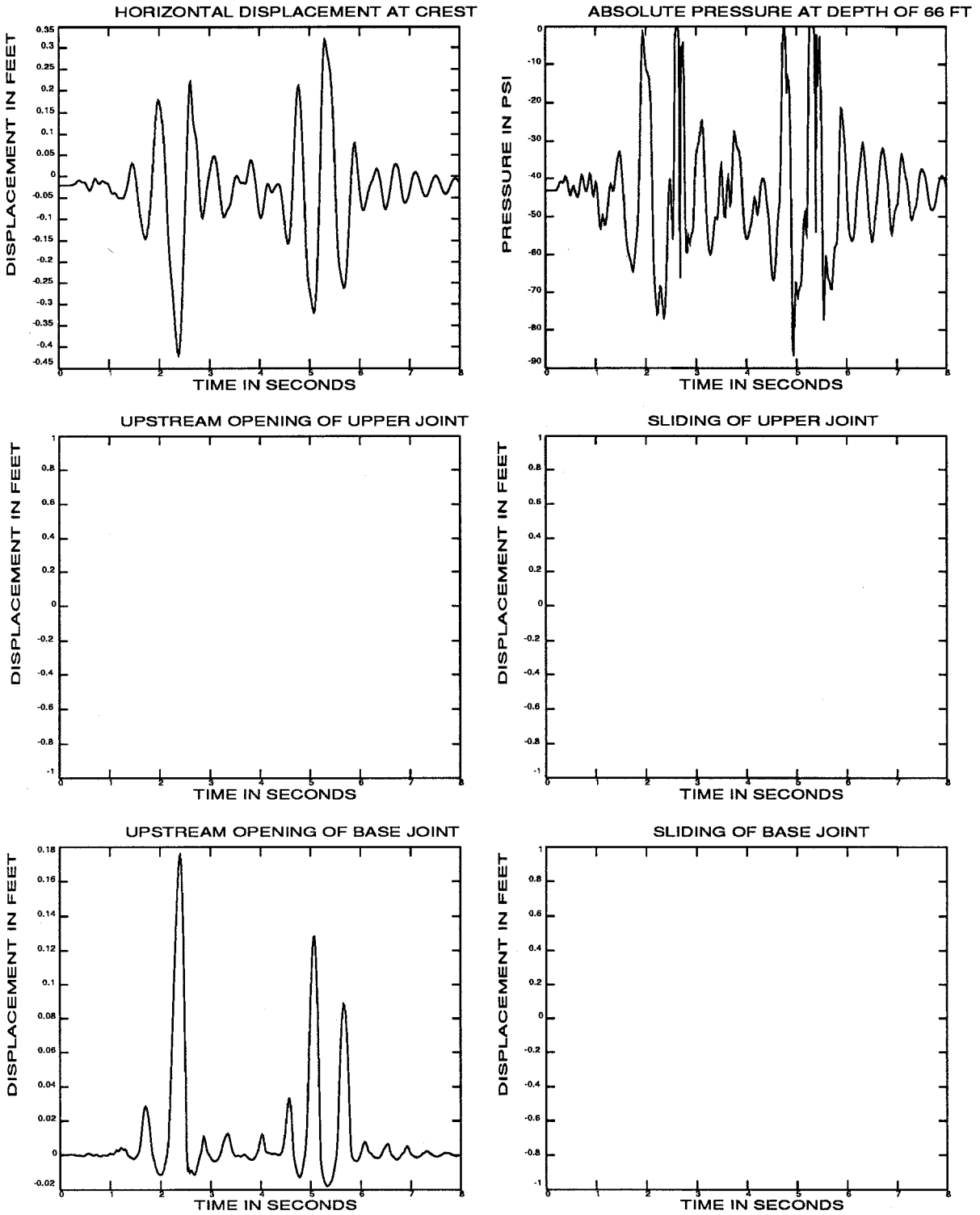

a. Time history responses

Figure 14. Results of earthquake analysis of the straight-sided dam with full reservoir and keyed base. The earthquake time scale equals one.

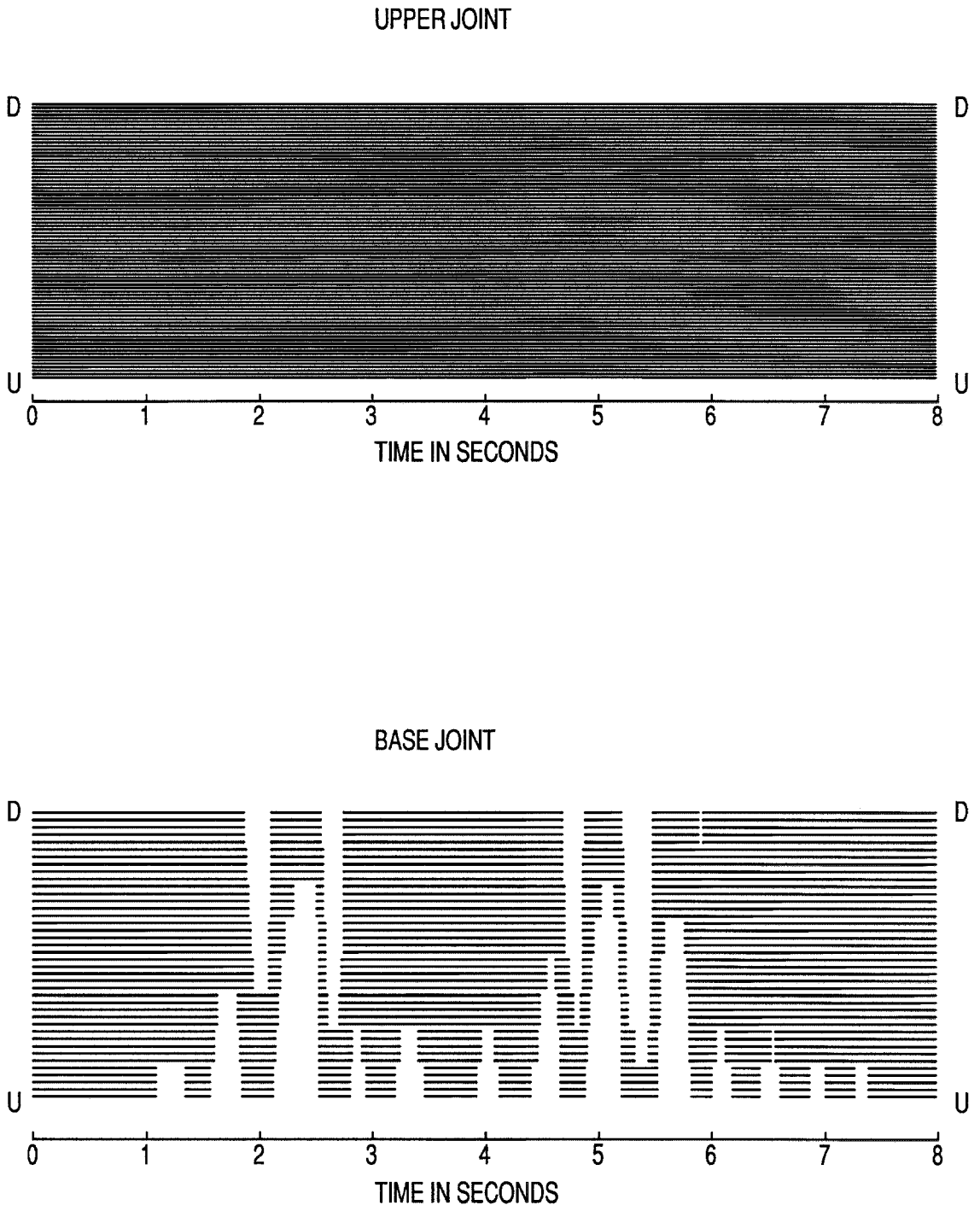

Figure 14b. Contact time histories of joints

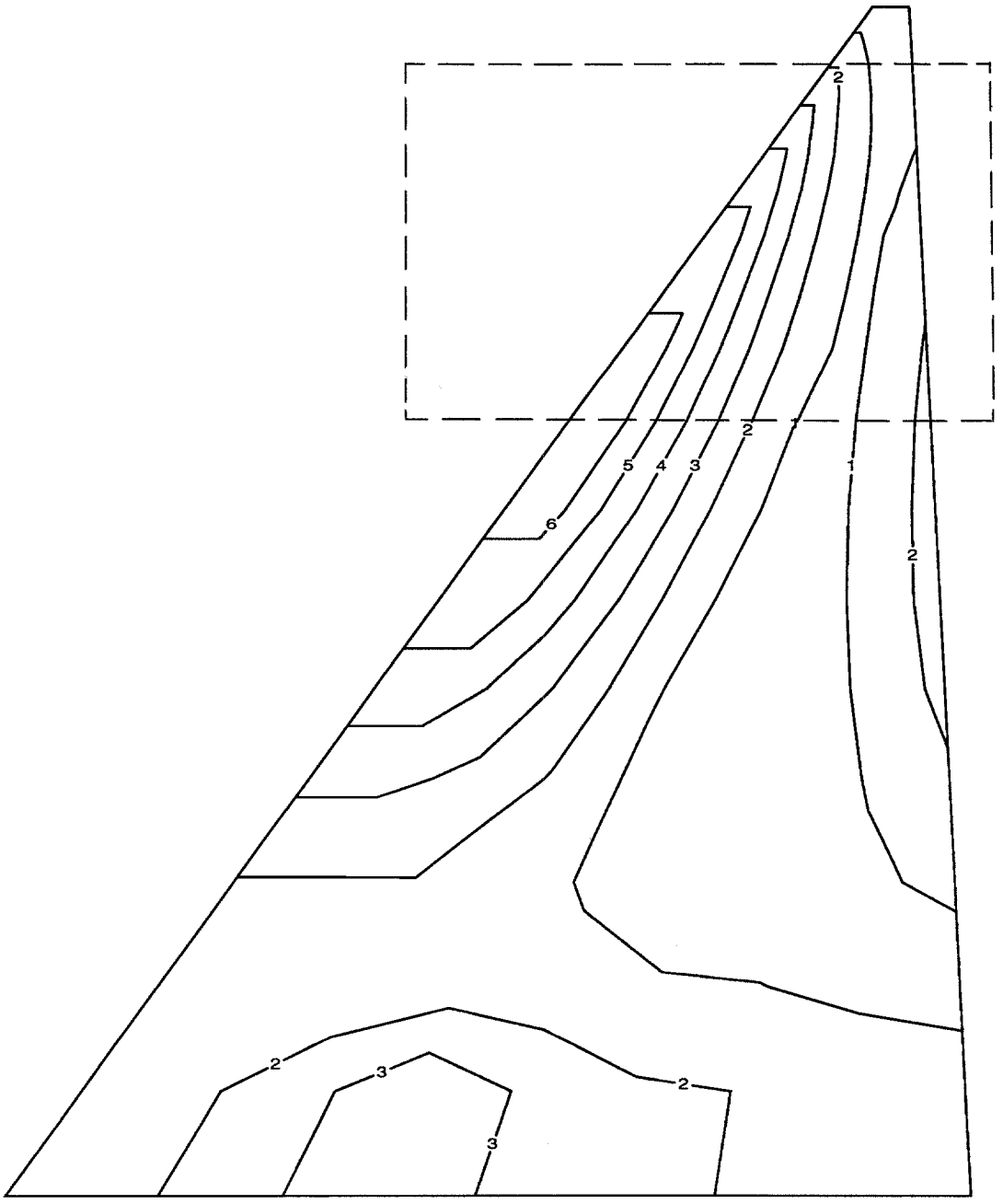

Figure 14c. Contours of maximum principal tensile stress (static plus dynamic). Stress vectors within the boxed region are shown in part d.

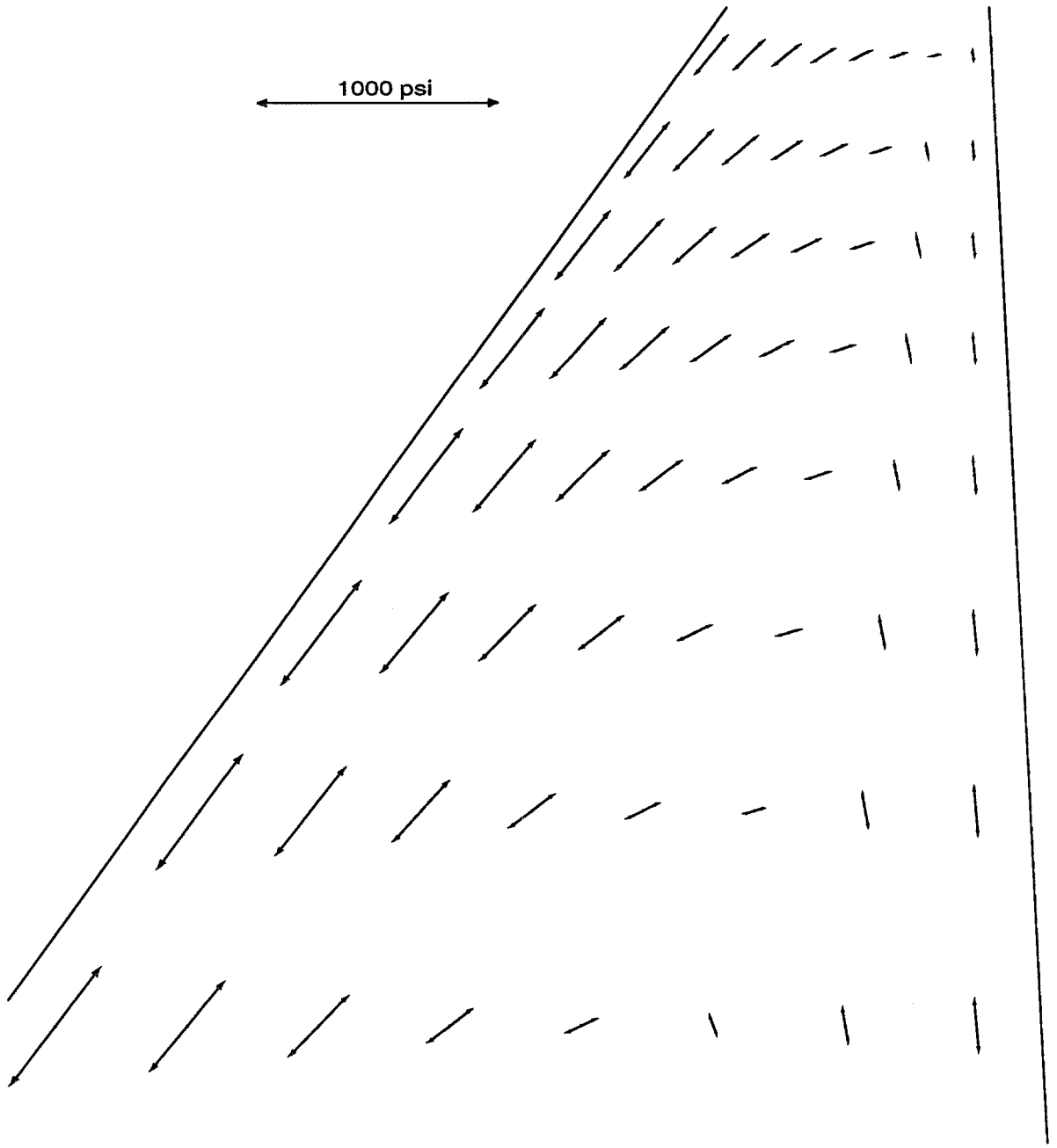

Figure 14d. Vectors of maximum principal tensile stress (static plus dynamic) in the neck region. See part c for region plotted.

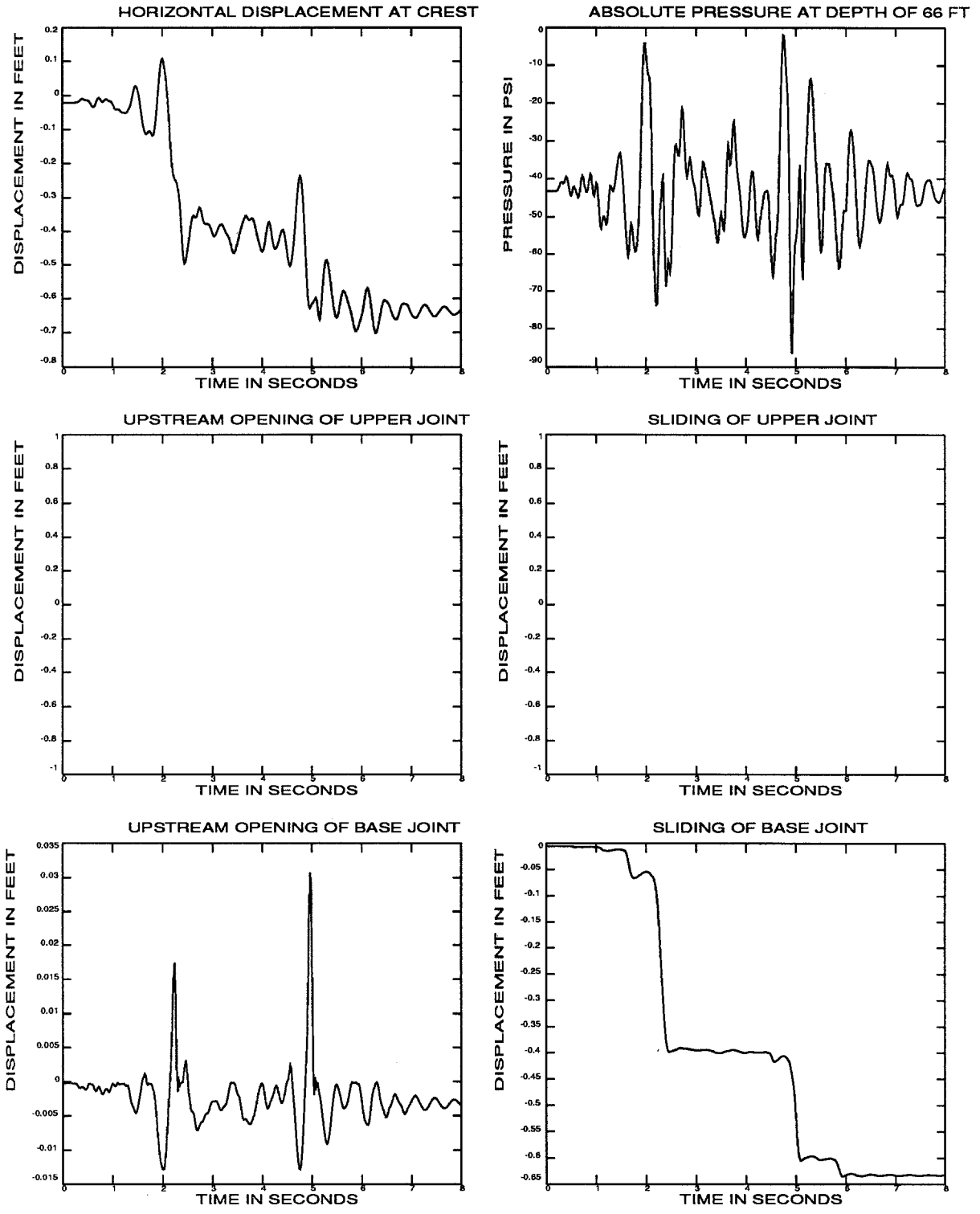

a. Time history responses

Figure 15. Results of earthquake analysis of the straight-sided dam with full reservoir and unkeyed base. The earthquake time scale equals one.

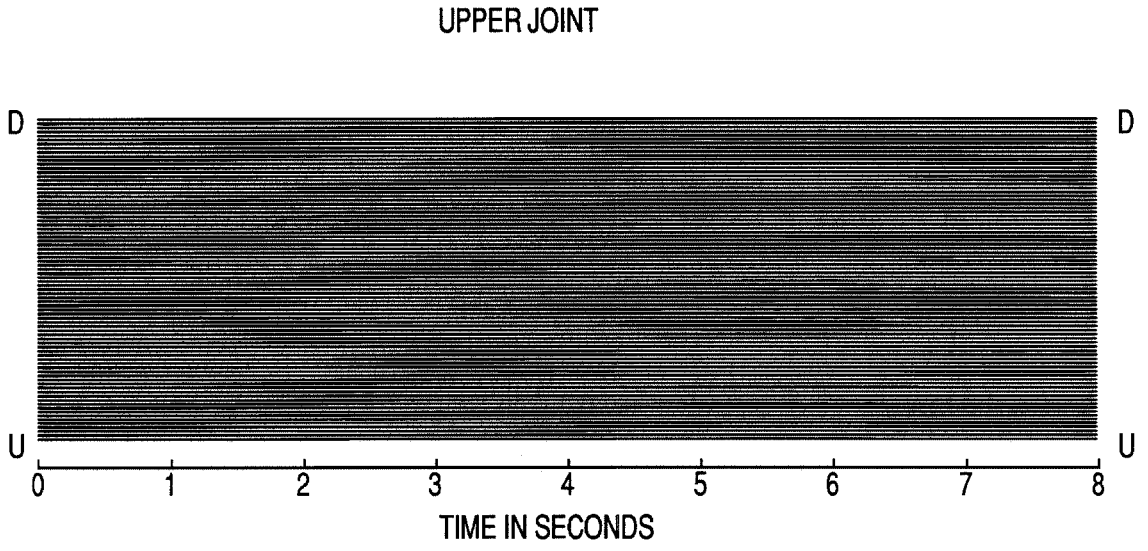

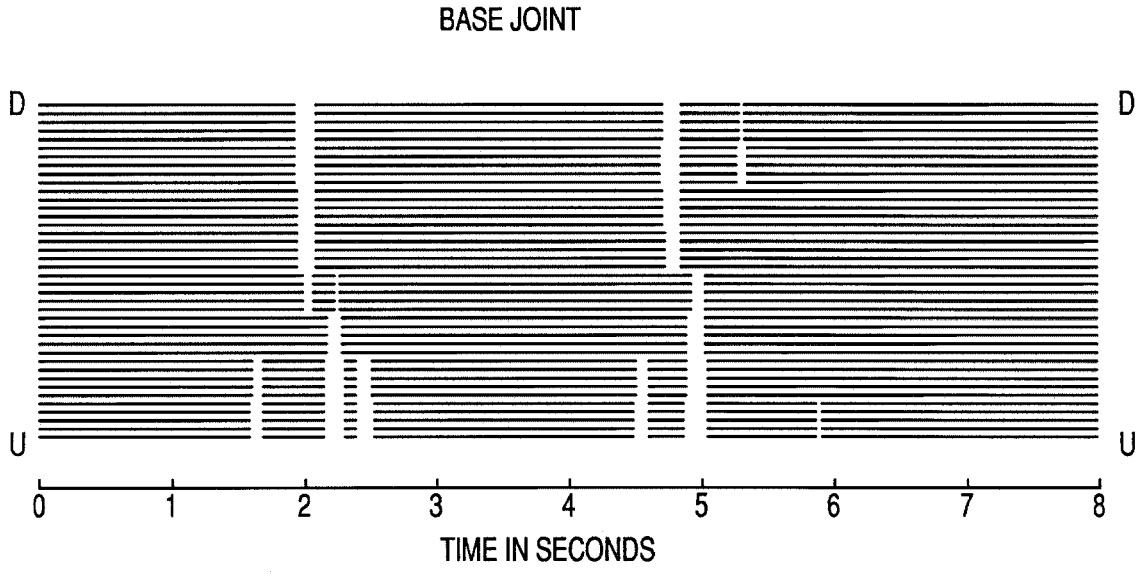

Figure 15b. Contact time histories of joints

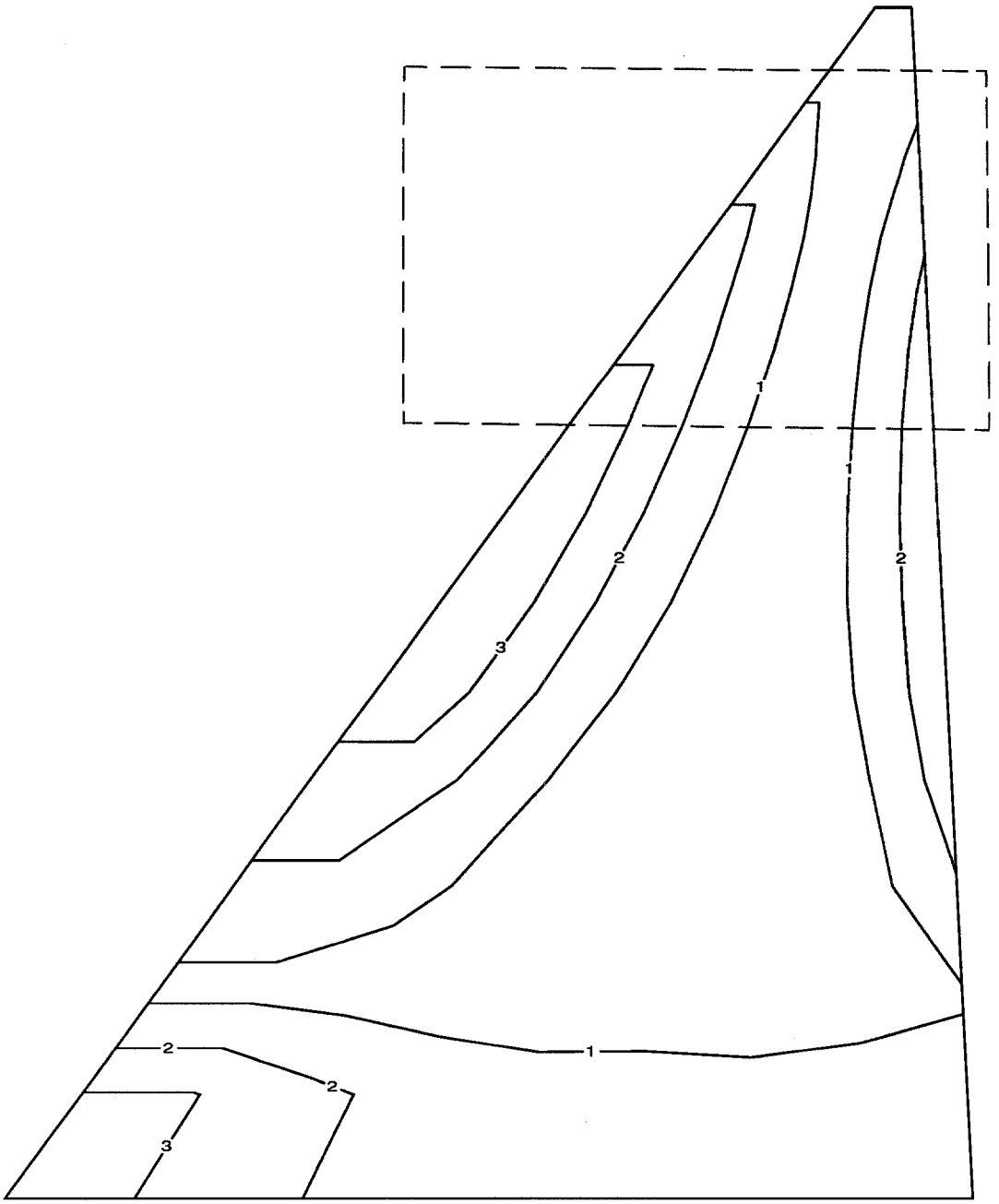

Figure 15c. Contours of maximum principal tensile stress (static plus dynamic). Stress vectors within the boxed region are shown in part d.

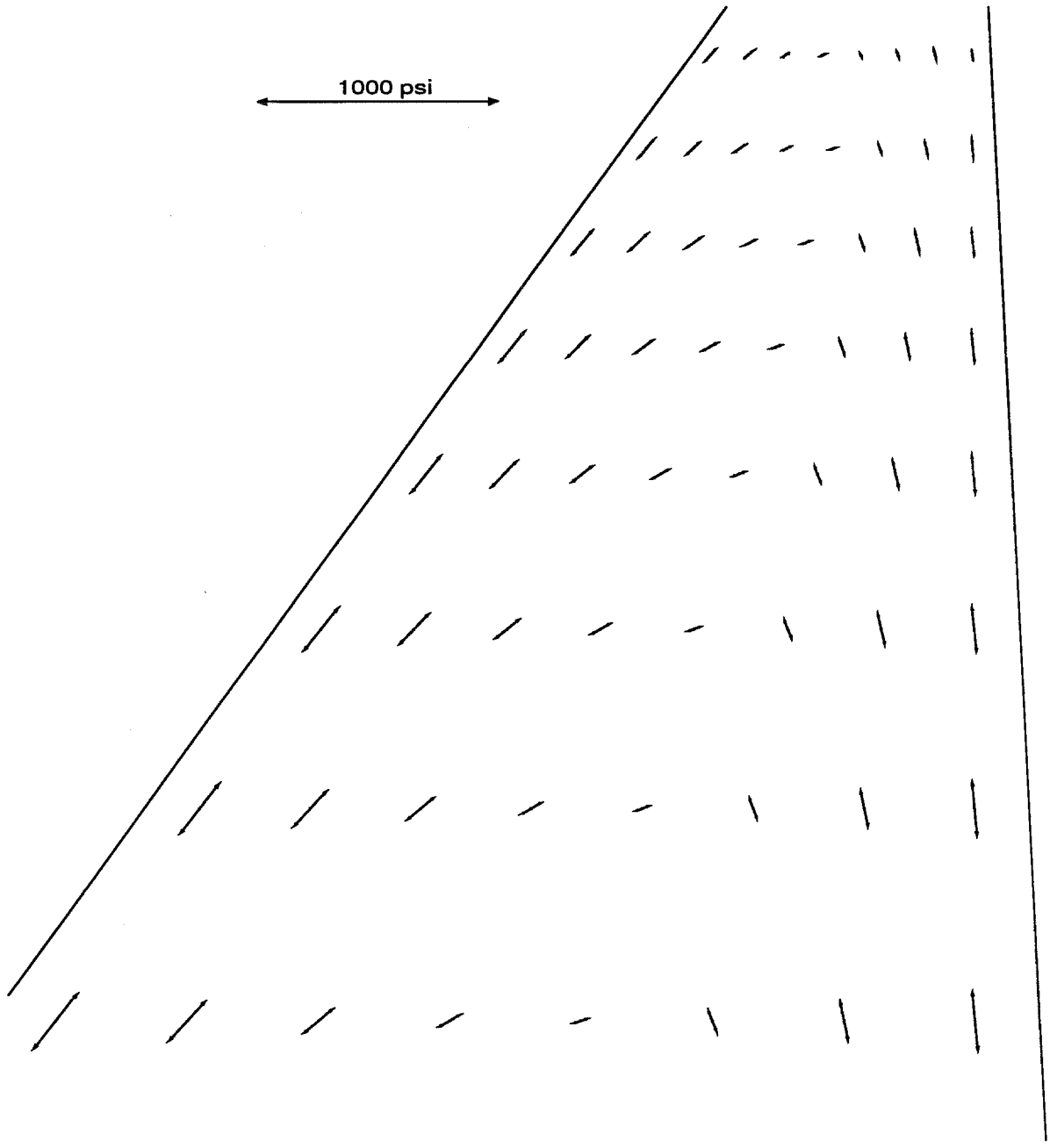

Figure 15d. Vectors of maximum principal tensile stress (static plus dynamic) in the neck region. See part c for region plotted.

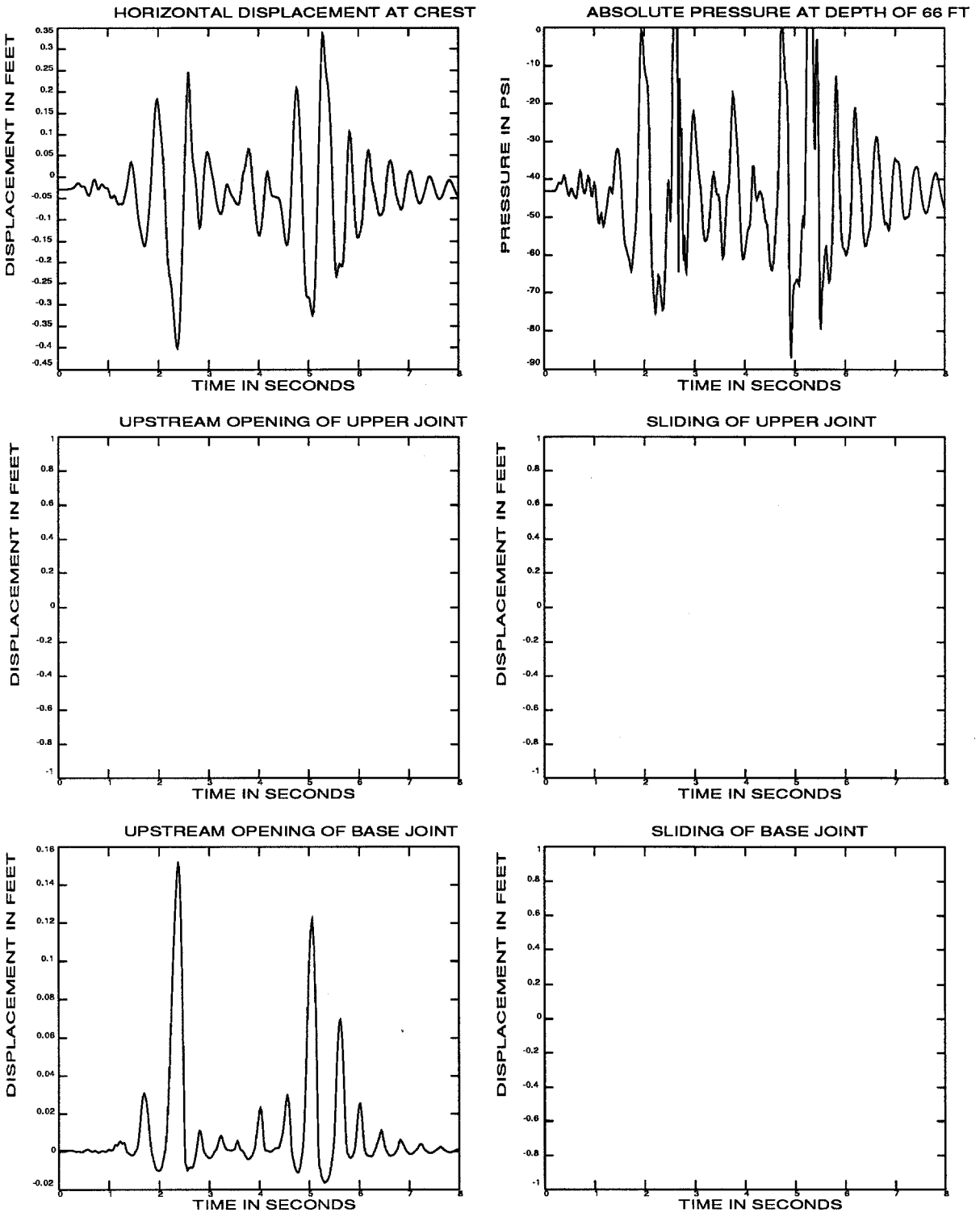

a. Time history responses

Figure 16. Results of earthquake analysis of the light-weight crest dam with full reservoir and keyed base. The earthquake time scale equals one.

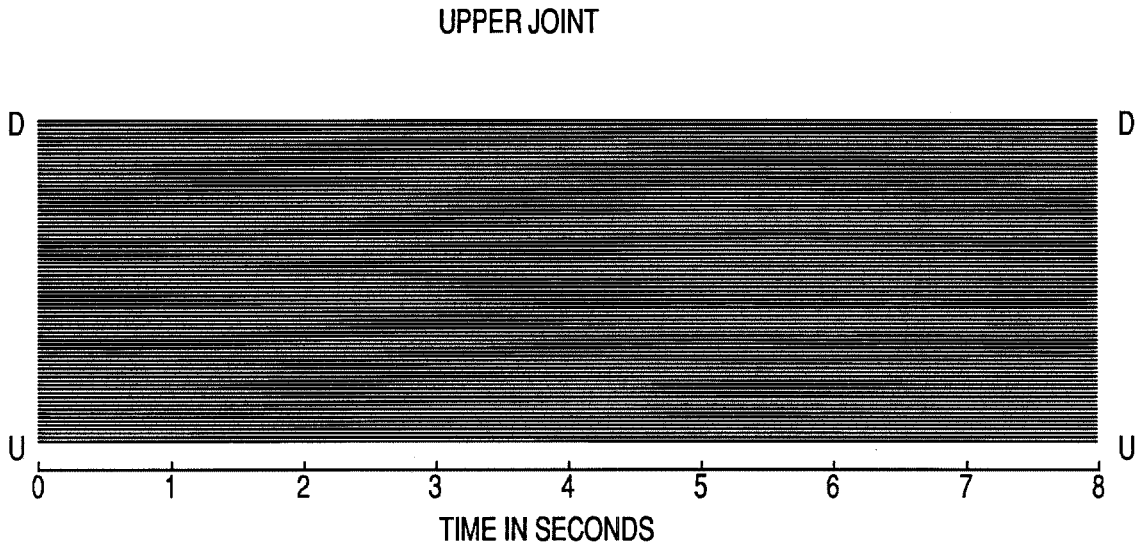

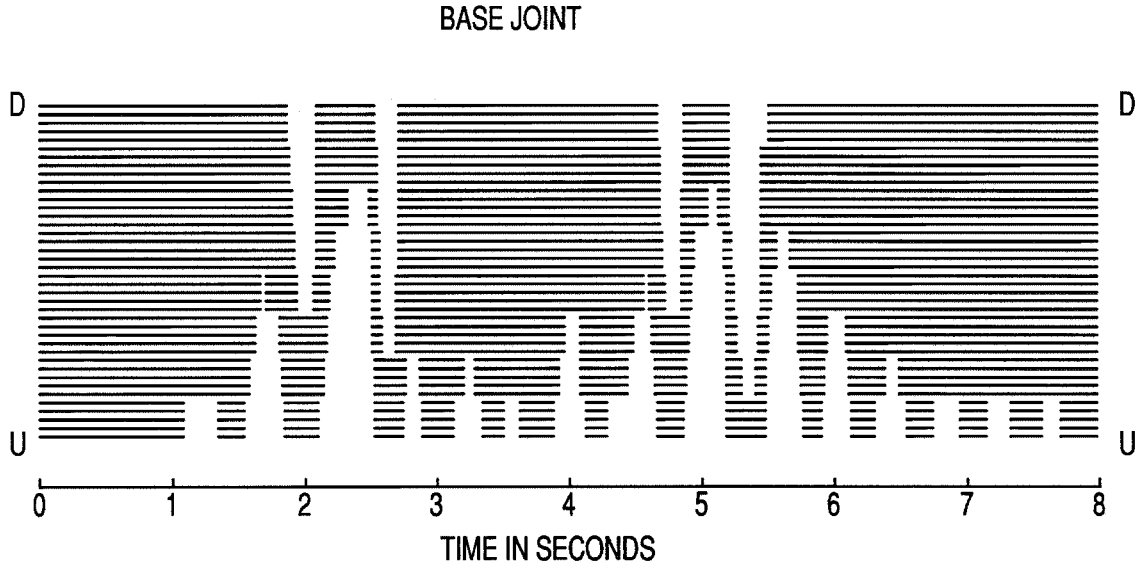

Figure 16b. Contact time histories of joints

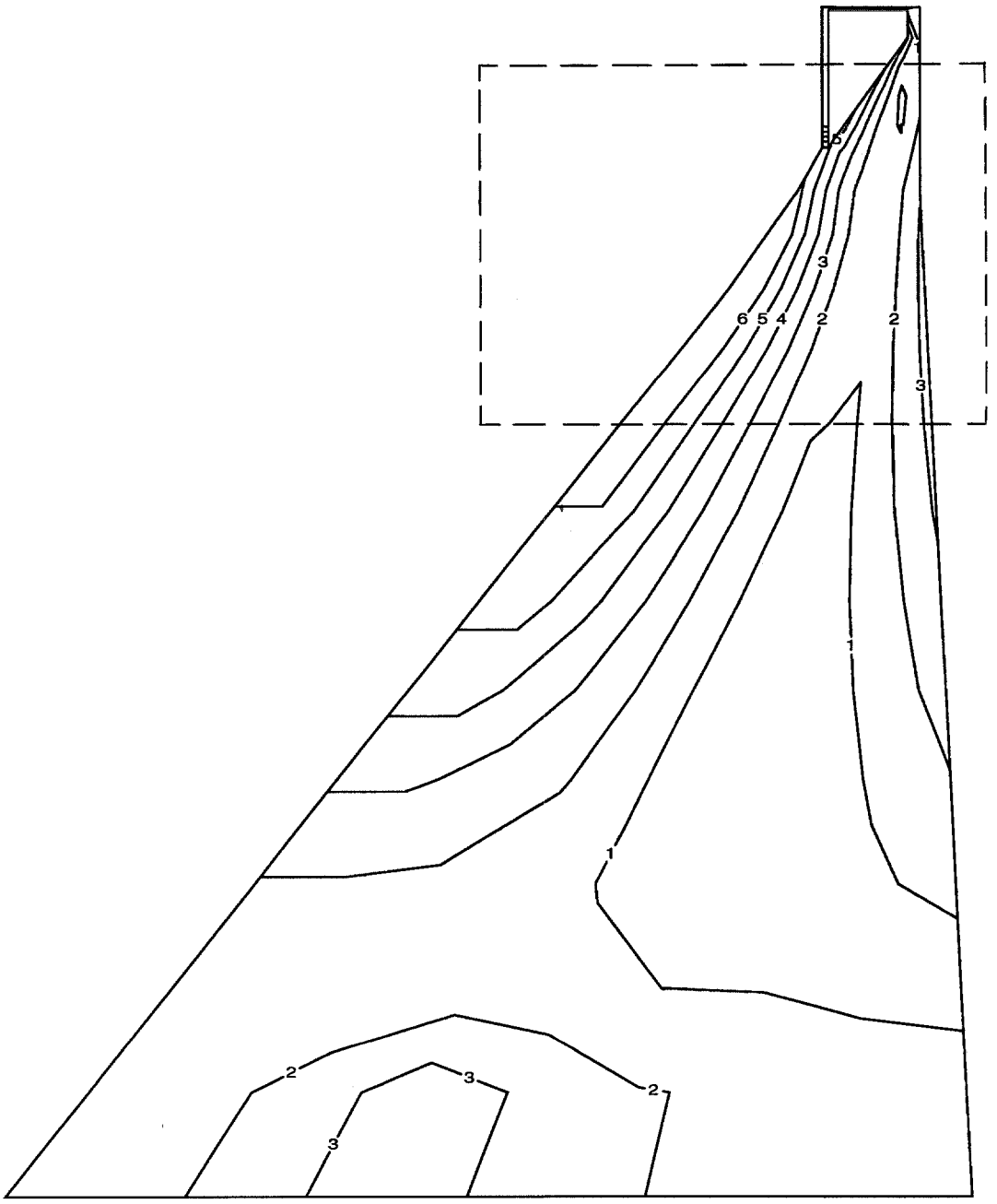

Figure 16c. Contours of maximum principal tensile stress (static plus dynamic). Stress vectors within the boxed region are shown in part d.

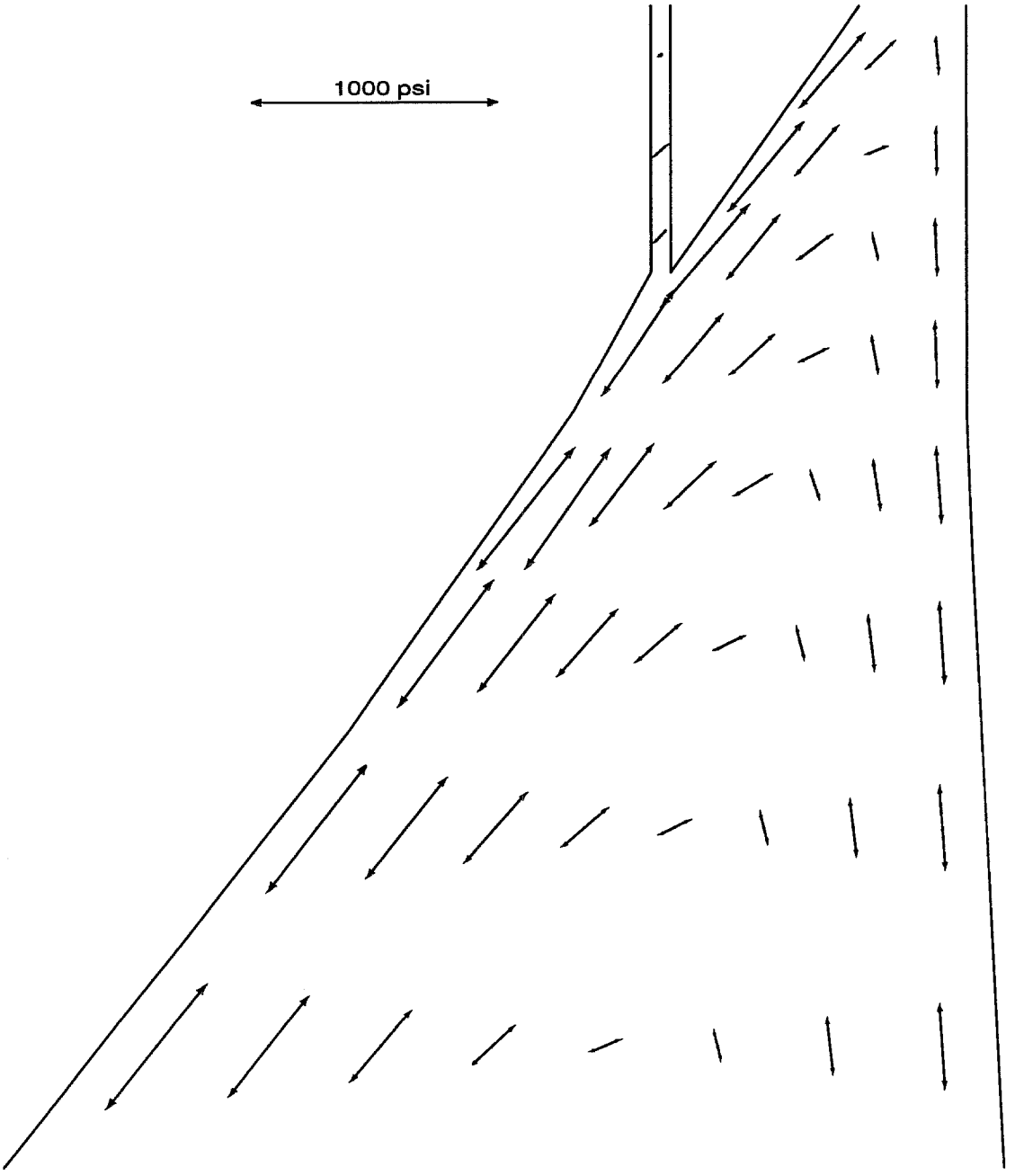

Figure 16d. Vectors of maximum principal tensile stress (static plus dynamic) in the neck region. See part c for region plotted.

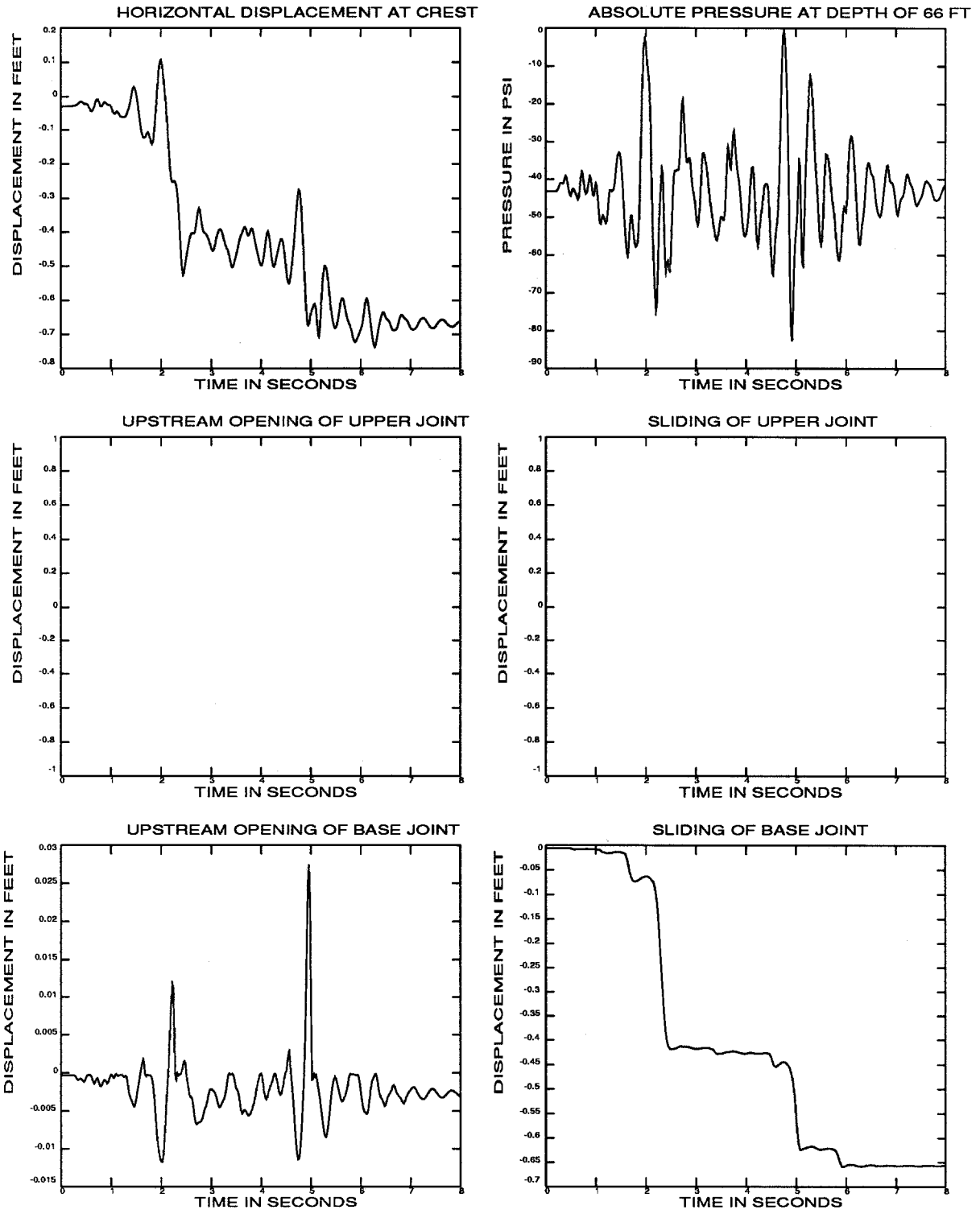

a. Time history responses

Figure 17. Results of earthquake analysis of the light-weight crest dam with full reservoir and unkeyed base. The earthquake time scale equals one.

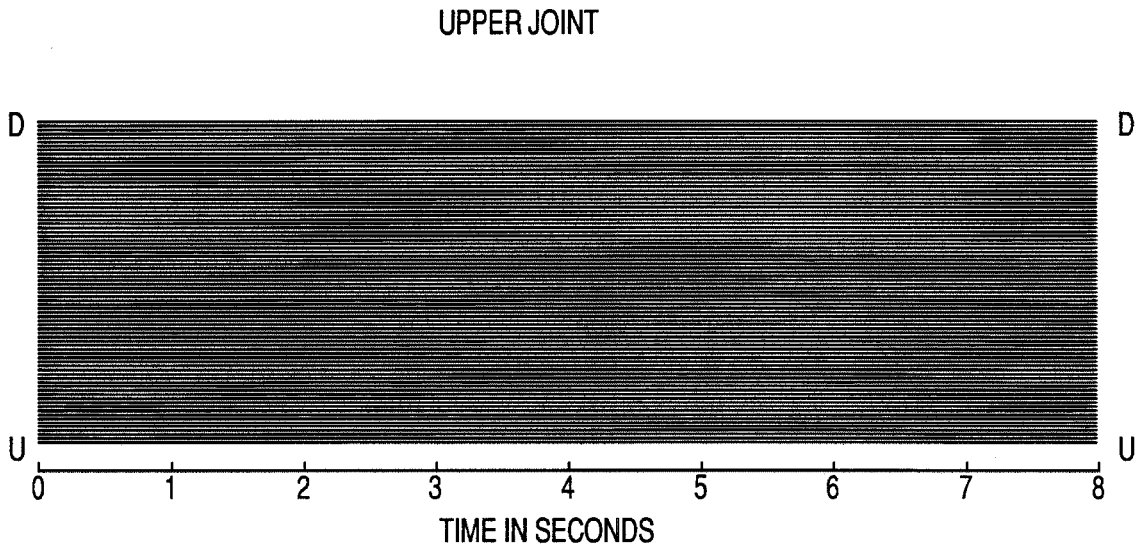

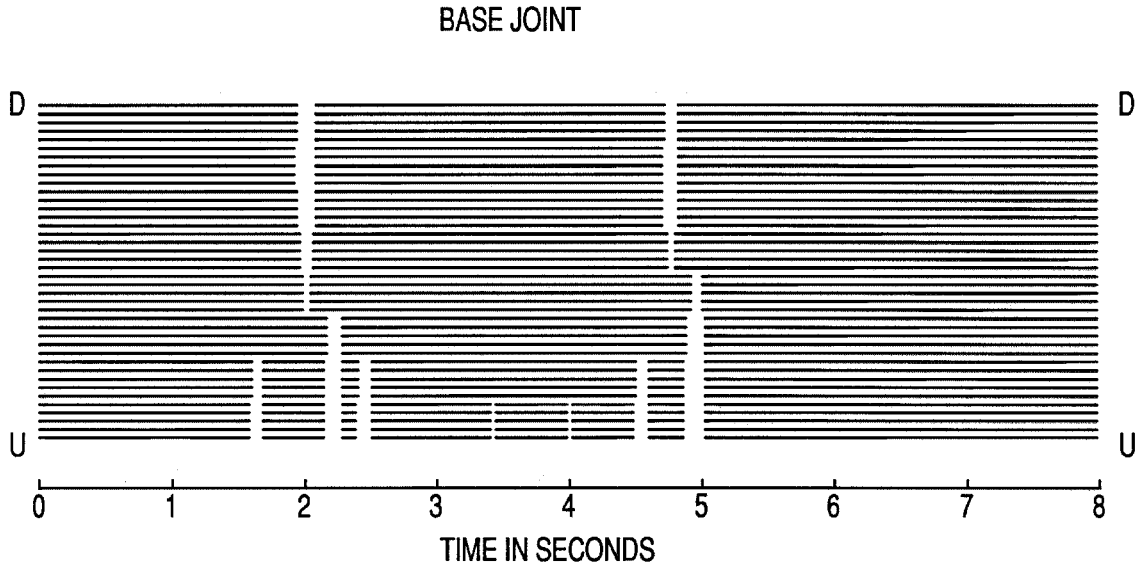

Figure 17b. Contact time histories of joints

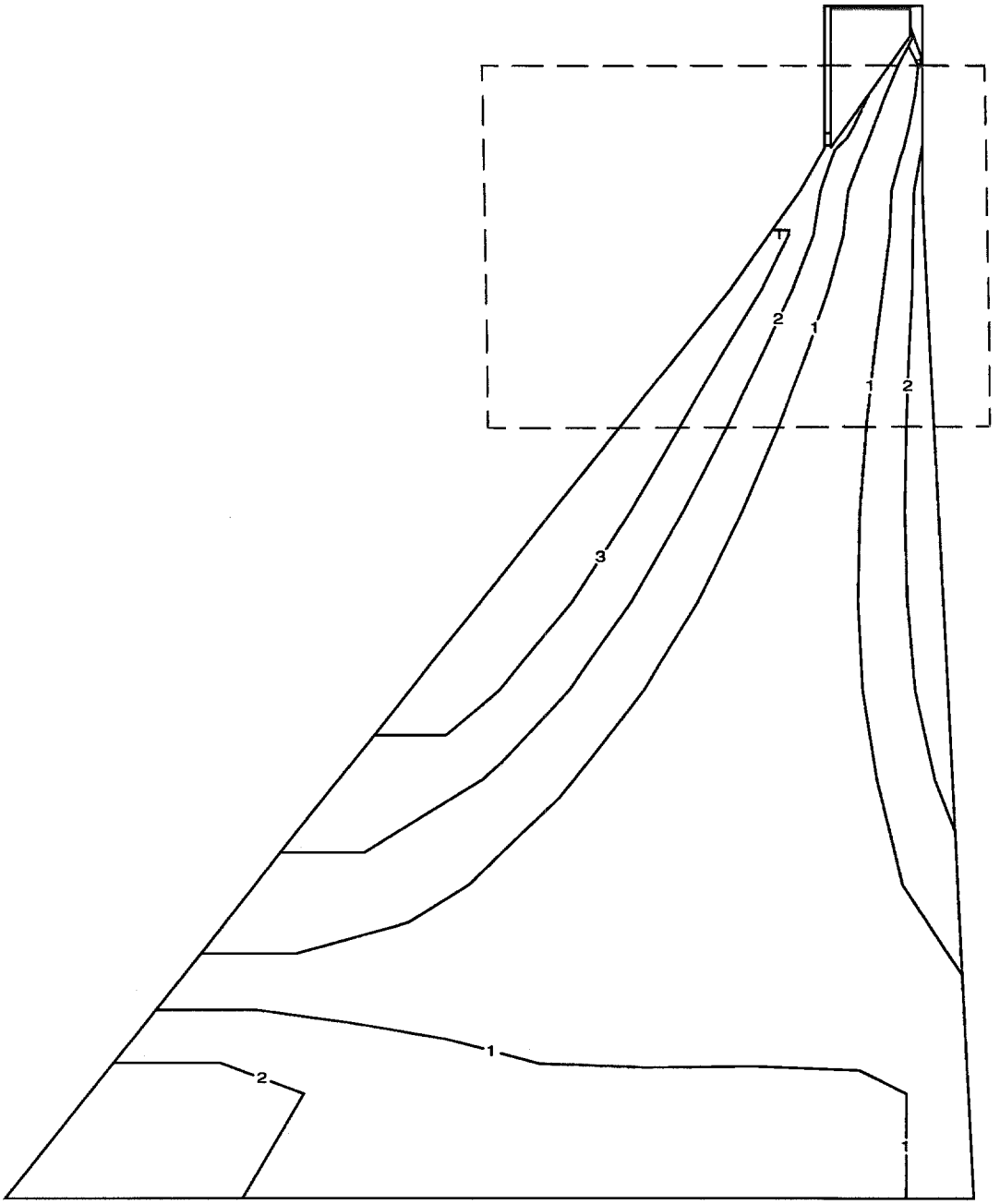

Figure 17c. Contours of maximum principal tensile stress (static plus dynamic). Stress vectors within the boxed region are shown in part d.

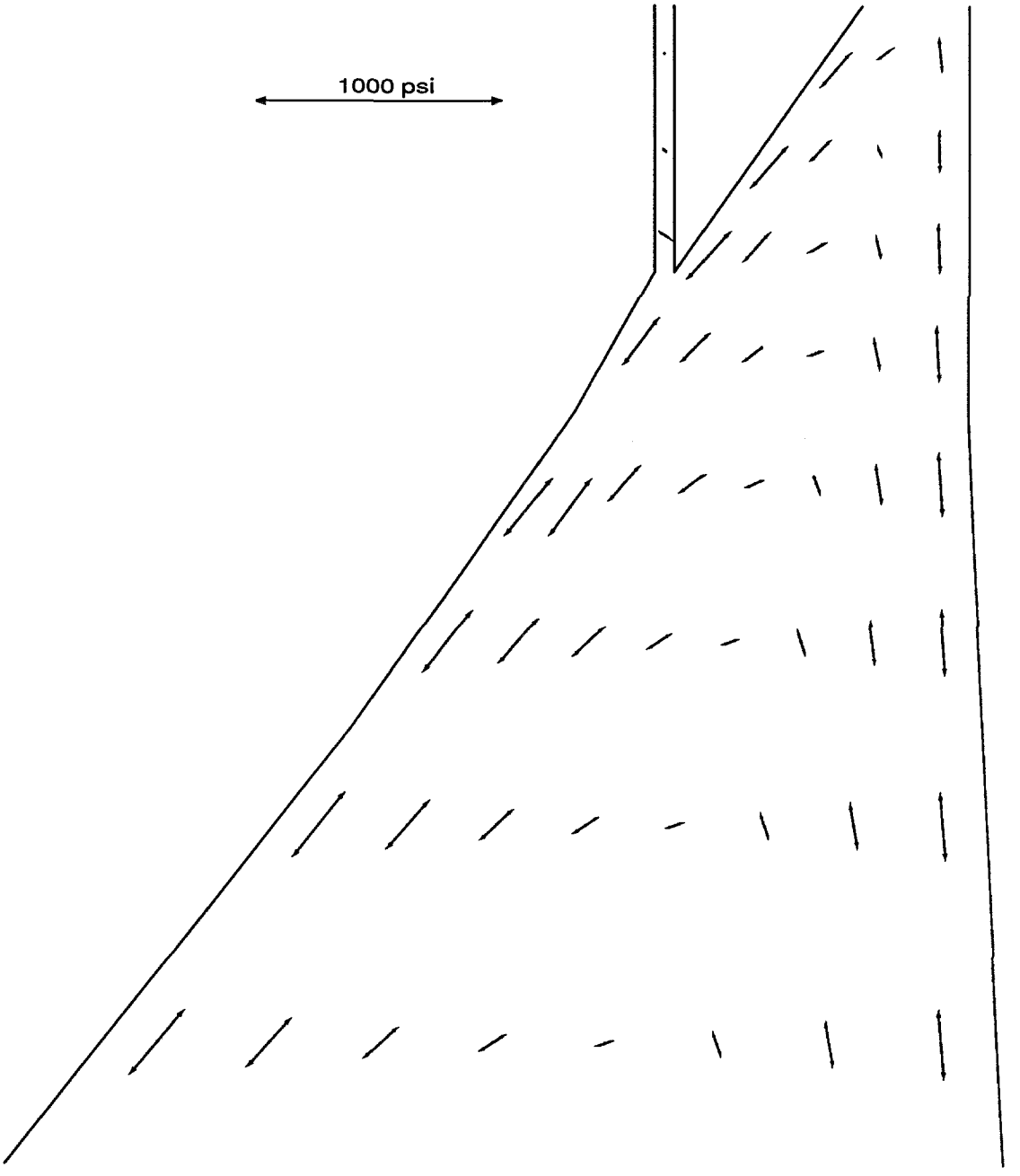

Figure 17d. Vectors of maximum principal tensile stress (static plus dynamic) in the neck region. See part c for region plotted.

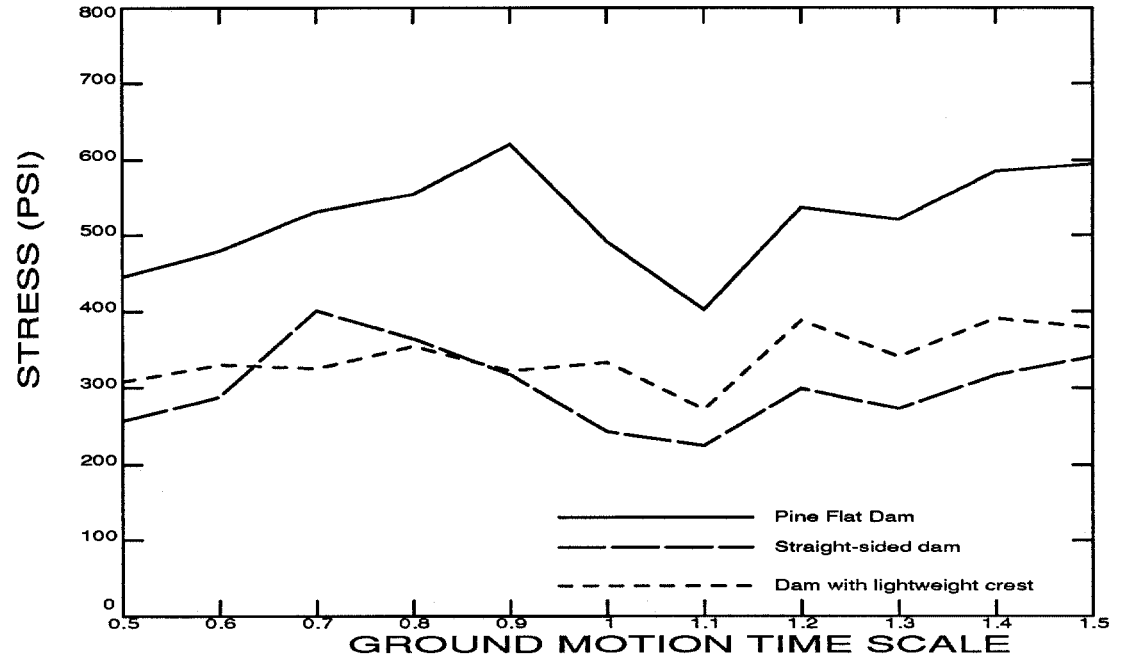

a. Upstream face

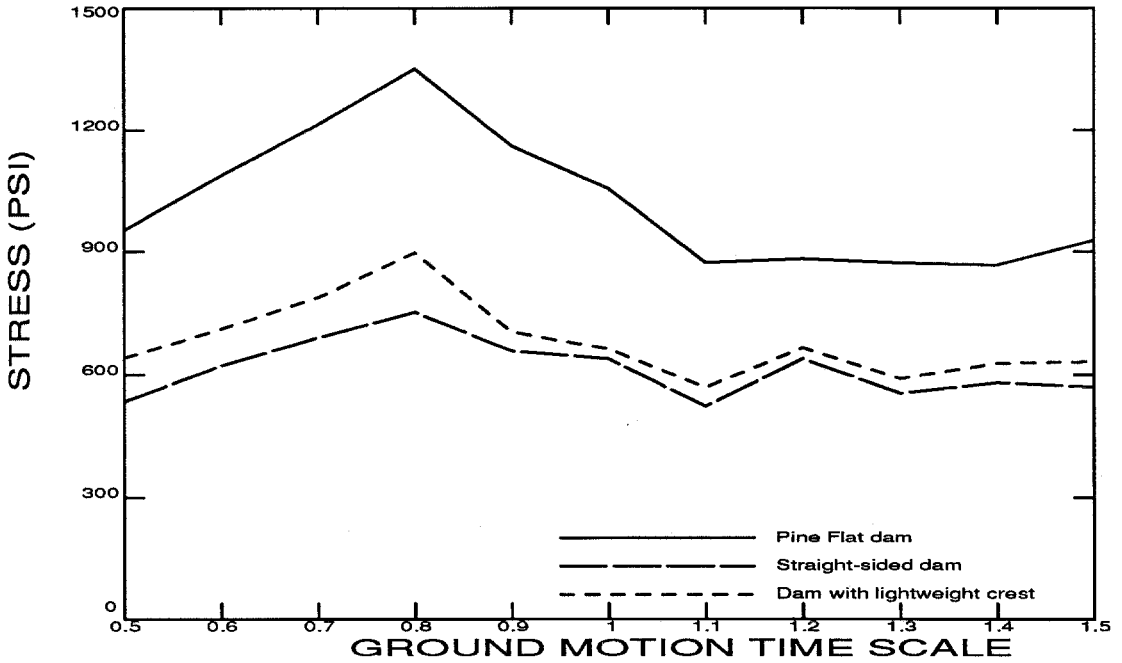

b. Downstream face

Figure 18. Maximum principal tensile stresses (static plus dynamic) as a function of ground motion time scale that occur at the faces of Pine Flat Dam and two dams with modified cross section — full reservoir and keyed base.

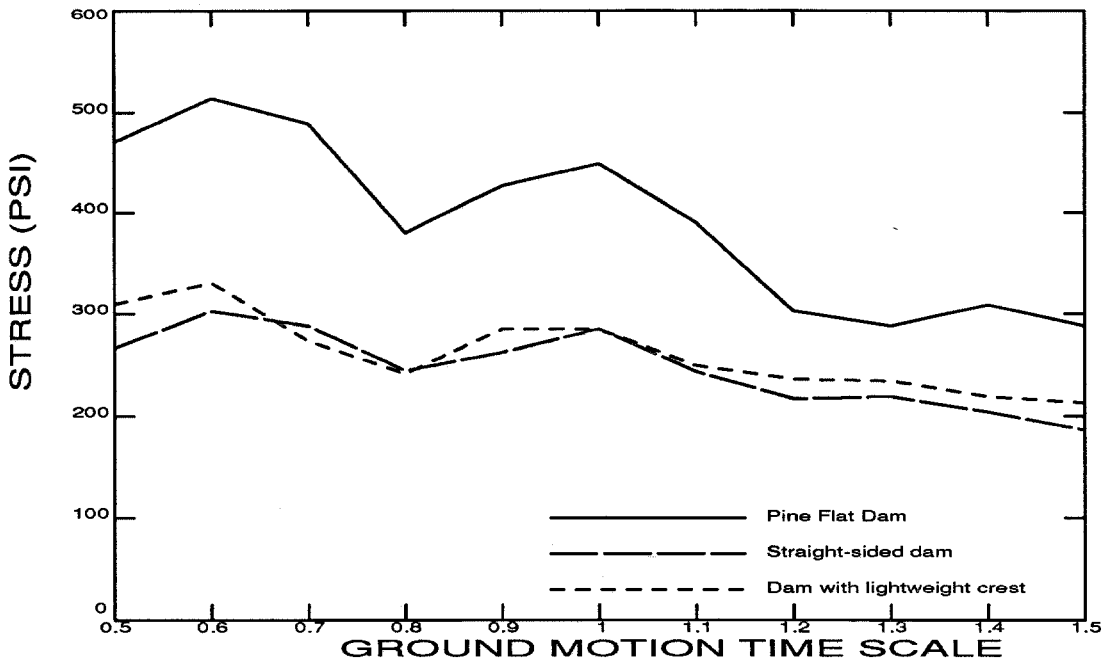

a. Upstream face

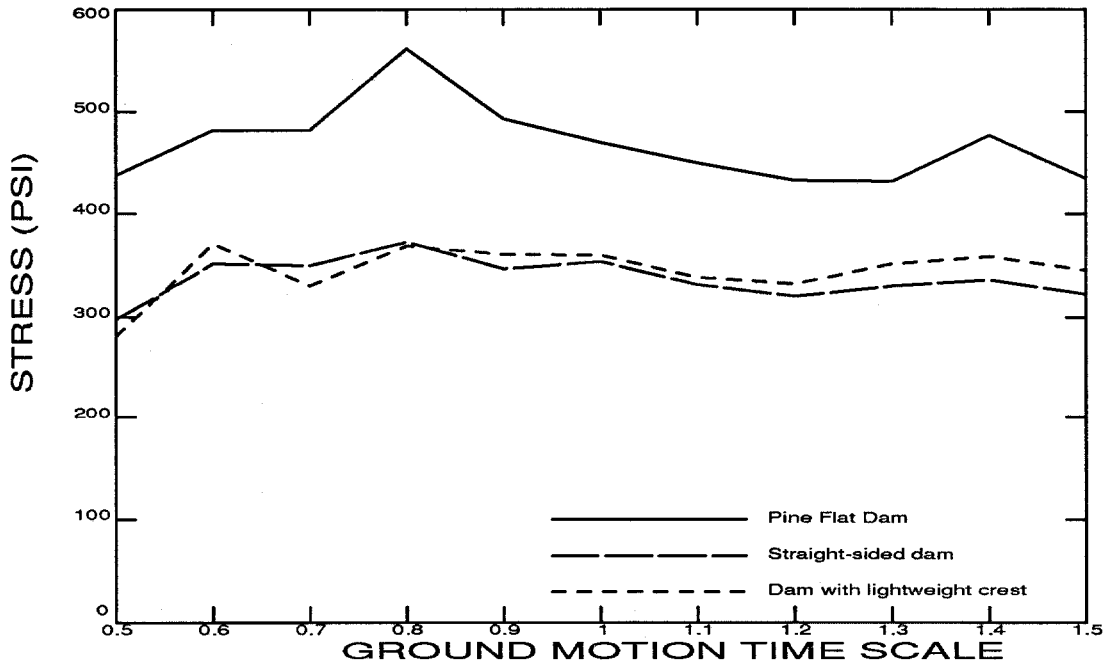

b. Downstream face

Figure 19. Maximum principal tensile stresses (static plus dynamic) as a function of ground motion time scale that occur at the faces of Pine Flat Dam and two dams with modified cross section — full reservoir and unkeyed base.

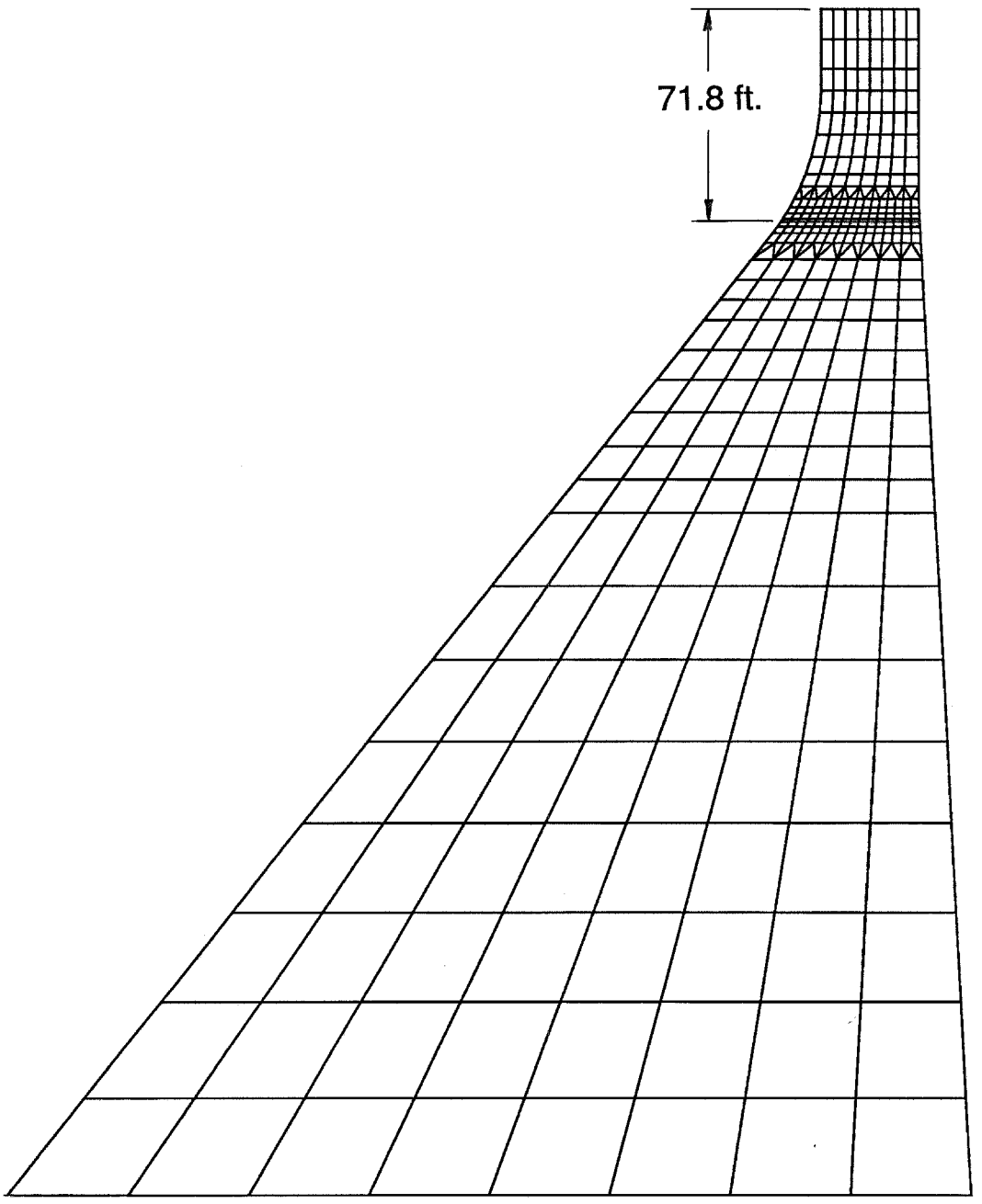

Figure 20. Finite element mesh of the dam with a horizontal joint in the neck region. The geometry is similar to the 400 foot high monolith of Pine Flat Dam.

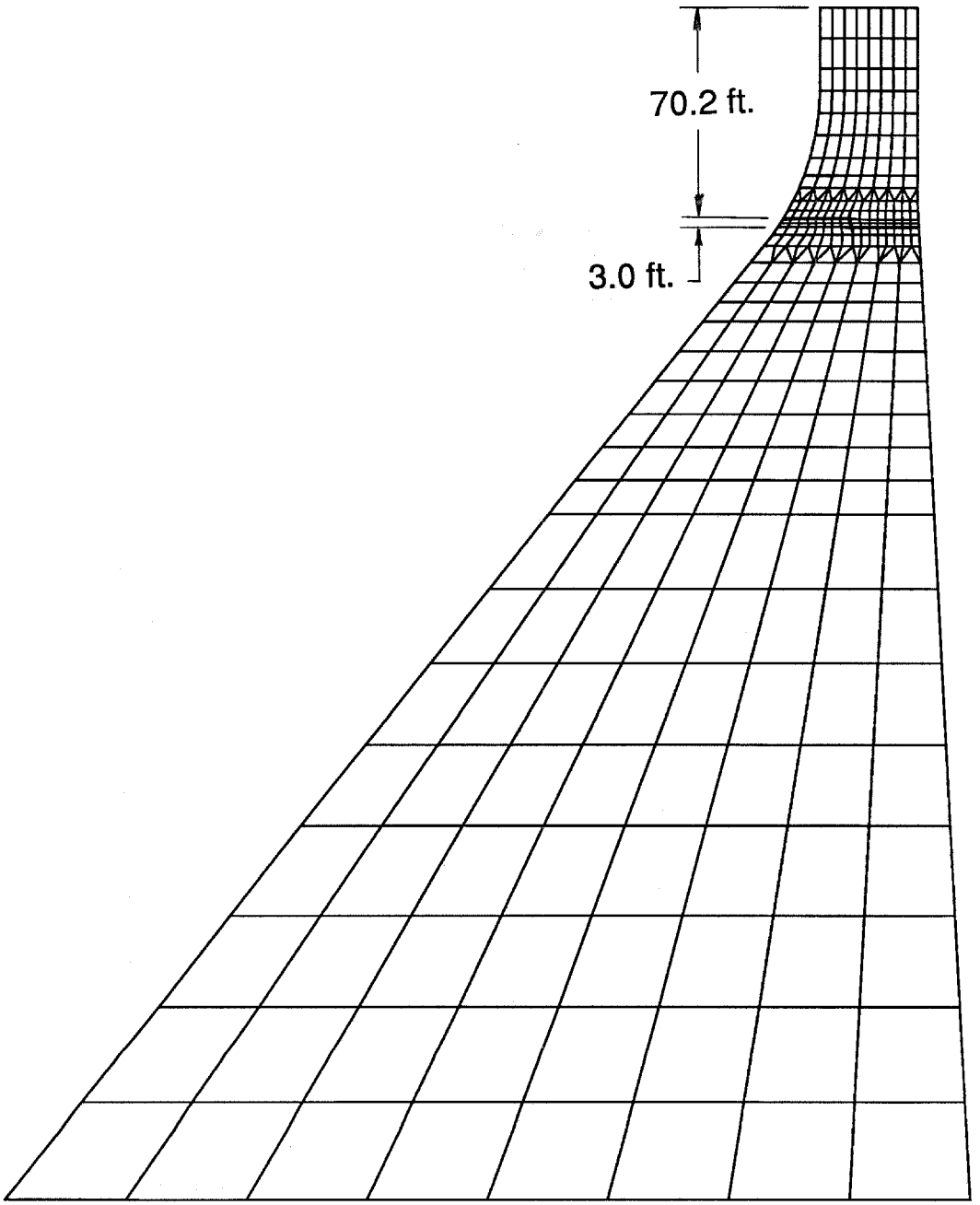

Figure 21. Finite element mesh of the dam with a stepped joint in the neck region. The geometry is similar to the 400 foot high monolith of Pine Flat Dam.

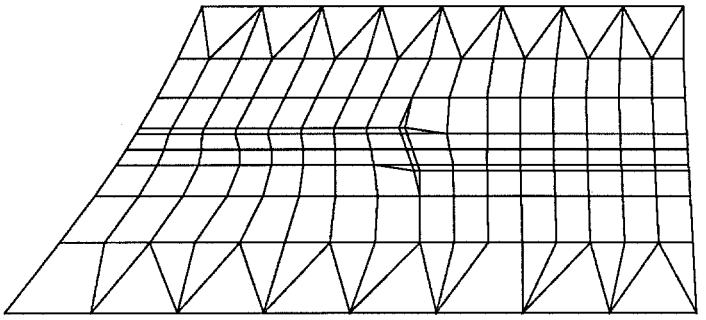

Figure 21 (Continued). Close-up of stepped joint.

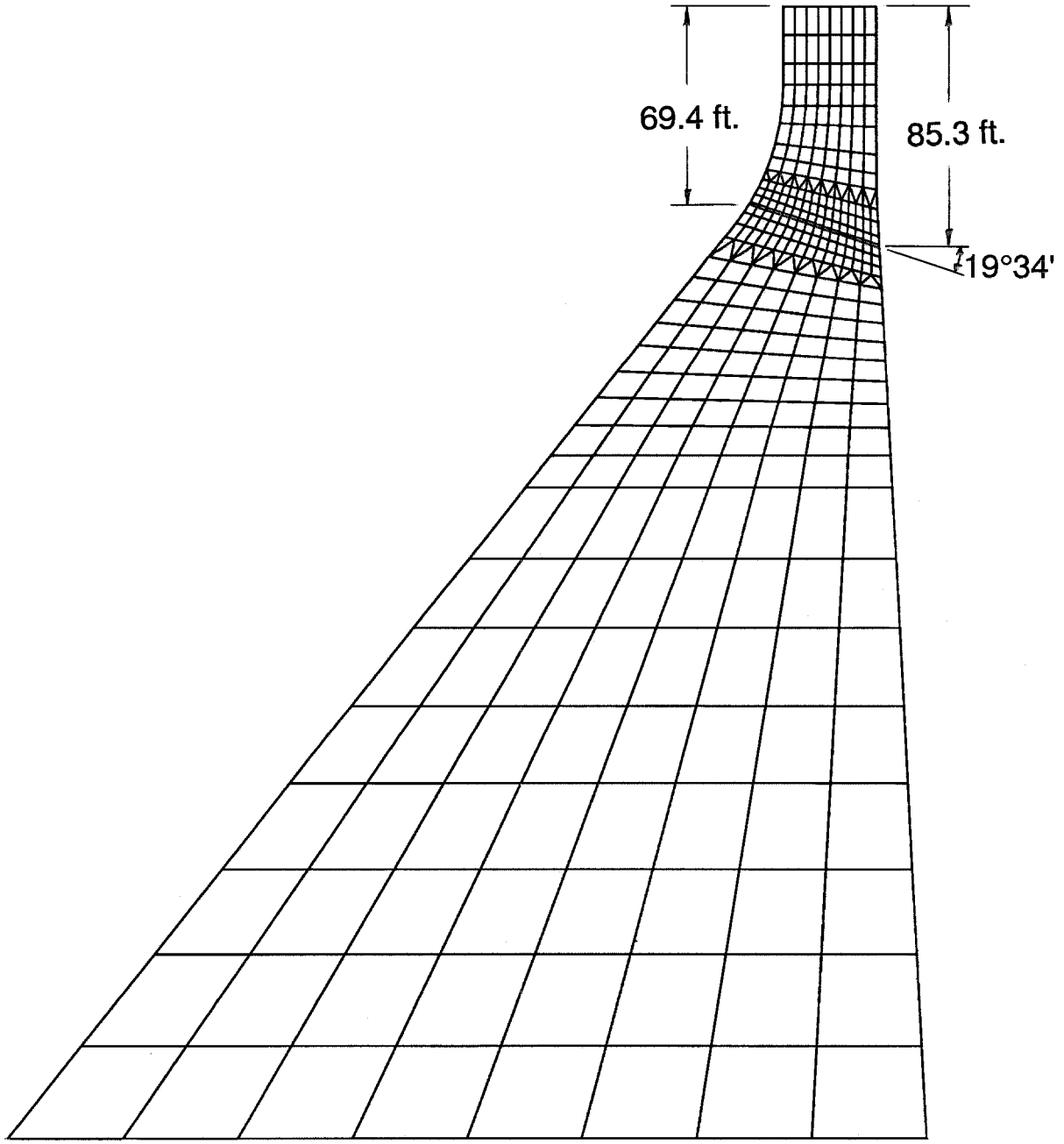

Figure 22. Finite element mesh of the dam with an inclined joint in the neck region. The geometry is similar to the 400 foot high monolith of Pine Flat Dam.

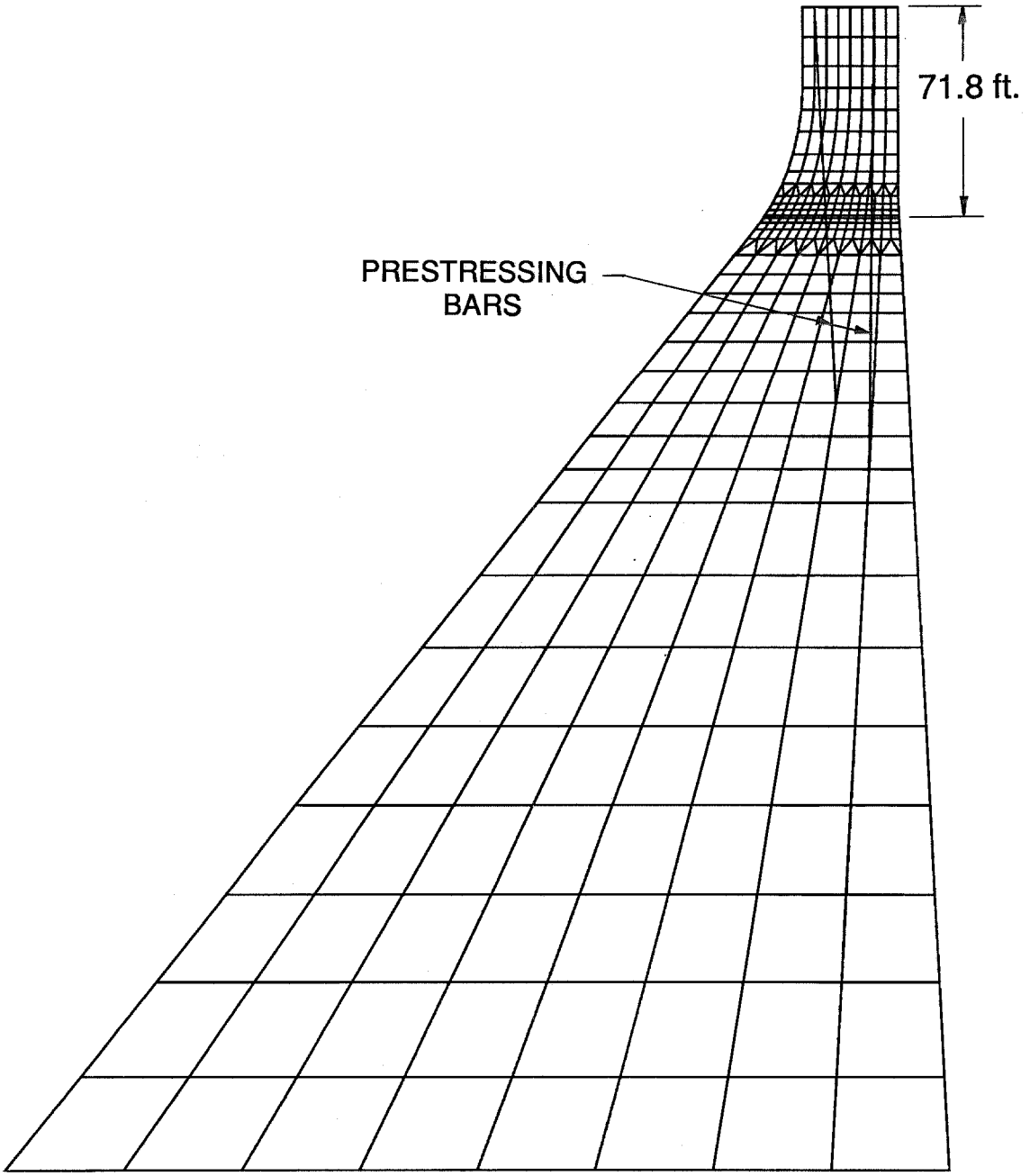

Figure 23. Finite element mesh of the dam with a horizontal joint and two prestressing bars in the neck region. The geometry is similar to the 400 foot high monolith of Pine Flat Dam.

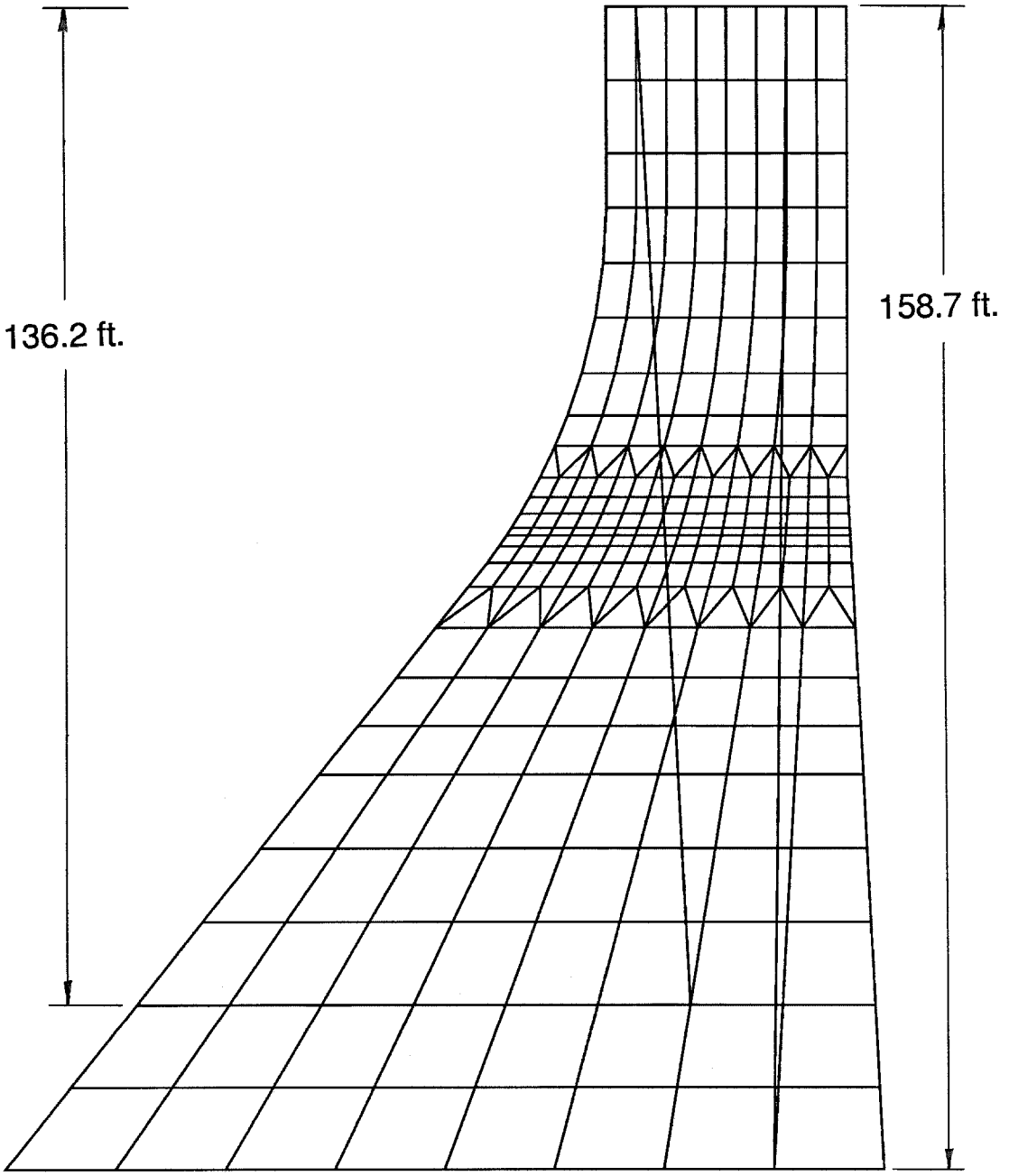

Figure 23 (Continued). Close-up of prestressed region.

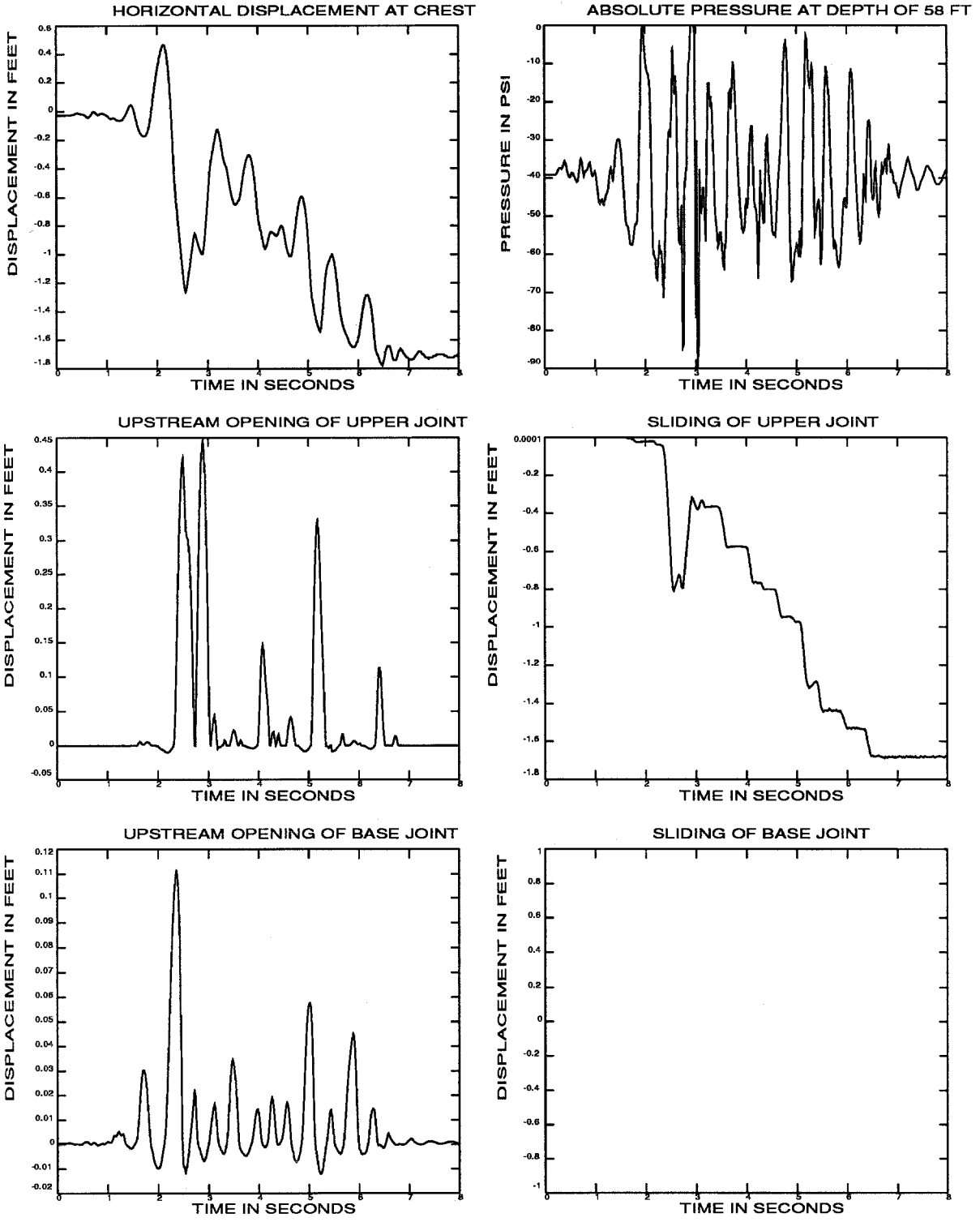

a. Time history responses

Figure 24. Results of earthquake analysis of the dam with a horizontal joint, full reservoir and keyed base. The earthquake time scale equals one.

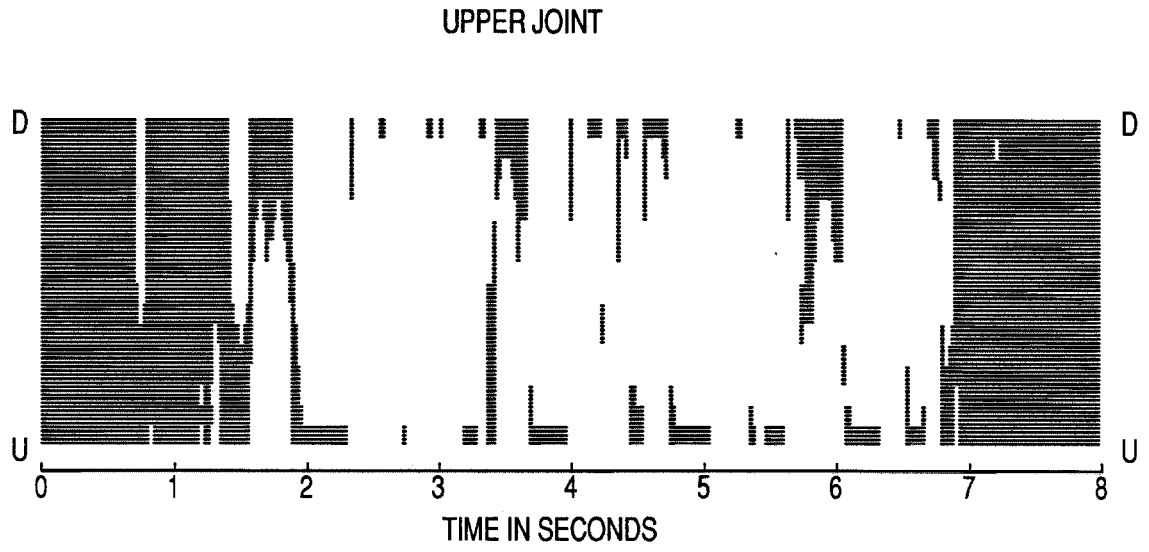

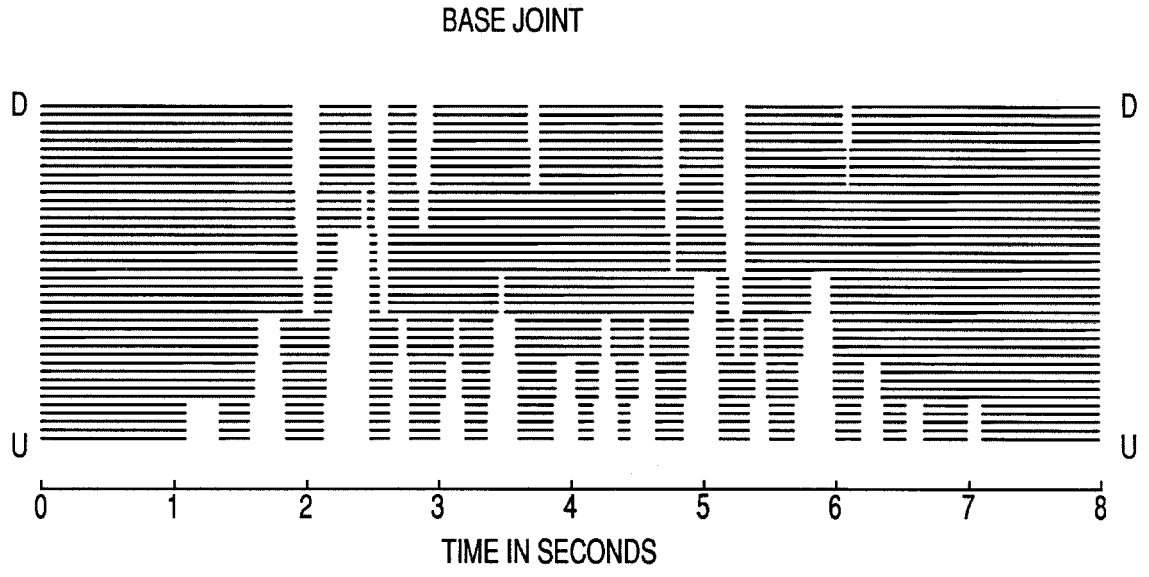

Figure 24b. Contact time histories of joints

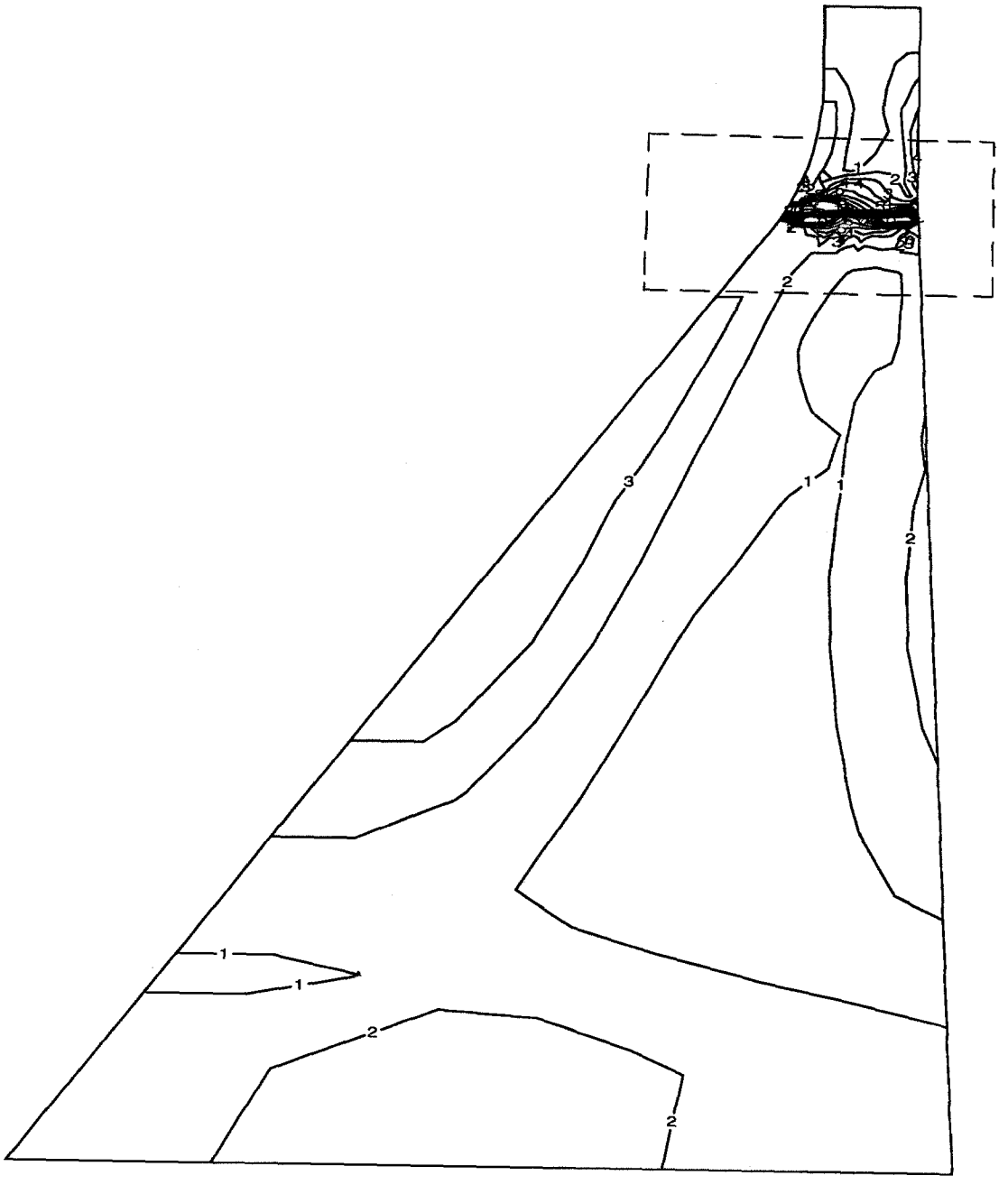

Figure 24c. Contours of maximum principal tensile stress (static plus dynamic). Stress vectors within the boxed region are shown in part d.

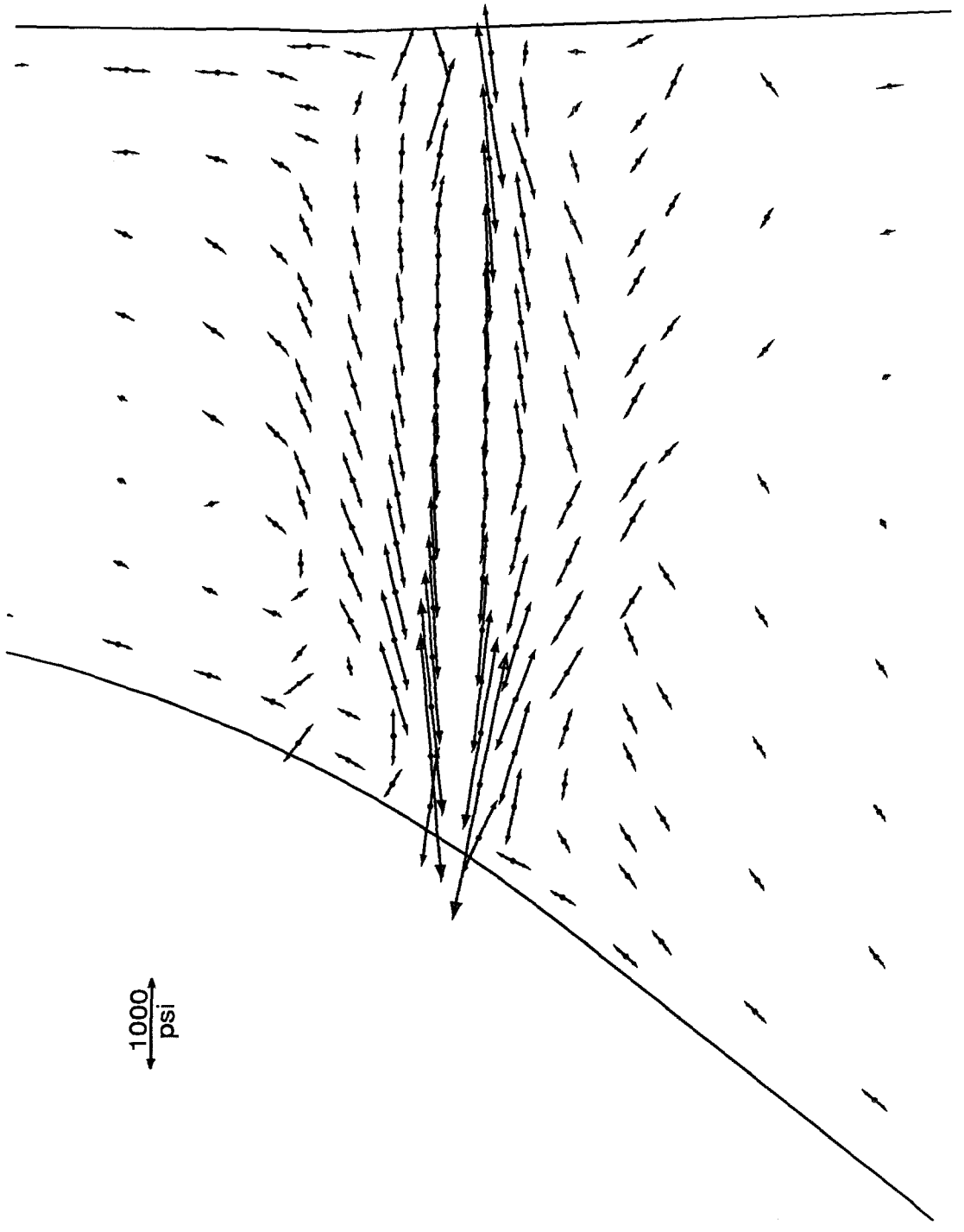

Figure 24d. Vectors of maximum principal tensile stress (static plus dynamic) in the neck region. See part c for region plotted.

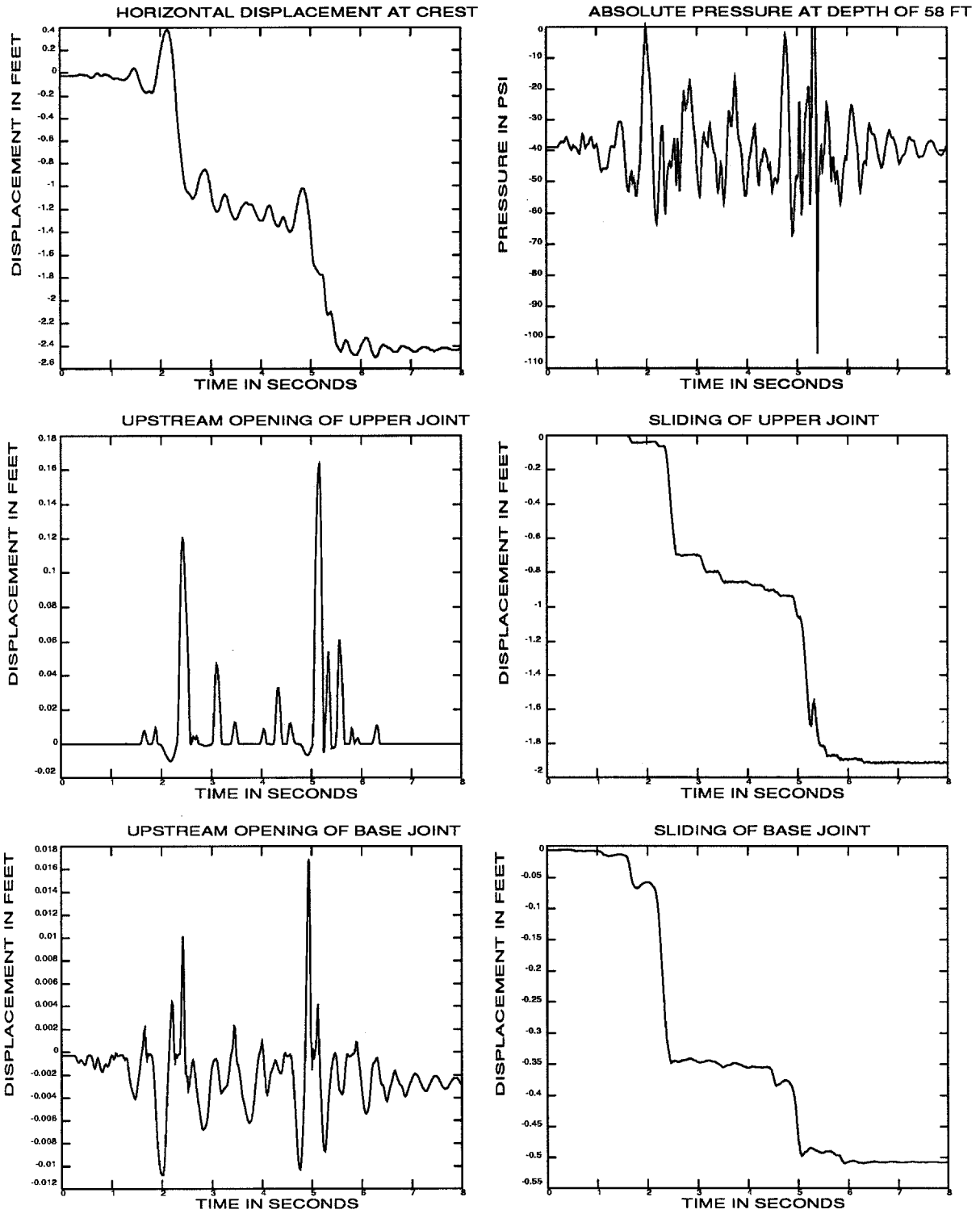

a. Time history responses

Figure 25. Results of earthquake analysis of the dam with a horizontal joint, full reservoir and unkeyed base. The earthquake time scale equals one.

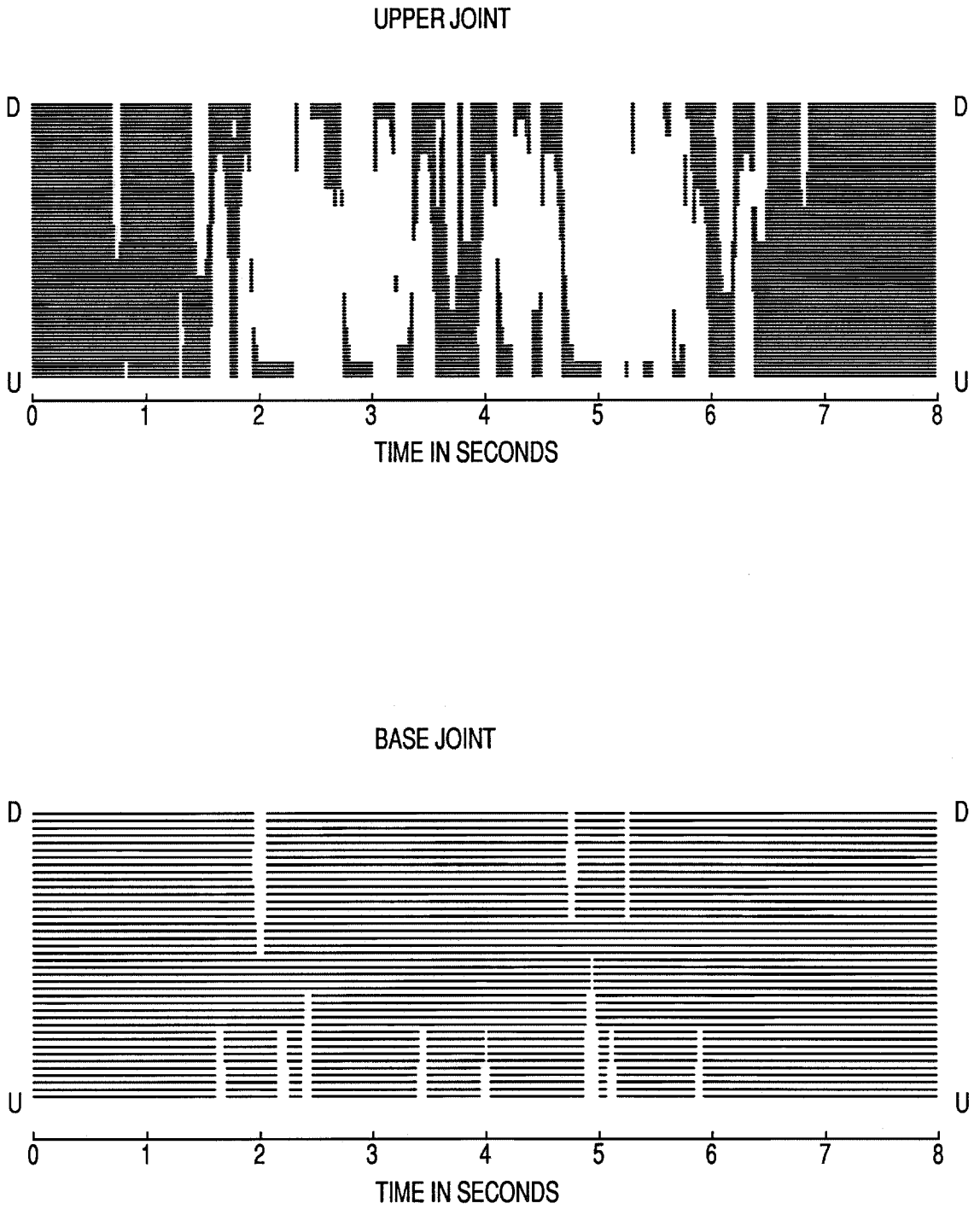

Figure 25b. Contact time histories of joints

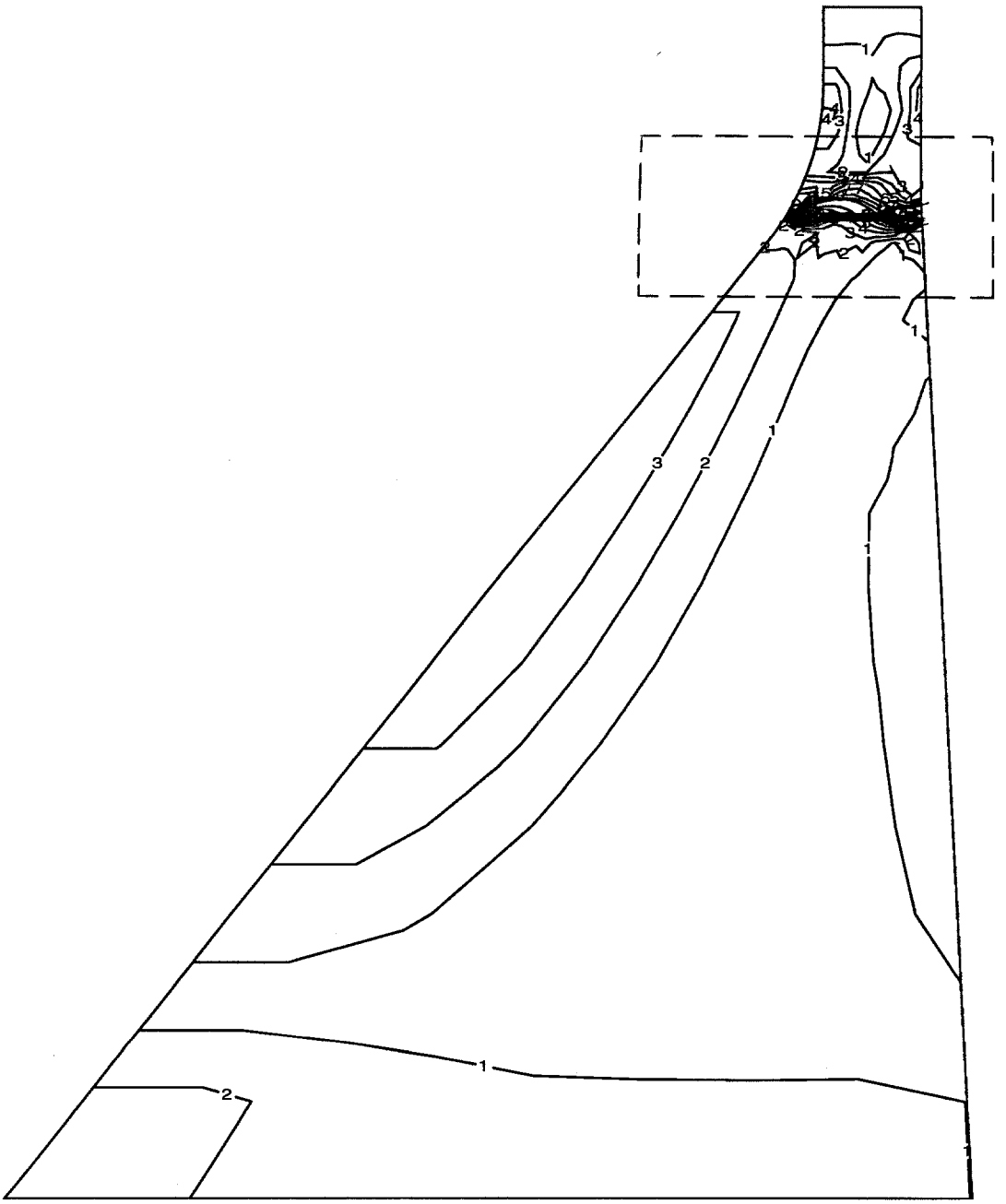

Figure 25c. Contours of maximum principal tensile stress (static plus dynamic). Stress vectors within the boxed region are shown in part d.

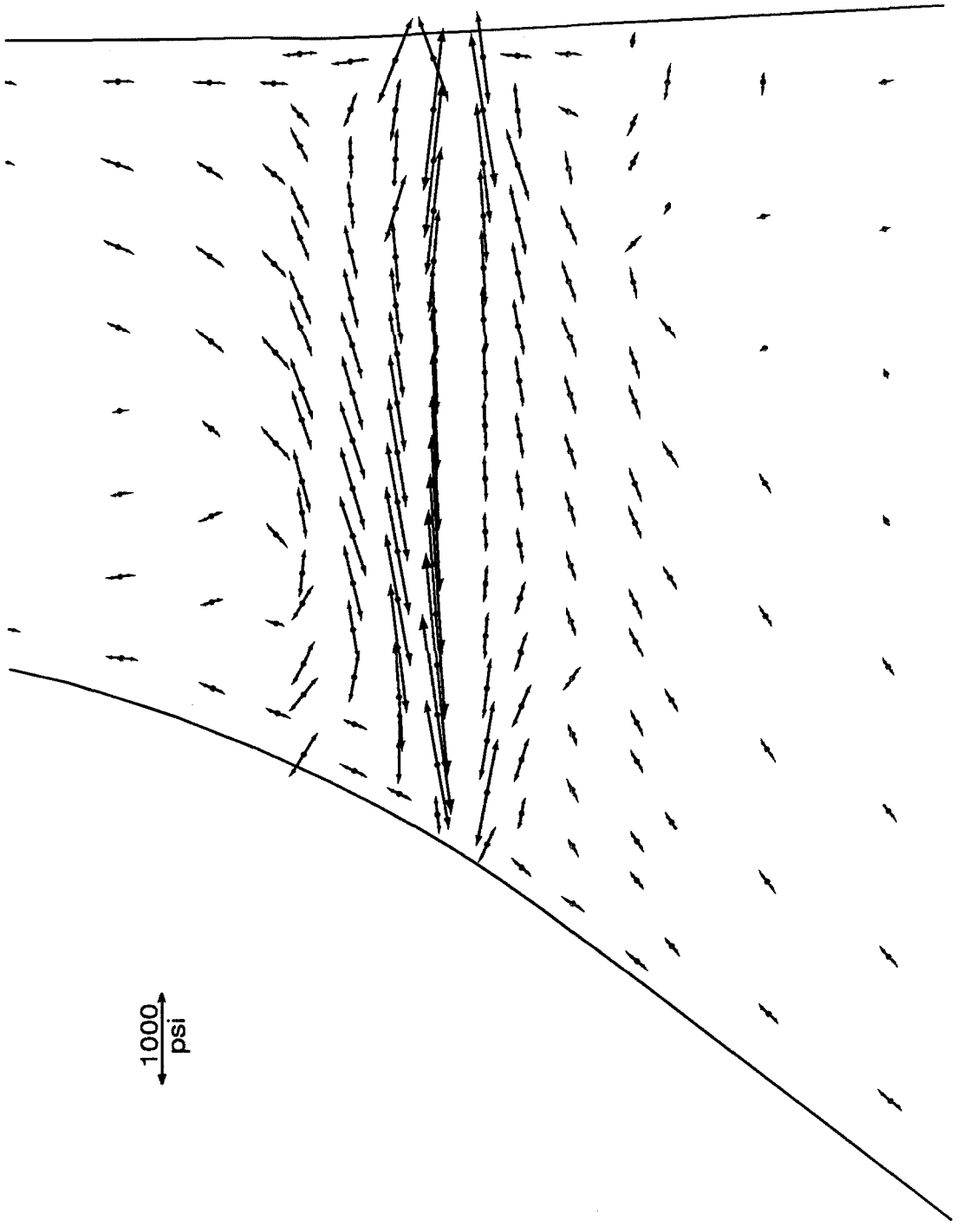

Figure 25d. Vectors of maximum principal tensile stress (static plus dynamic) in the neck region. See part c for region plotted.

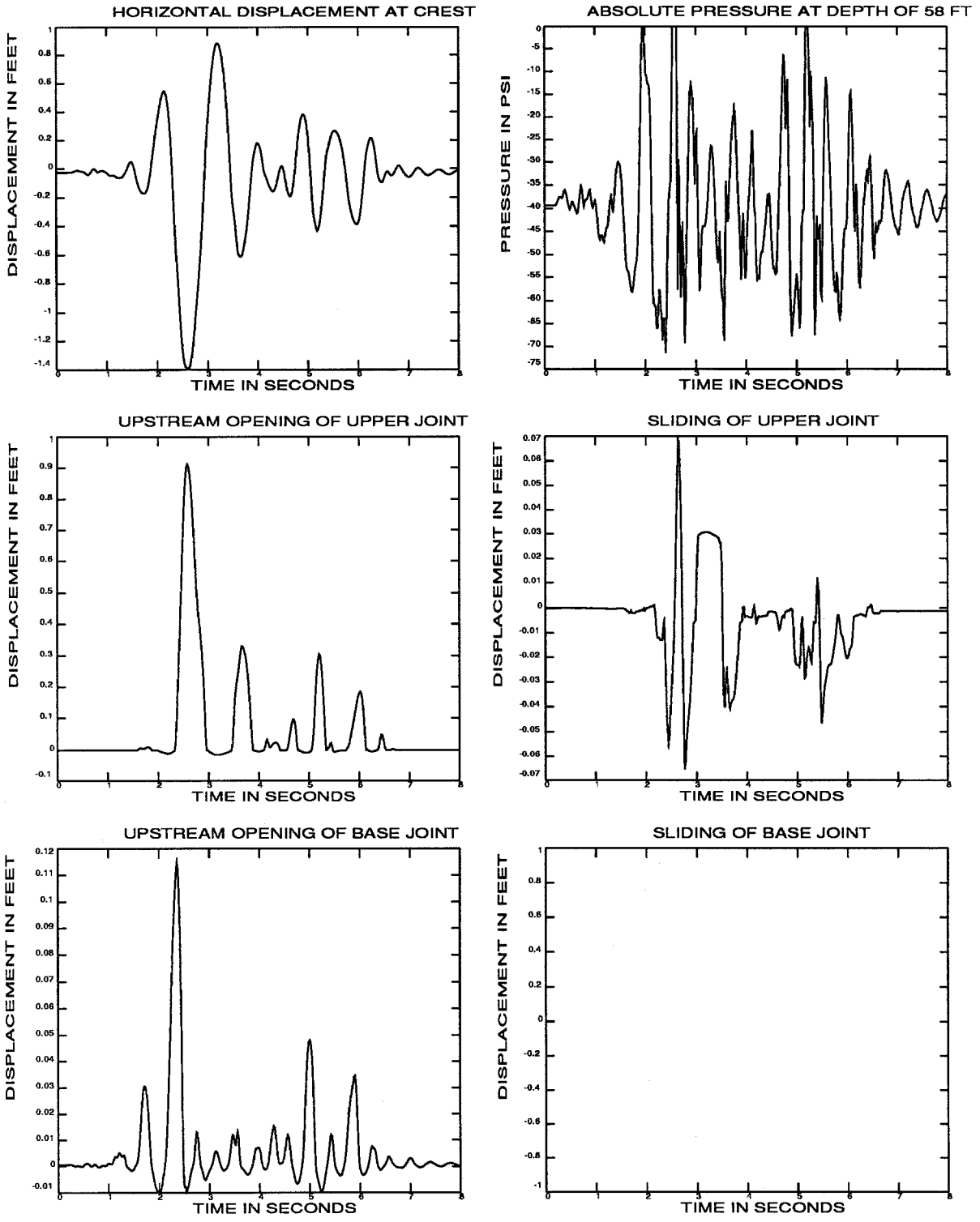

a. Time history responses

Figure 26. Results of earthquake analysis of the dam with a stepped joint, full reservoir and keyed base. The earthquake time scale equals one.

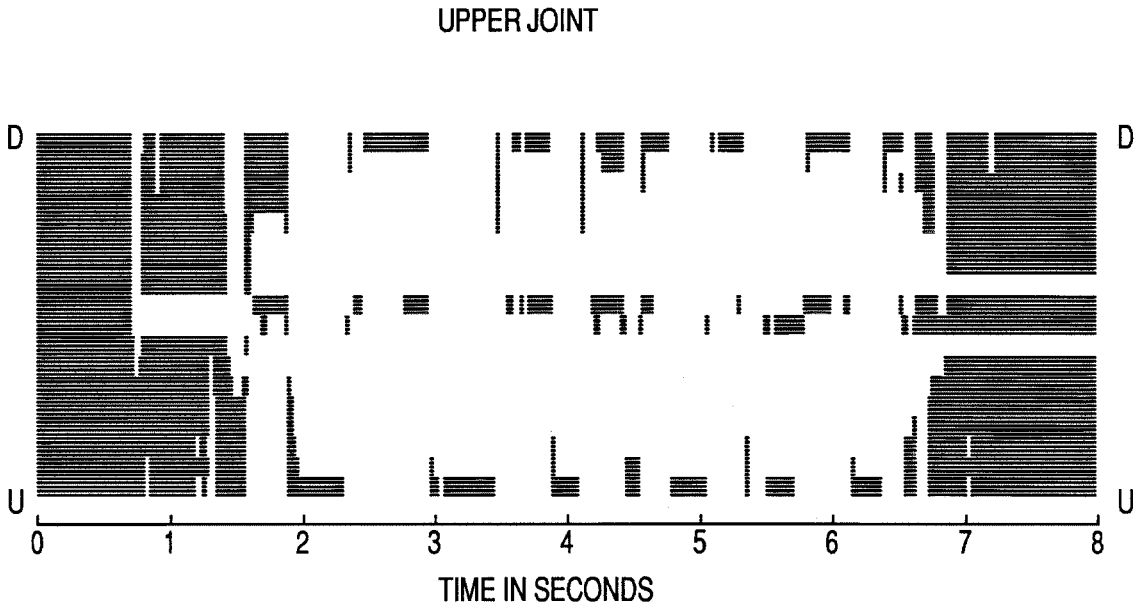

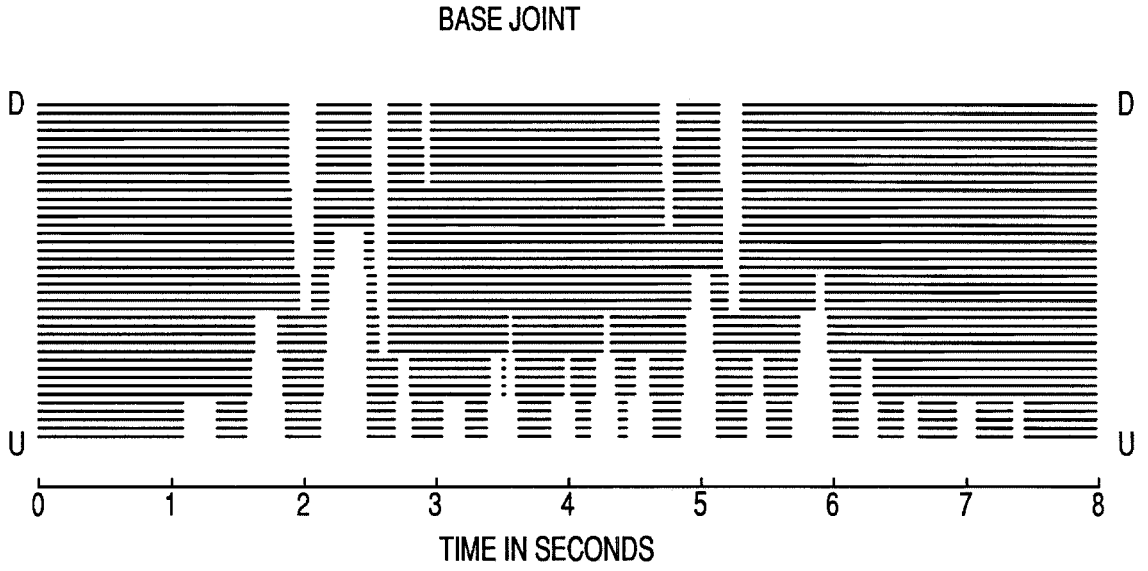

Figure 26b. Contact time histories of joints

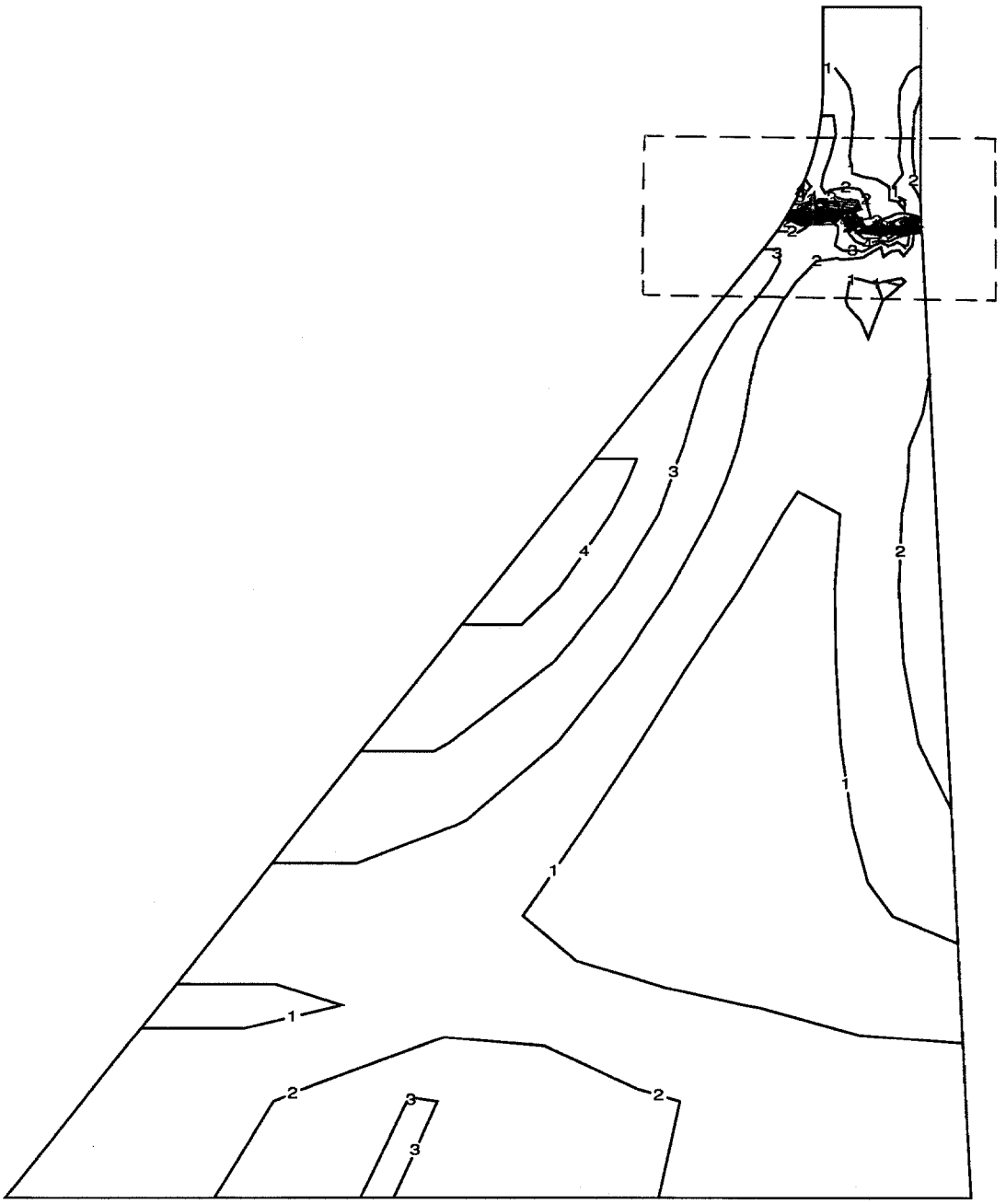

Figure 26c. Contours of maximum principal tensile stress (static plus dynamic). Stress vectors within the boxed region are shown in part d.

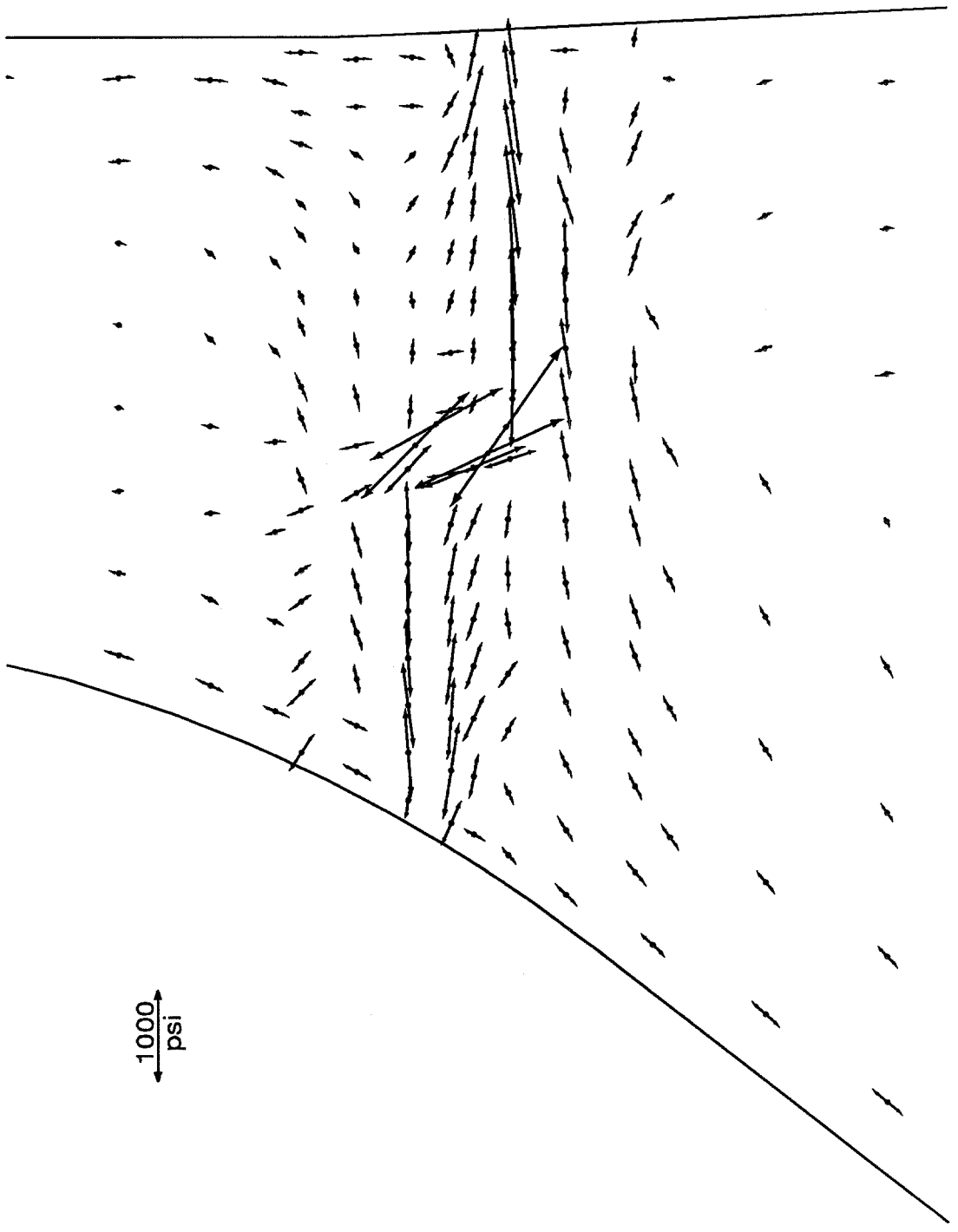

Figure 26d. Vectors of maximum principal tensile stress (static plus dynamic) in the neck region. See part c for region plotted.

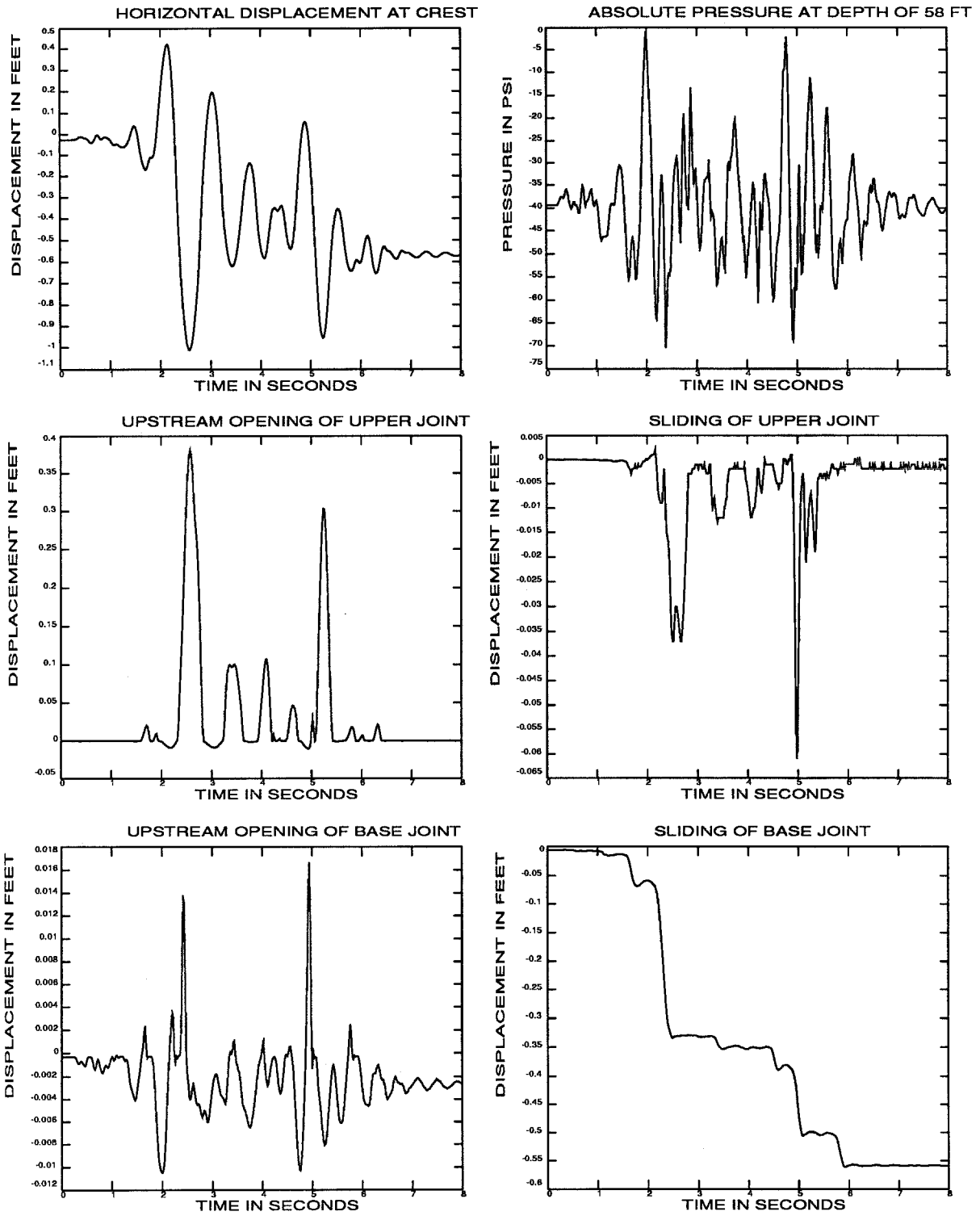

a. Time history responses

Figure 27. Results of earthquake analysis of the dam with a stepped joint, full reservoir and unkeyed base. The earthquake time scale equals one.

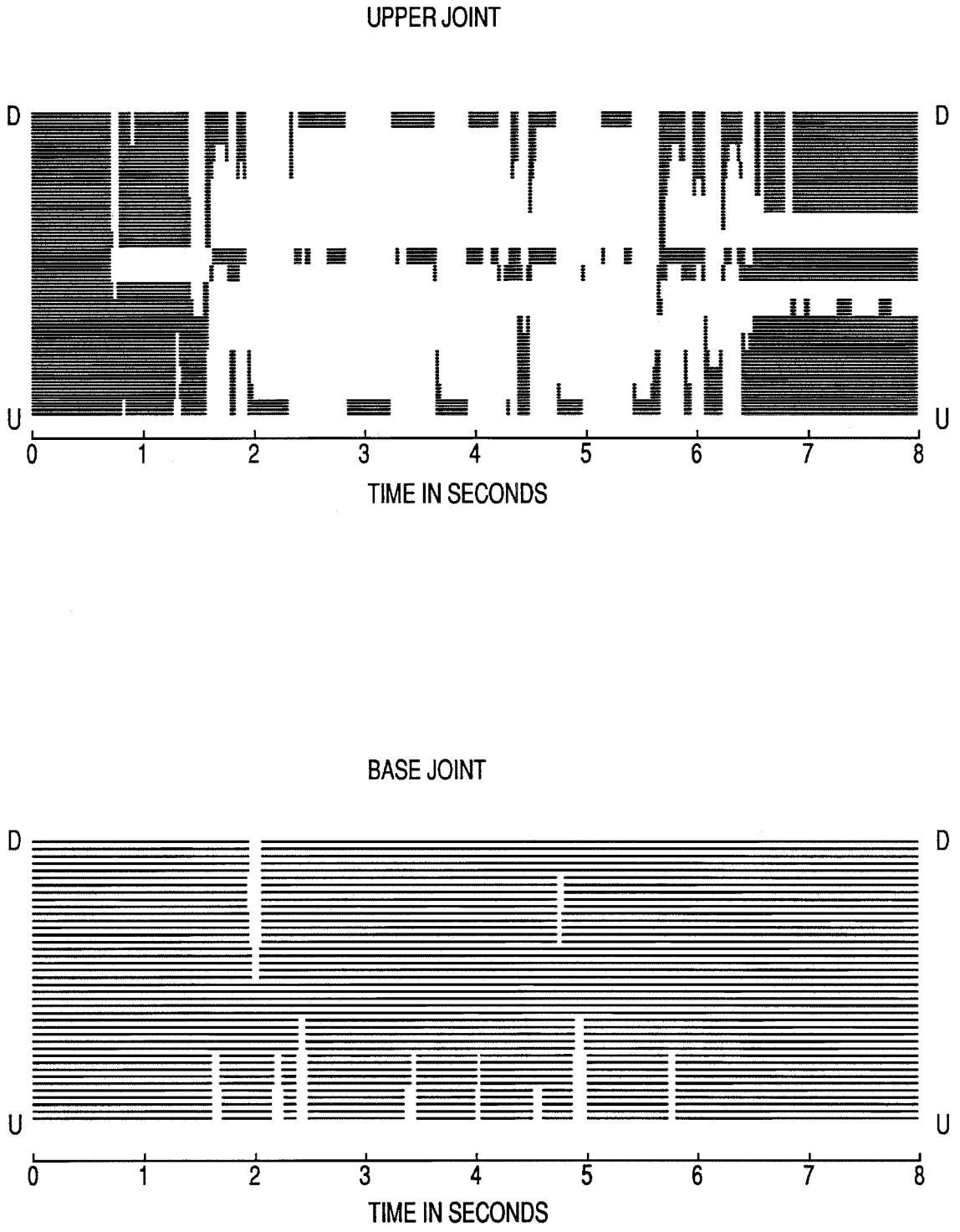

Figure 27b. Contact time histories of joints

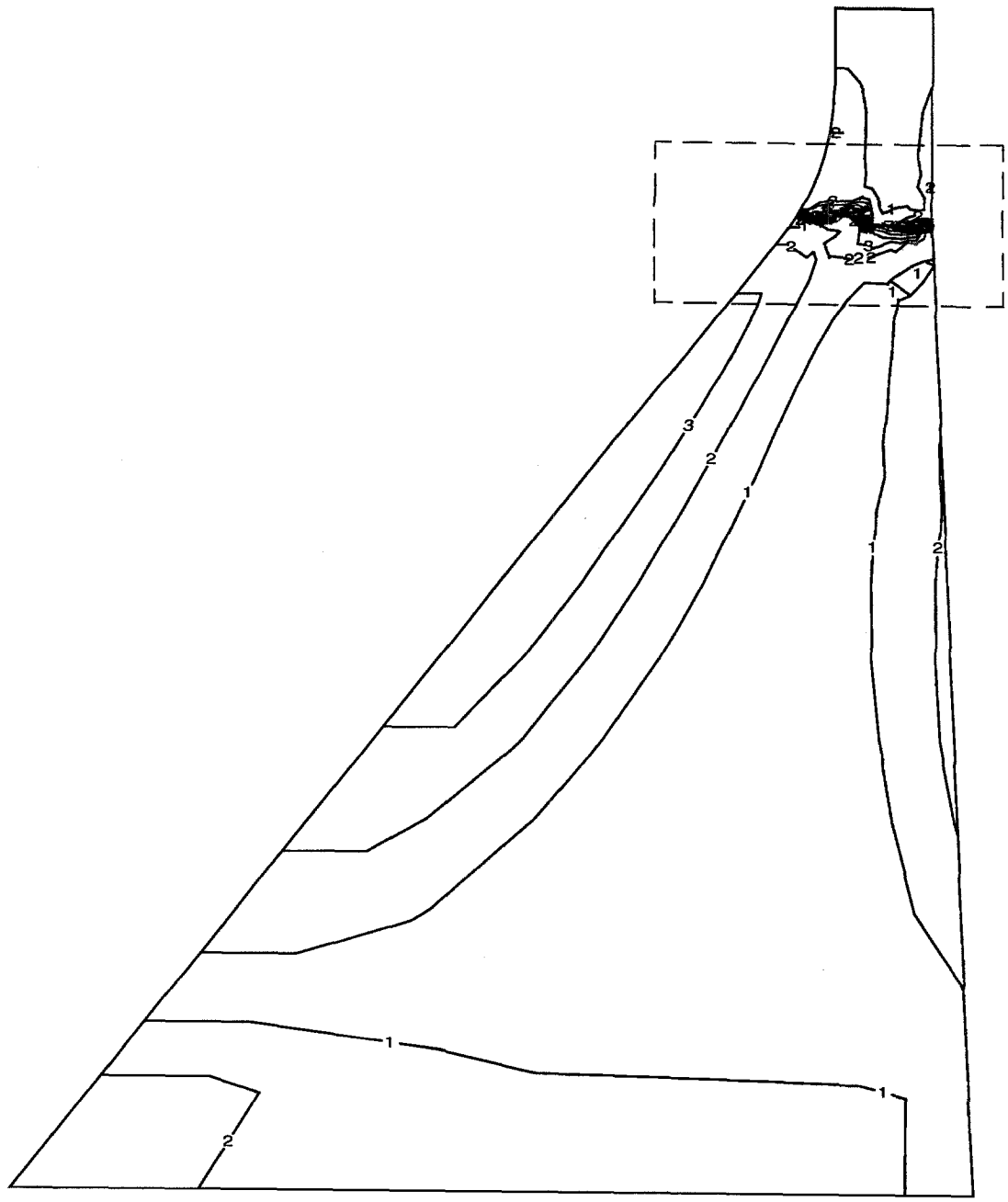

Figure 27c. Contours of maximum principal tensile stress (static plus dynamic). Stress vectors within the boxed region are shown in part d.

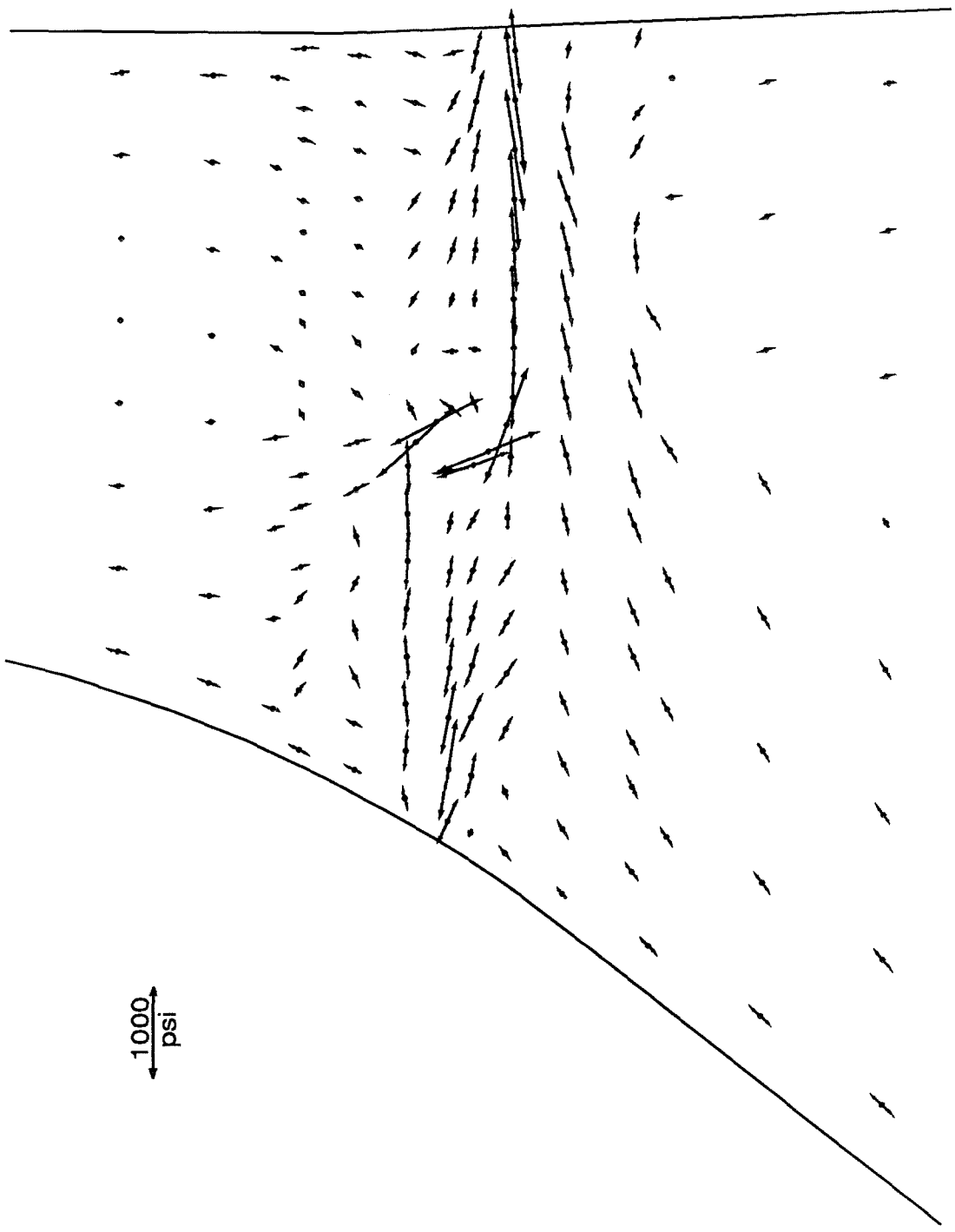

Figure 27d. Vectors of maximum principal tensile stress (static plus dynamic) in the neck region. See part c for region plotted.

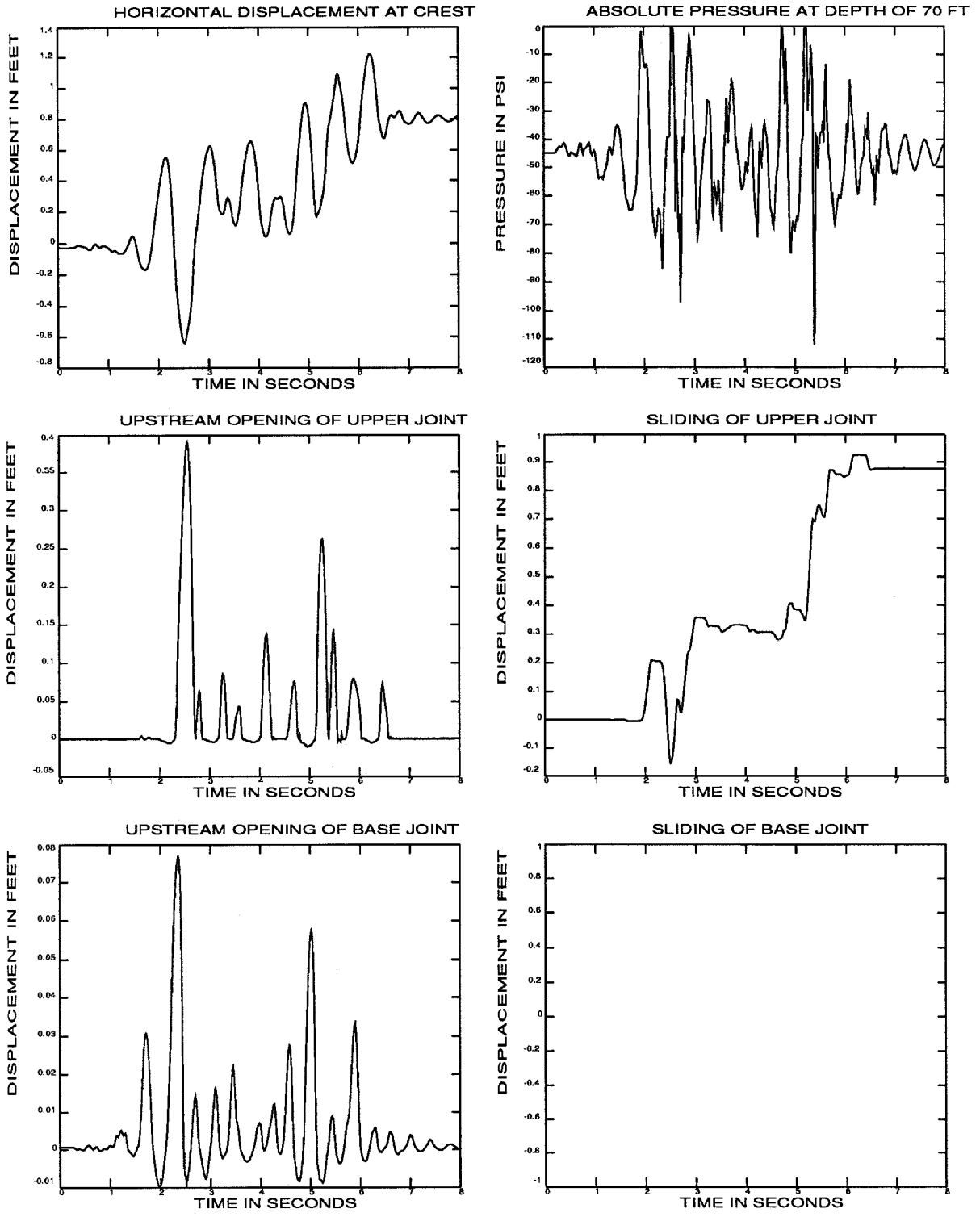

a. Time history responses

Figure 28. Results of earthquake analysis of the dam with an inclined joint, full reservoir and keyed base. The earthquake time scale equals one.

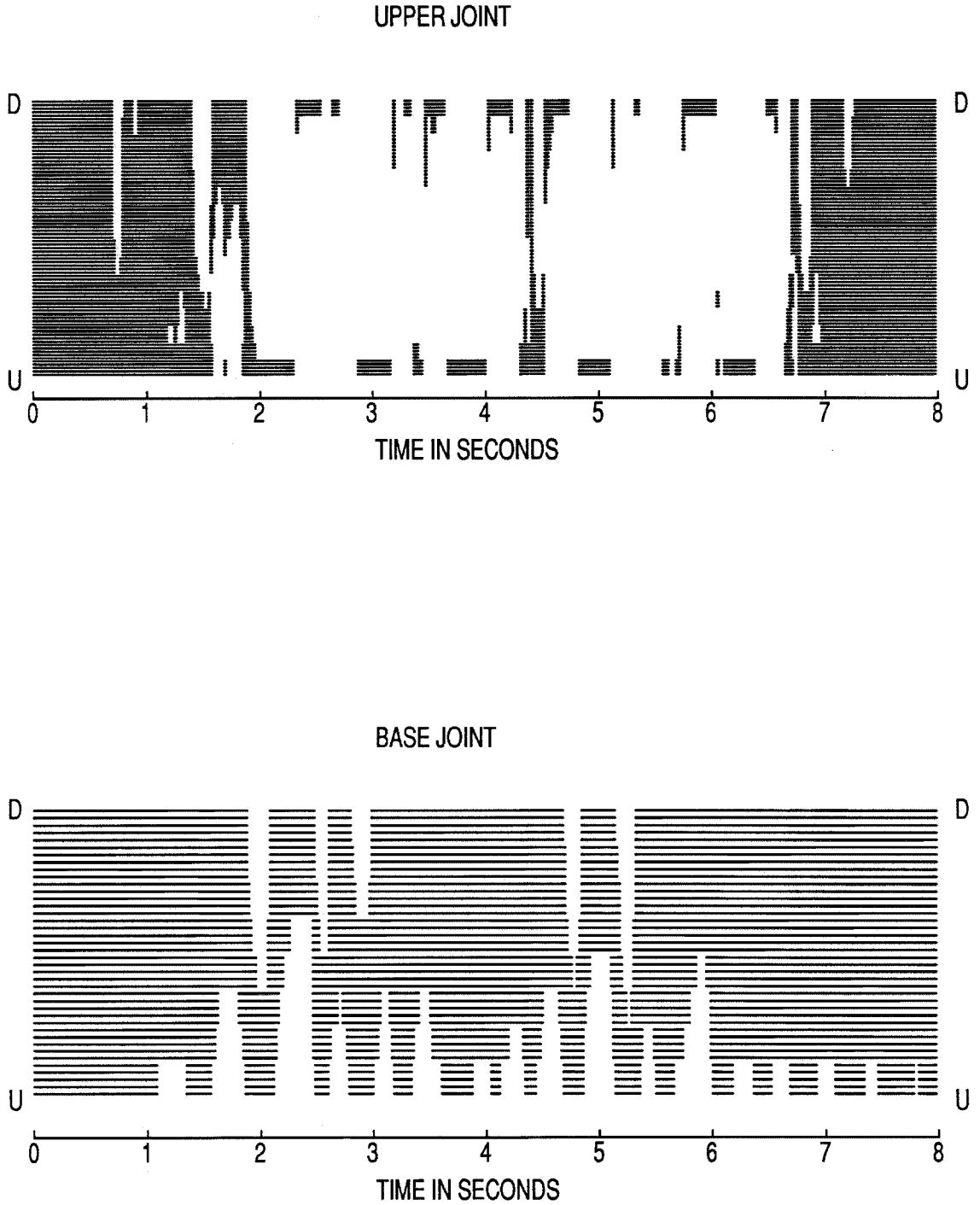

Figure 28b. Contact time histories of joints

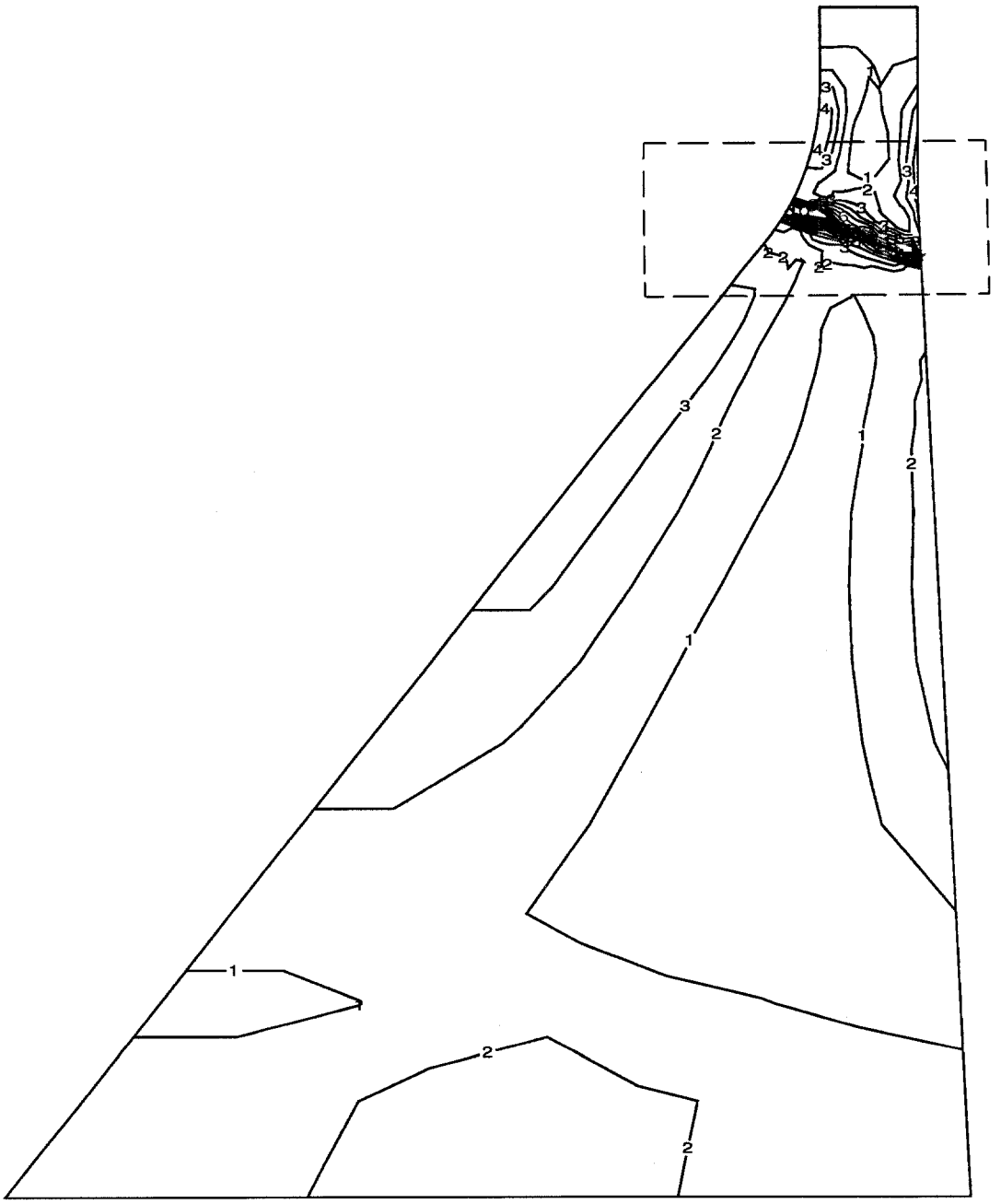

Figure 28c. Contours of maximum principal tensile stress (static plus dynamic). Stress vectors within the boxed region are shown in part d.

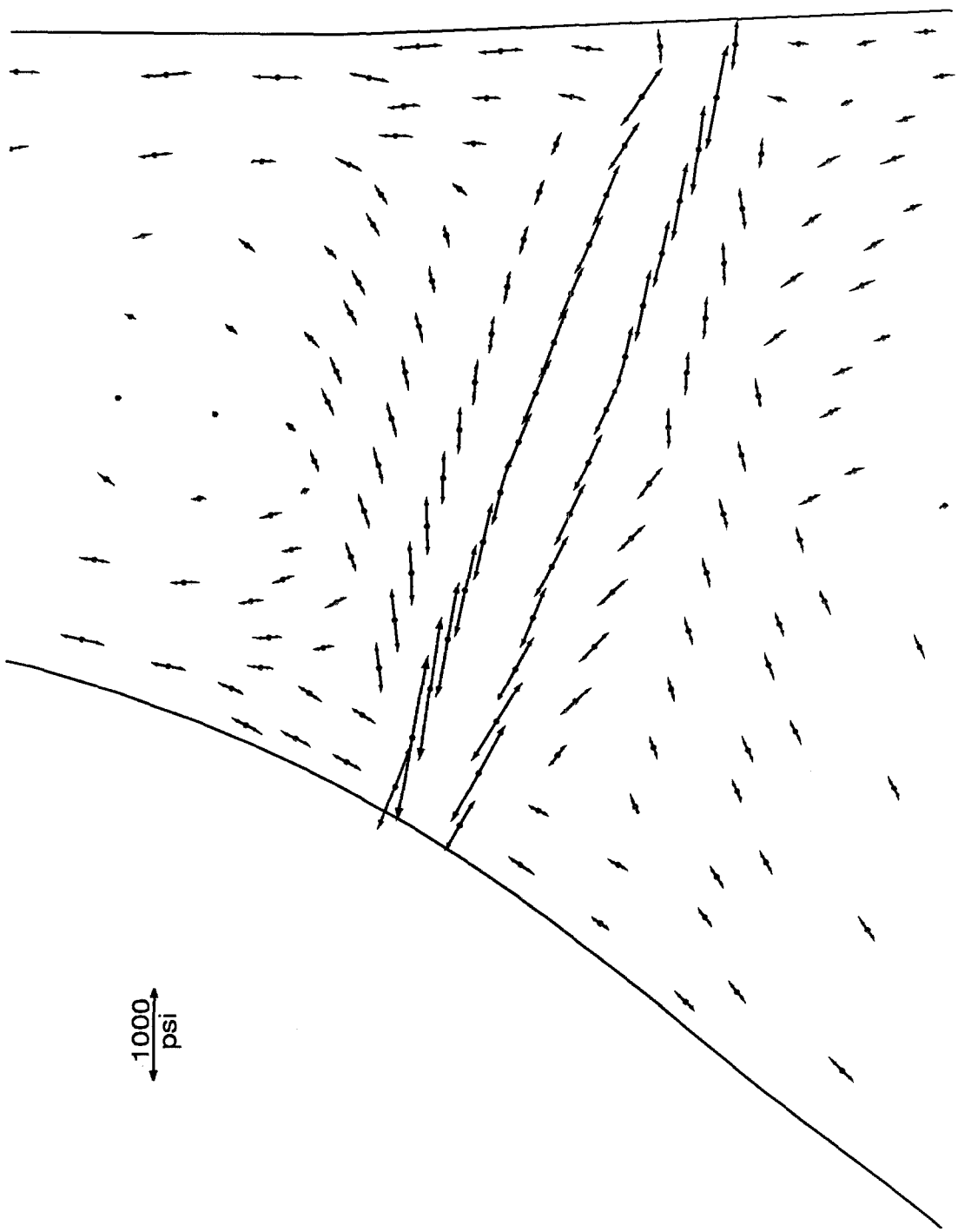

Figure 28d. Vectors of maximum principal tensile stress (static plus dynamic) in the neck region. See part c for region plotted.

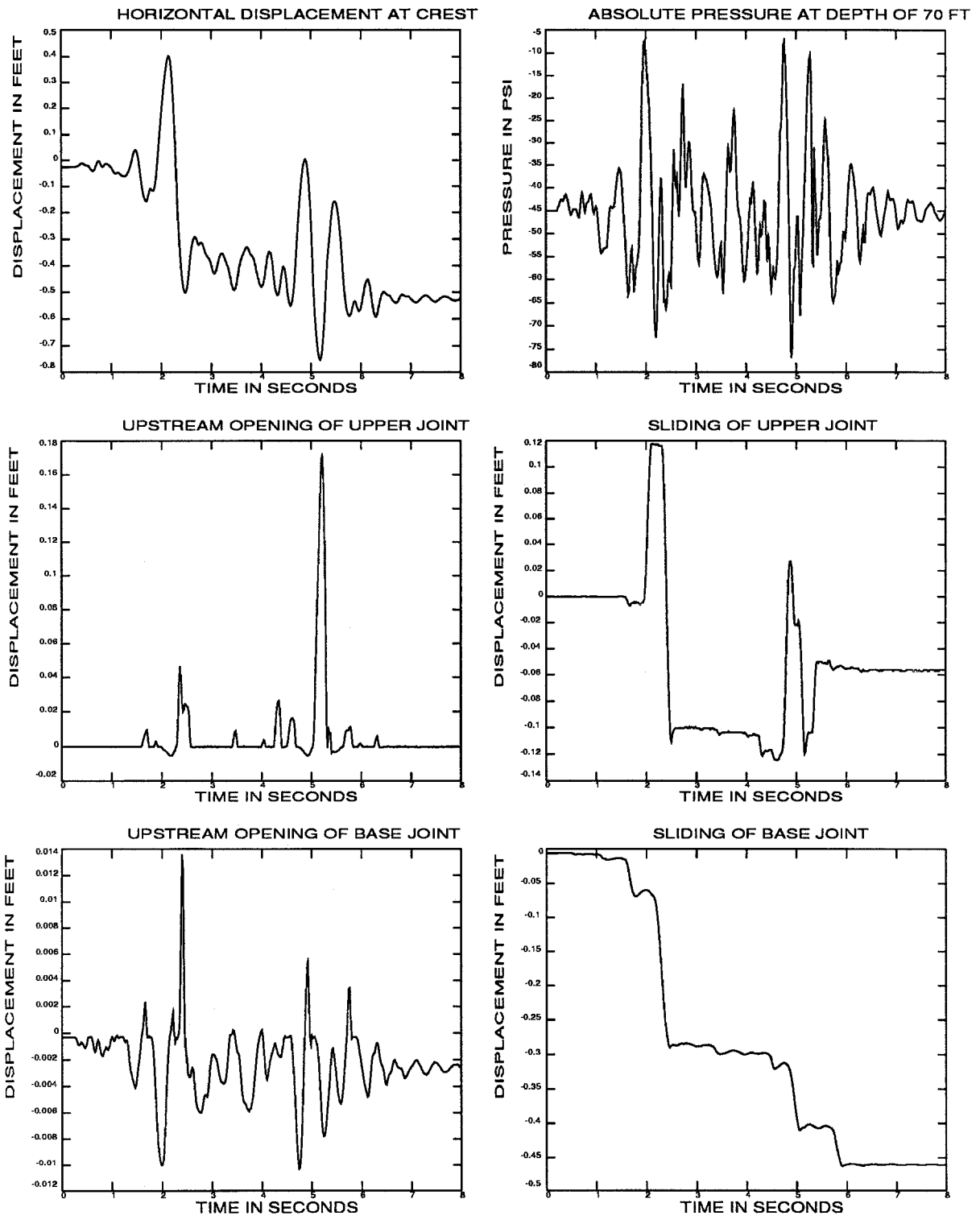

a. Time history responses

Figure 29. Results of earthquake analysis of the dam with an inclined joint, full reservoir and unkeyed base. The earthquake time scale equals one.

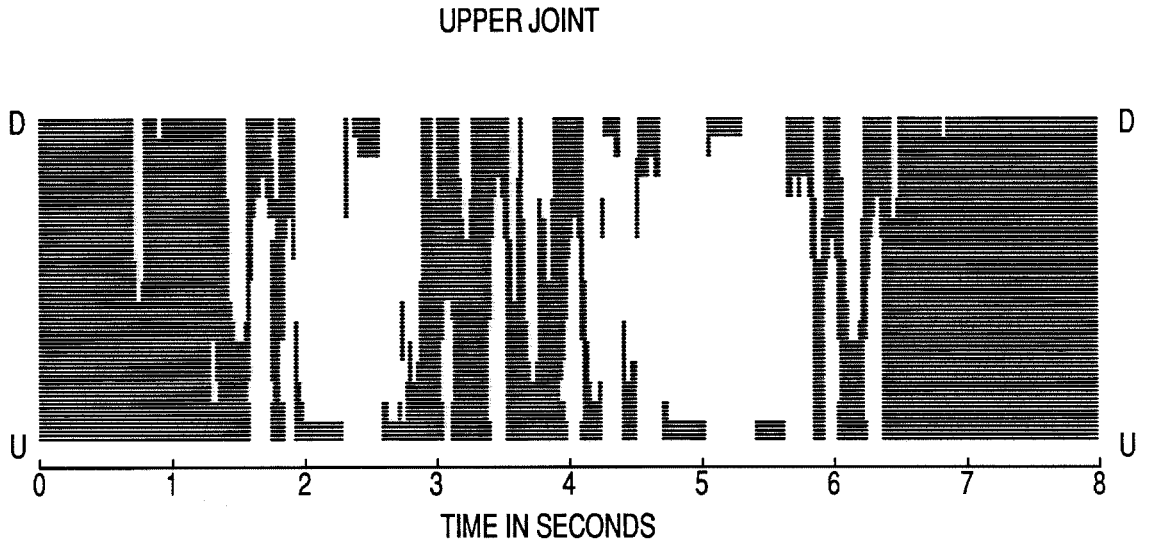

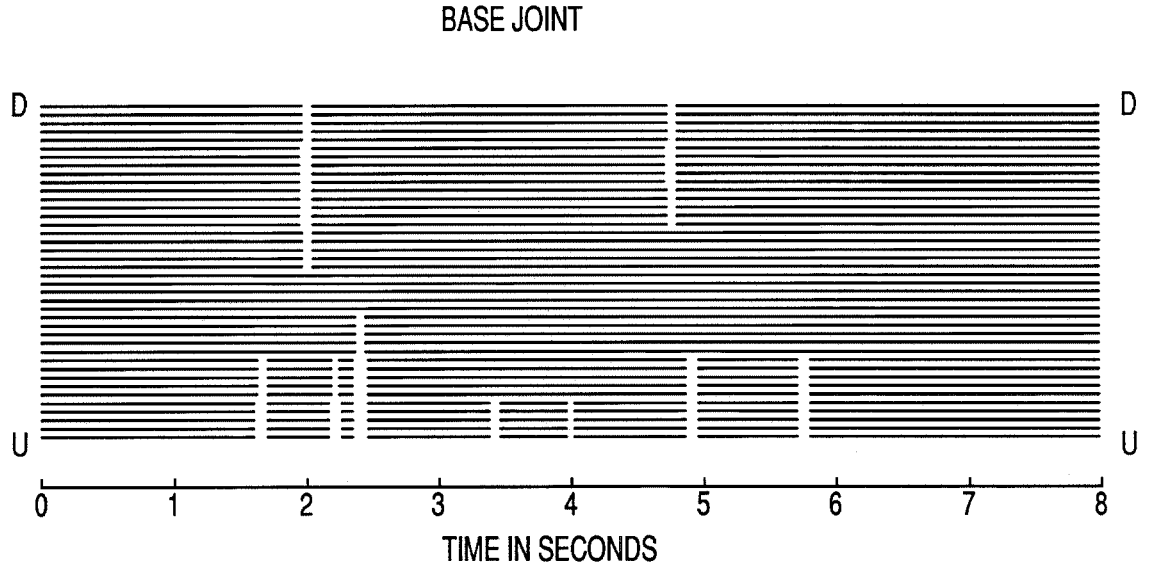

Figure 29b. Contact time histories of joints

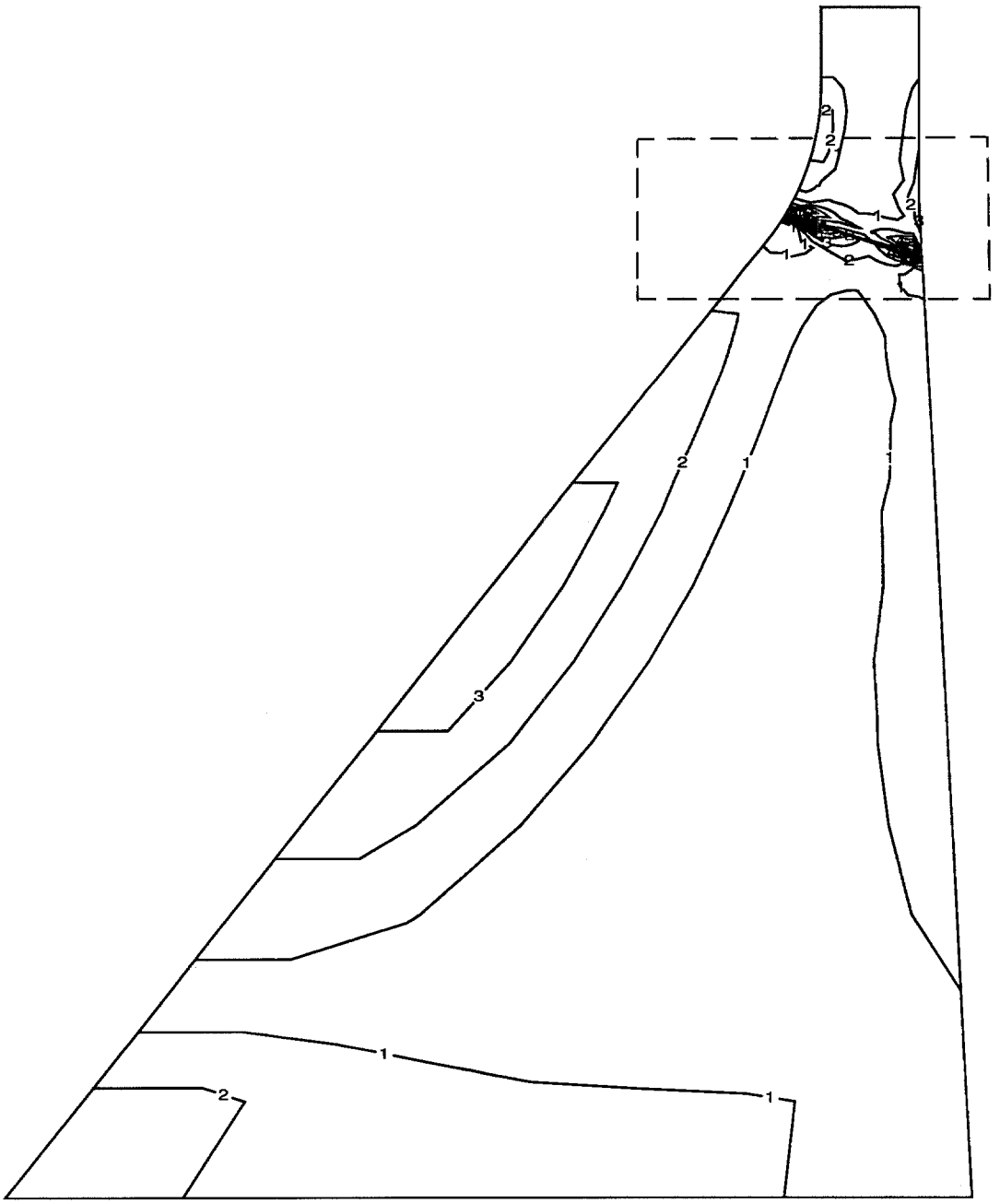

Figure 29c. Contours of maximum principal tensile stress (static plus dynamic). Stress vectors within the boxed region are shown in part d.

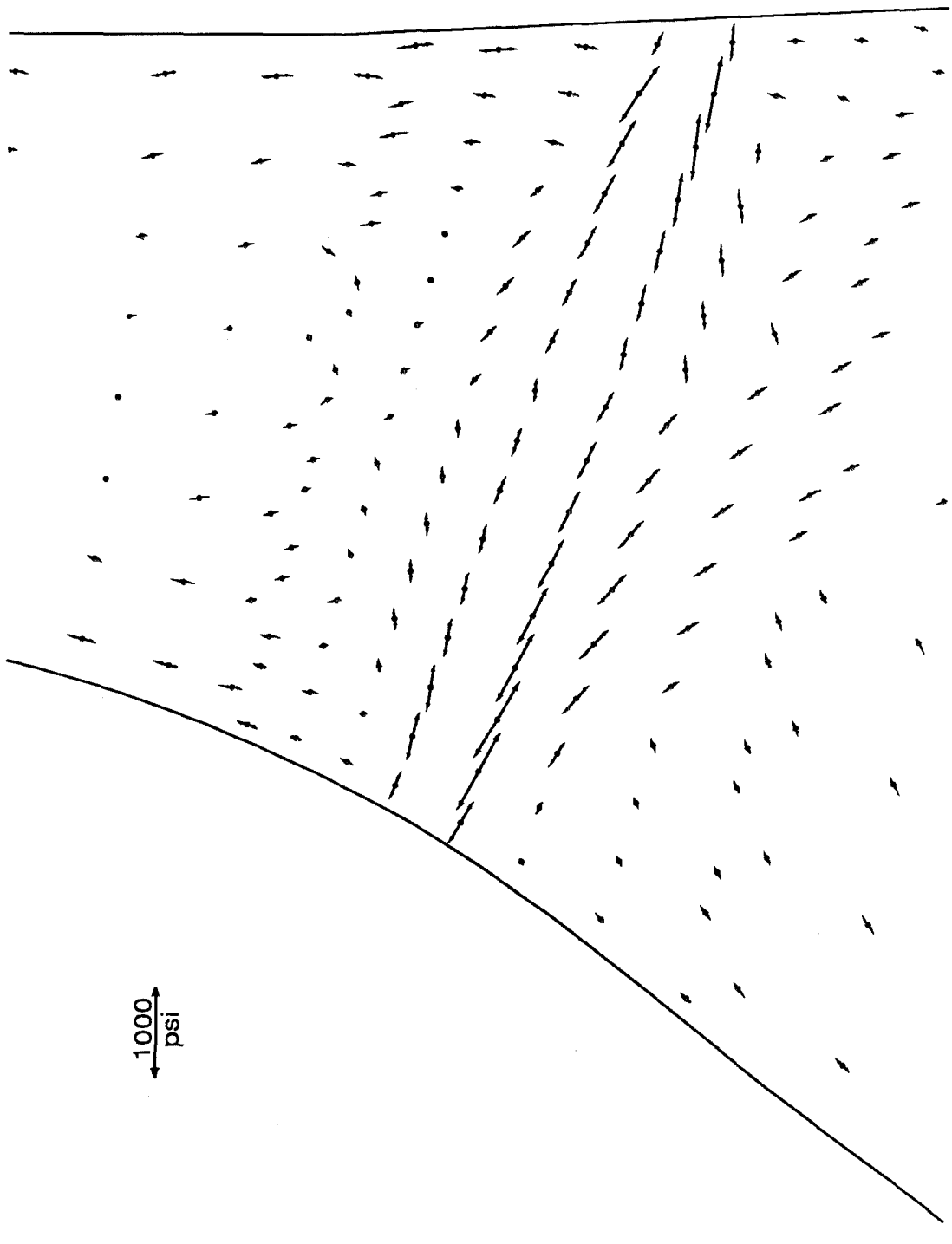

Figure 29d. Vectors of maximum principal tensile stress (static plus dynamic) in the neck region. See part c for region plotted.

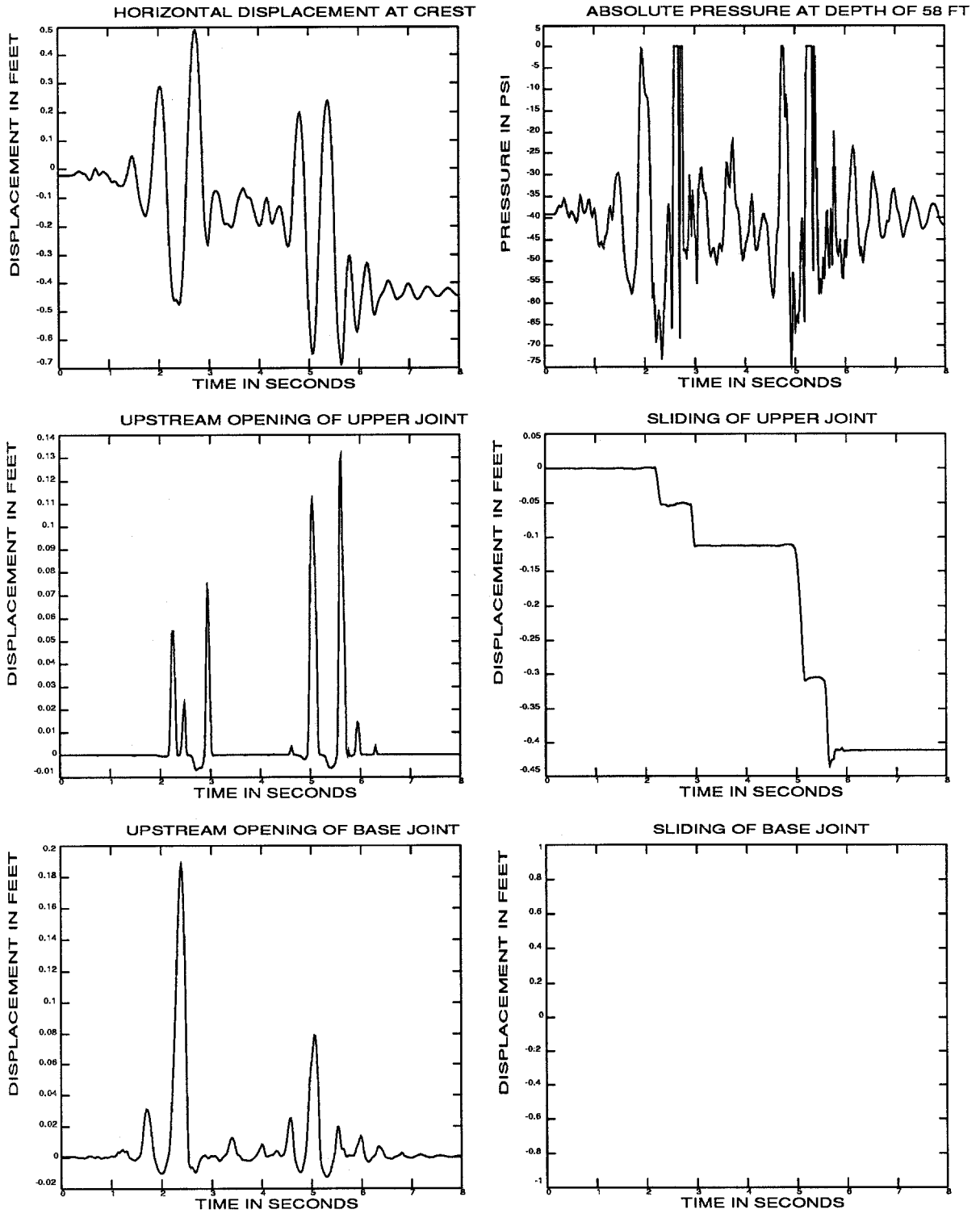

a. Time history responses

Figure 30. Results of earthquake analysis of the prestressed dam with a horizontal joint, full reservoir and keyed base. The earthquake time scale equals one.

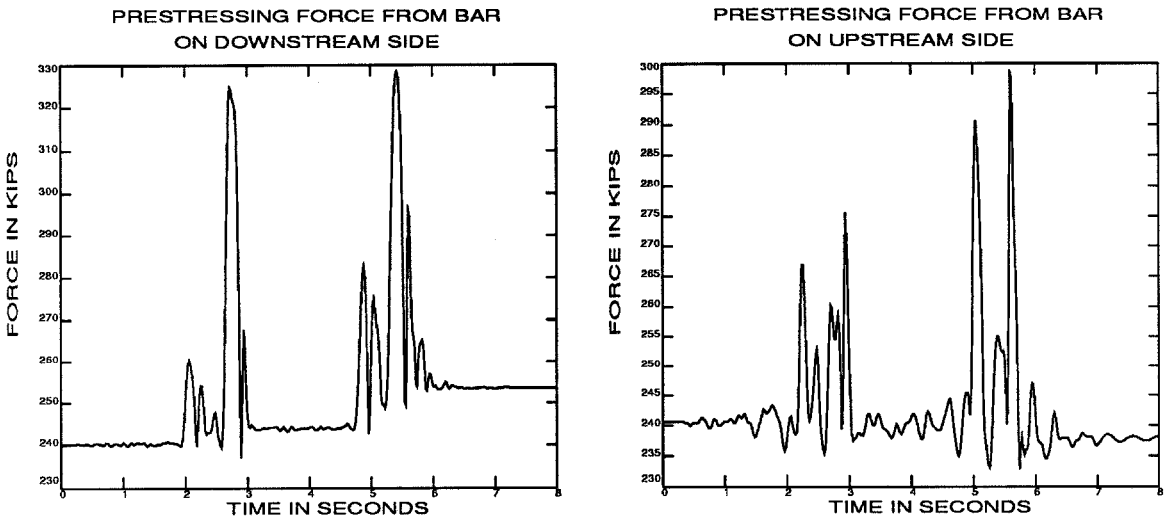

Figure 30a. (Continued)

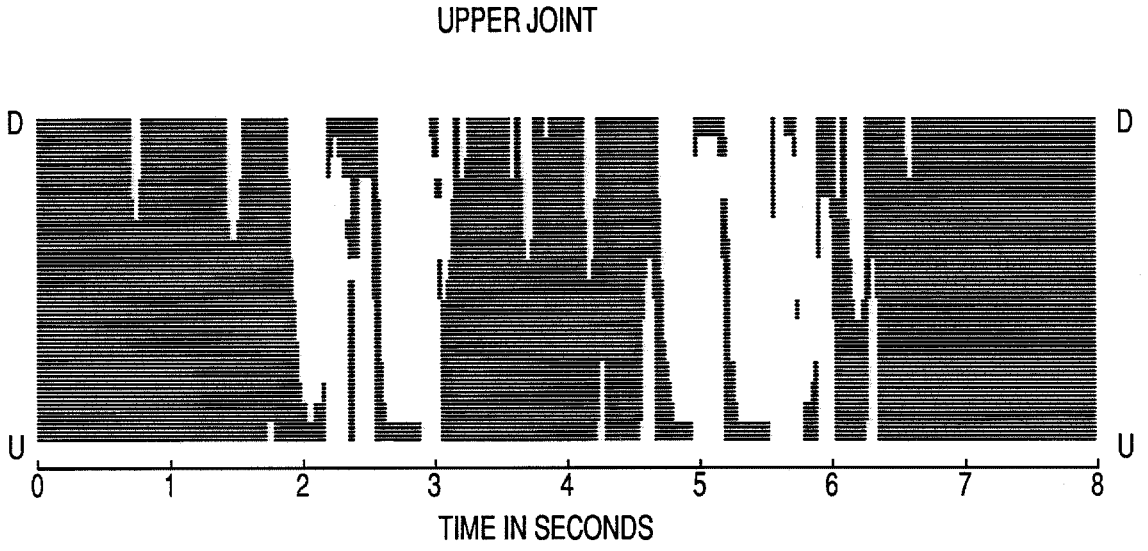

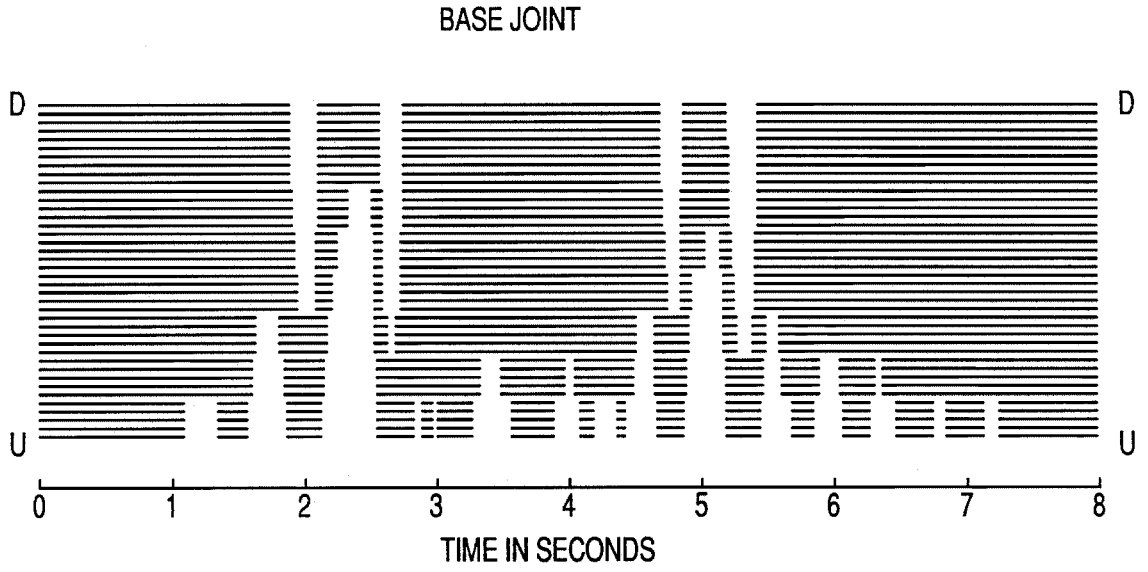

Figure 30b. Contact time histories of joints

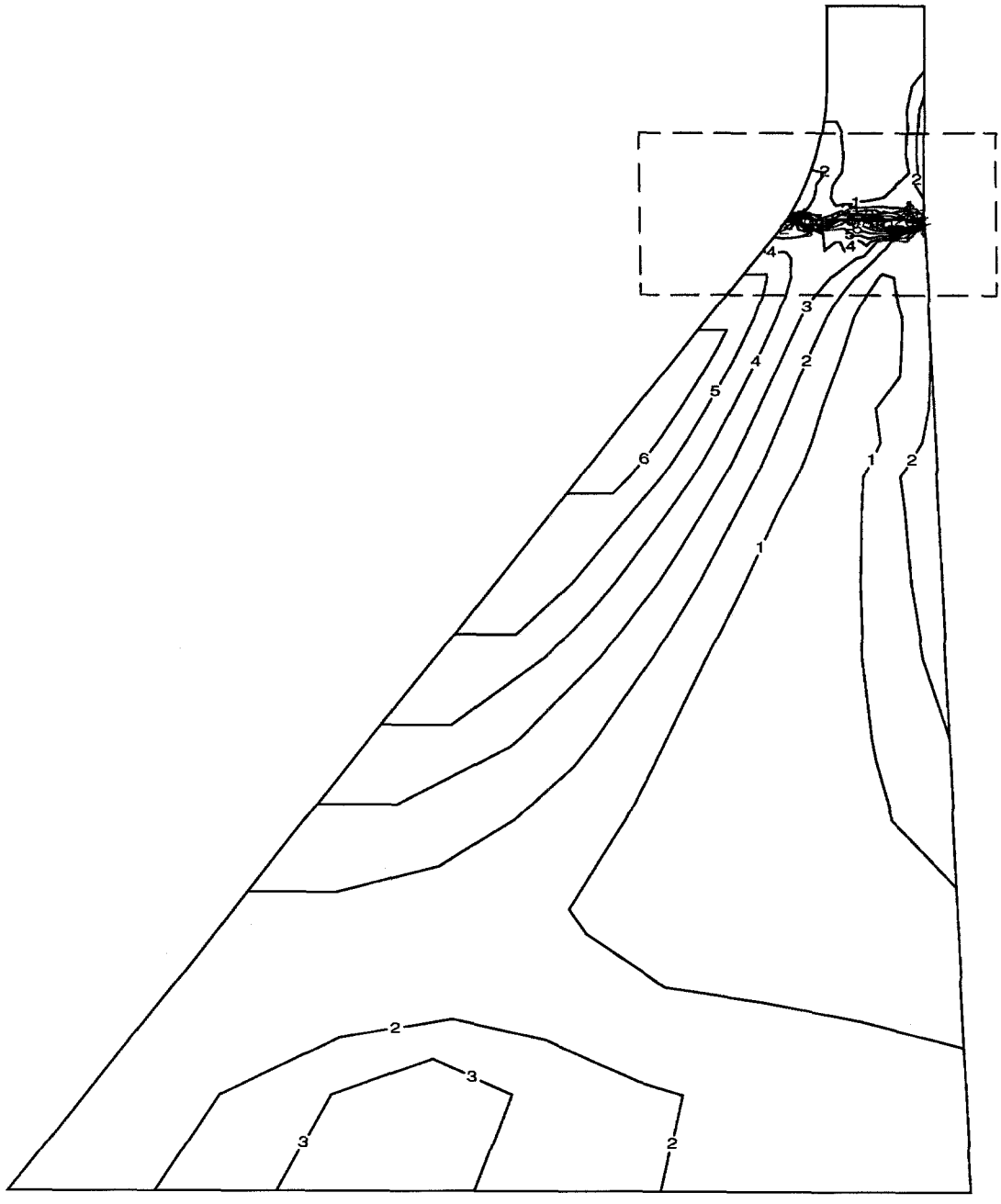

Figure 30c. Contours of maximum principal tensile stress (static plus dynamic). Stress vectors within the boxed region are shown in part d.

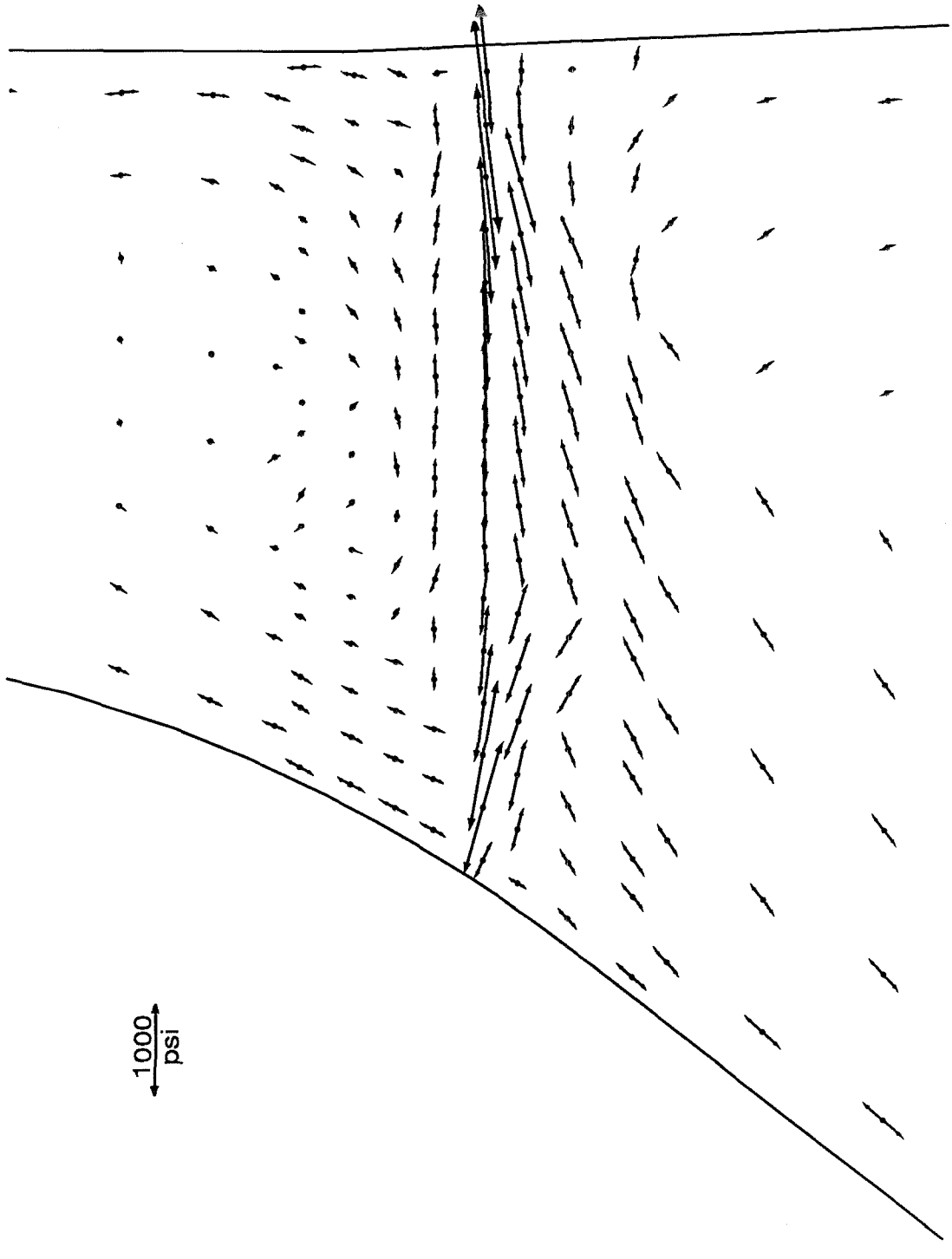

Figure 30d. Vectors of maximum principal tensile stress (static plus dynamic) in the neck region. See part c for region plotted.

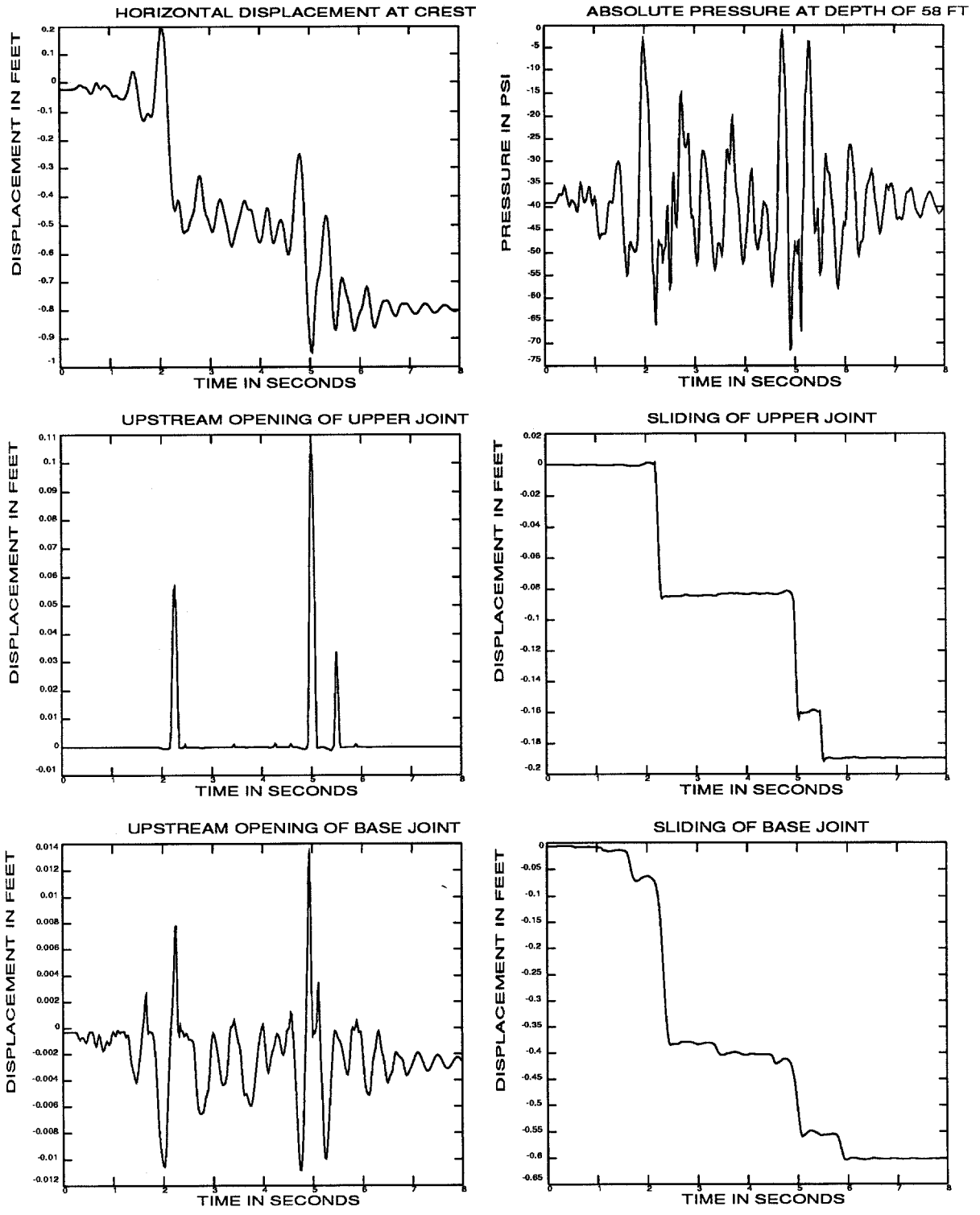

a. Time history responses

Figure 31. Results of earthquake analysis of the prestressed dam with a horizontal joint, full reservoir and unkeyed base. The earthquake time scale equals one.

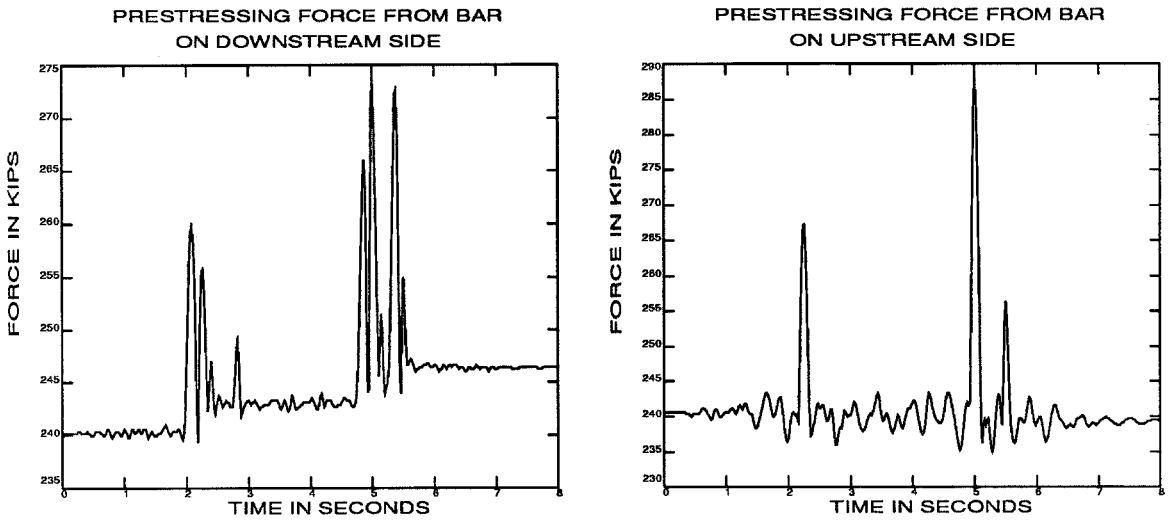

Figure 31a. (Continued)

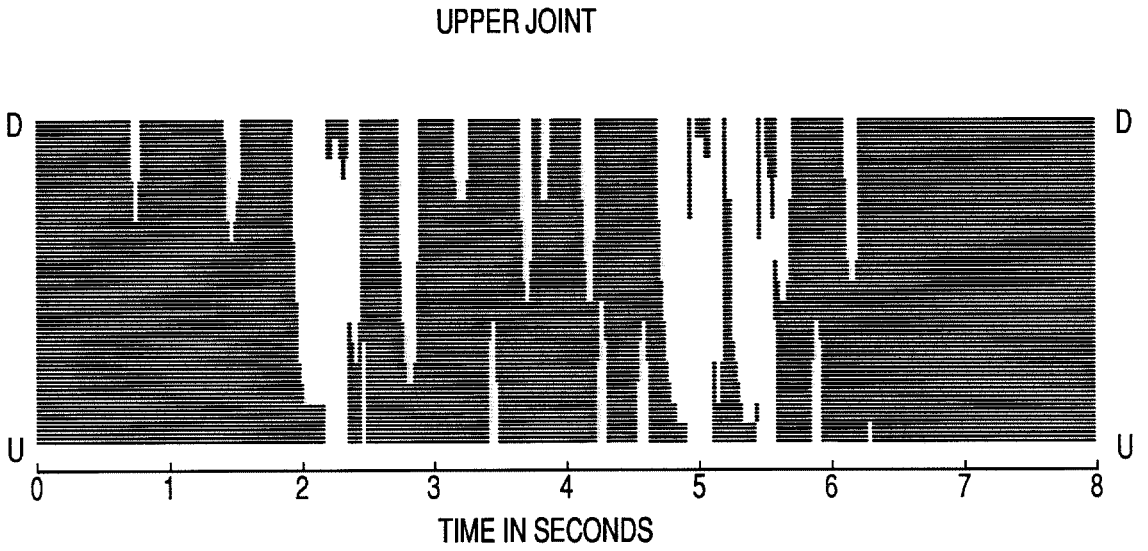

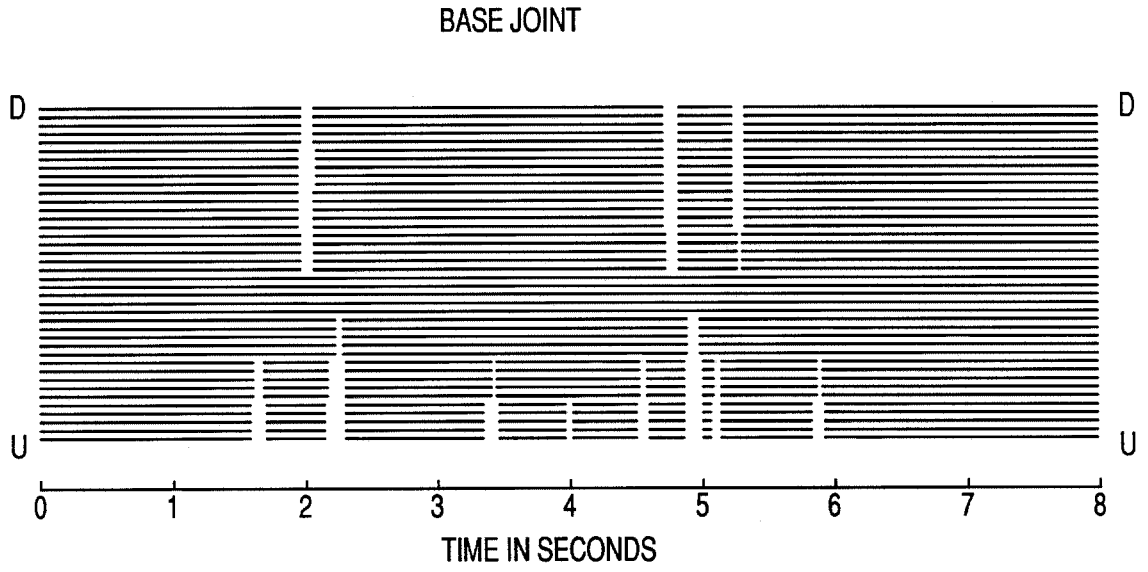

Figure 31b. Contact time histories of joints

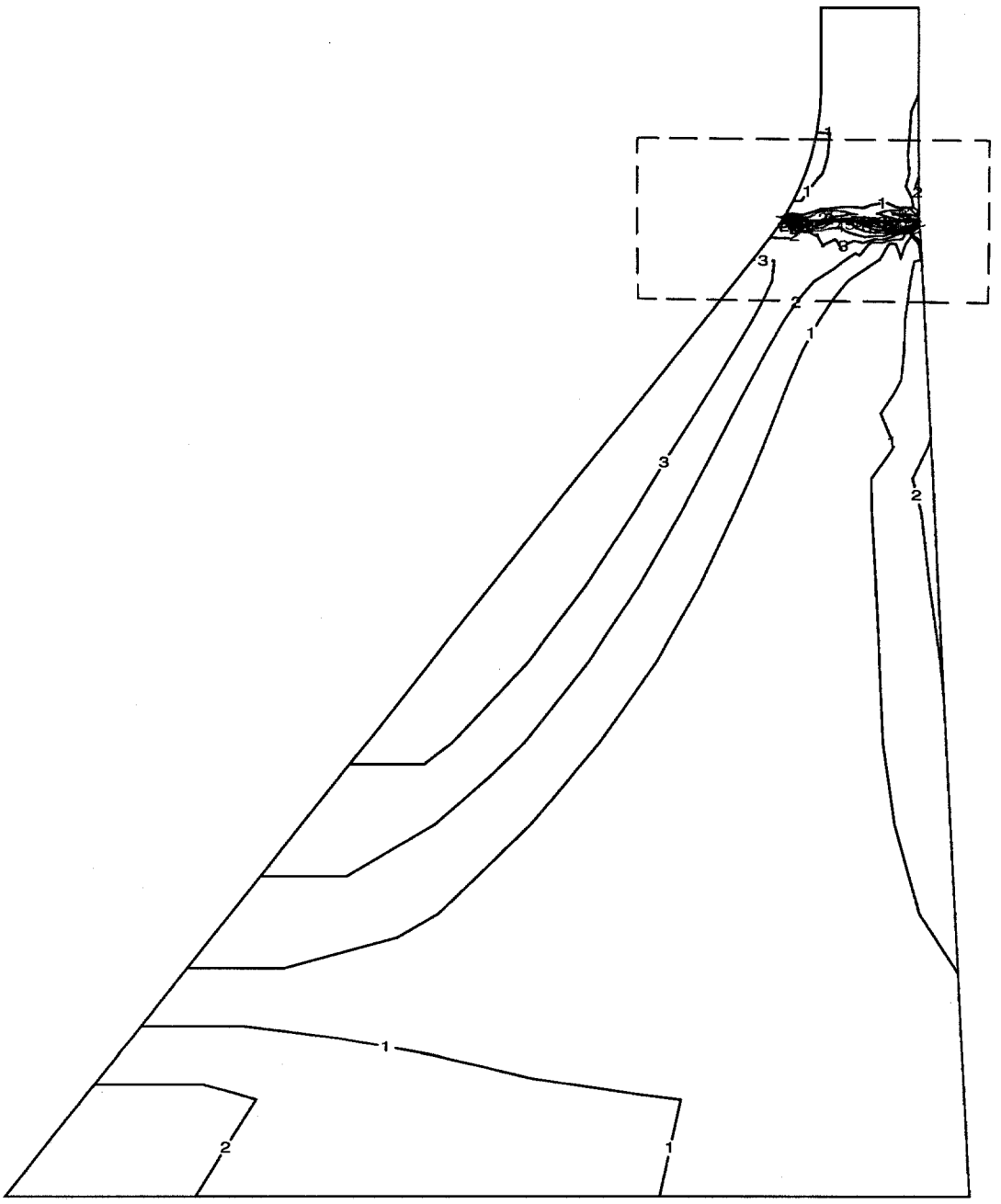

Figure 31c. Contours of maximum principal tensile stress (static plus dynamic). Stress vectors within the boxed region are shown in part d.

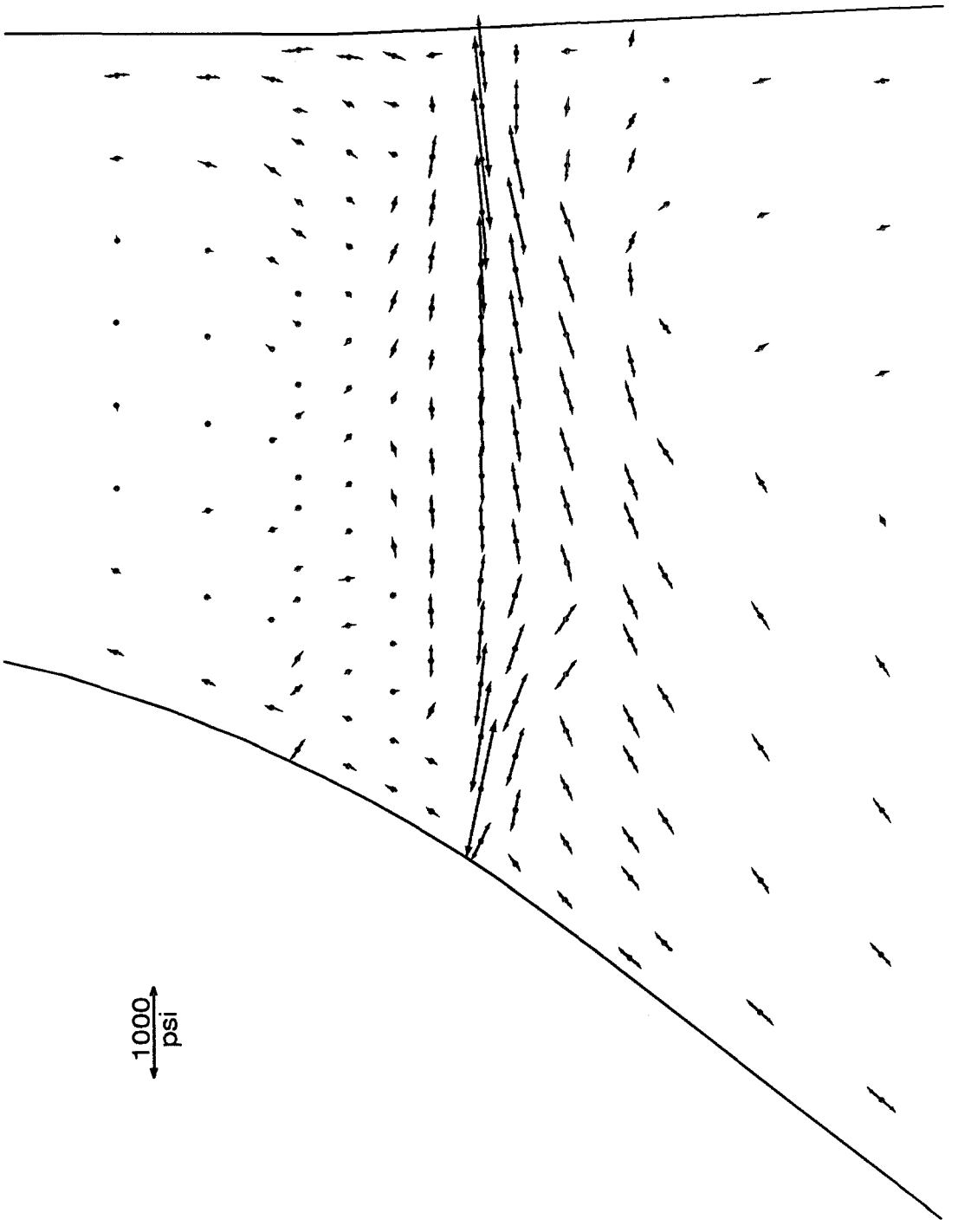

Figure 31d. Vectors of maximum principal tensile stress (static plus dynamic) in the neck region. See part c for region plotted.

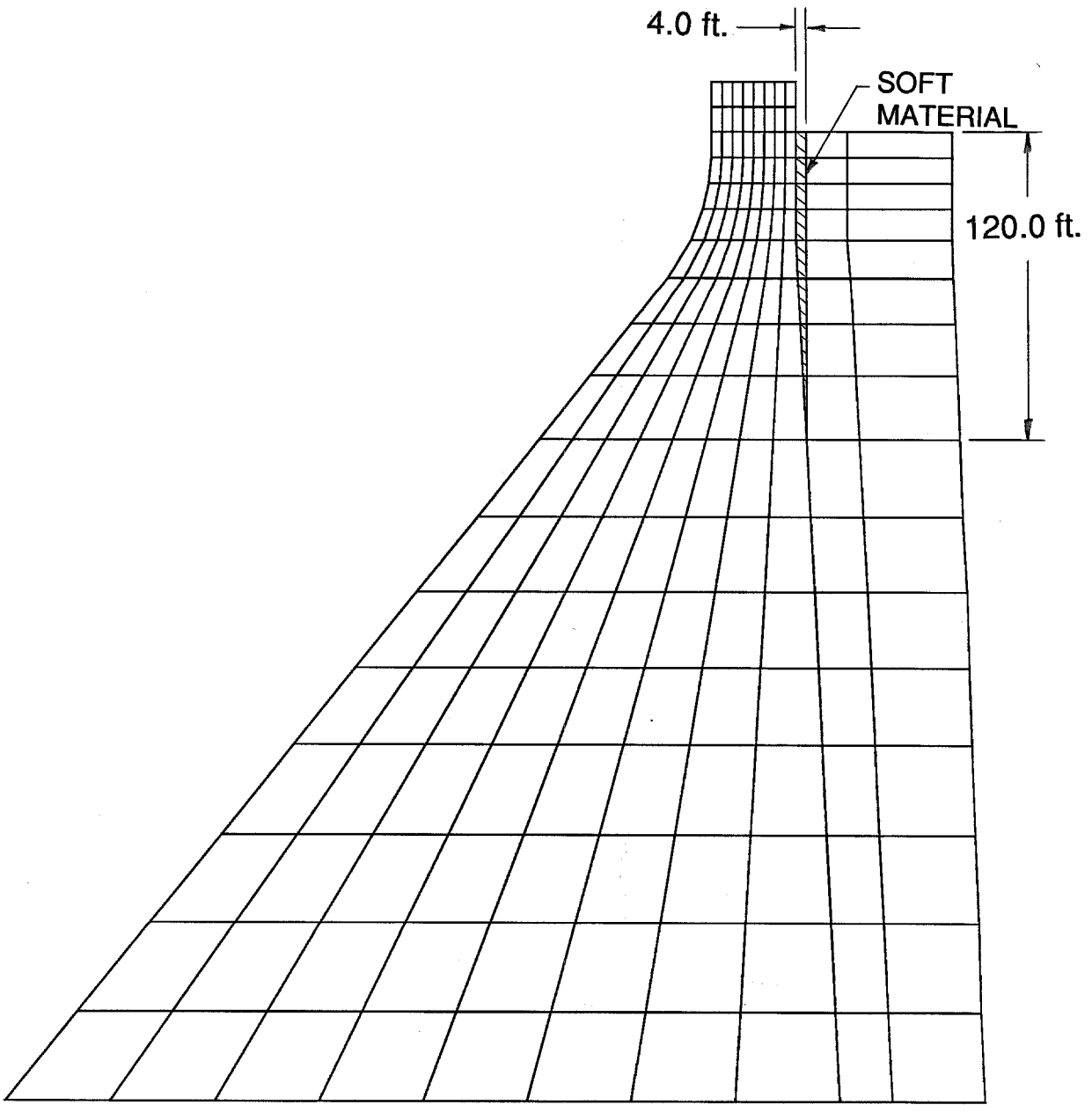

Figure 32. Finite element mesh of Pine Flat Dam and water with soft material adjacent to the dam face.

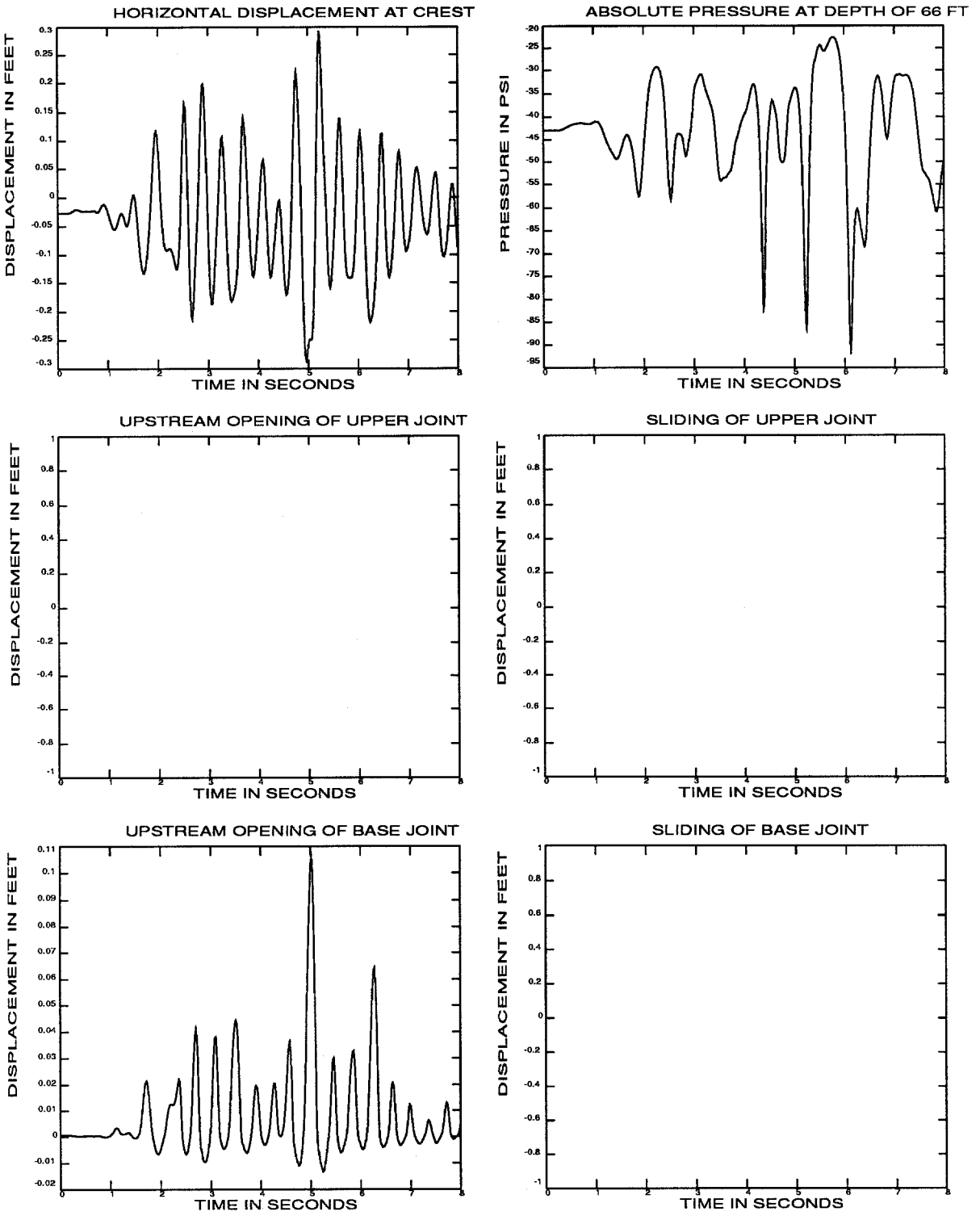

a. Time history responses

Figure 33. Results of earthquake analysis of Pine Flat Dam with full reservoir and keyed base and isolated with a layer of soft material. The earthquake time scale equals one.

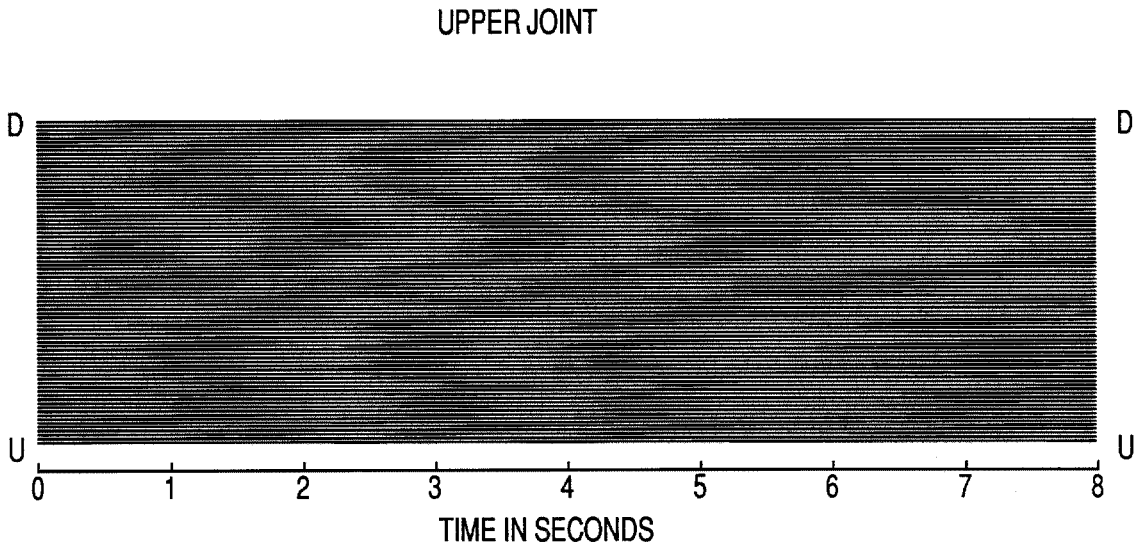

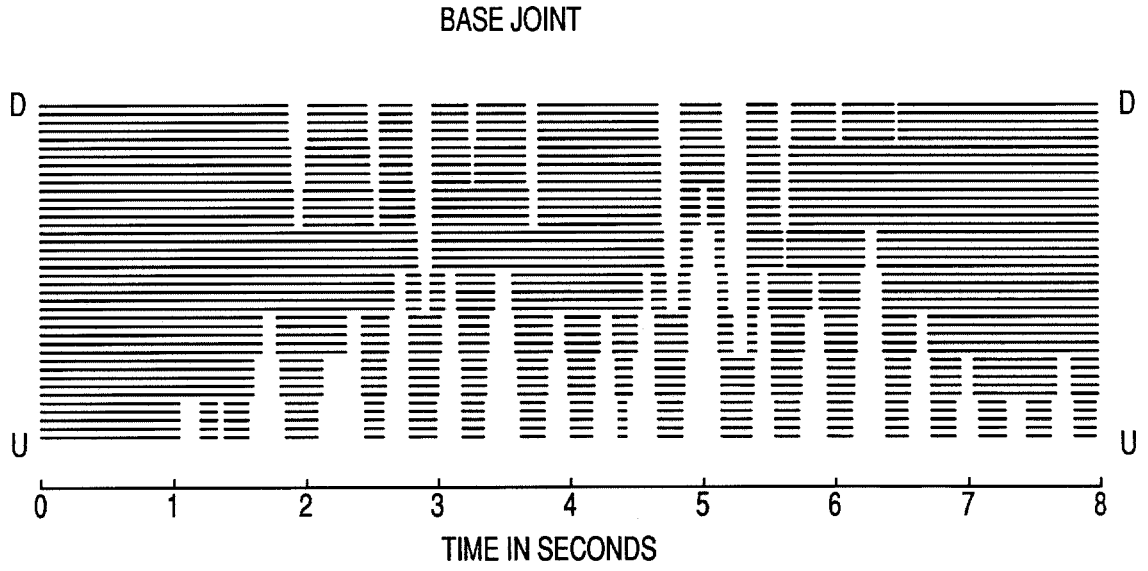

Figure 33b. Contact time histories of joints

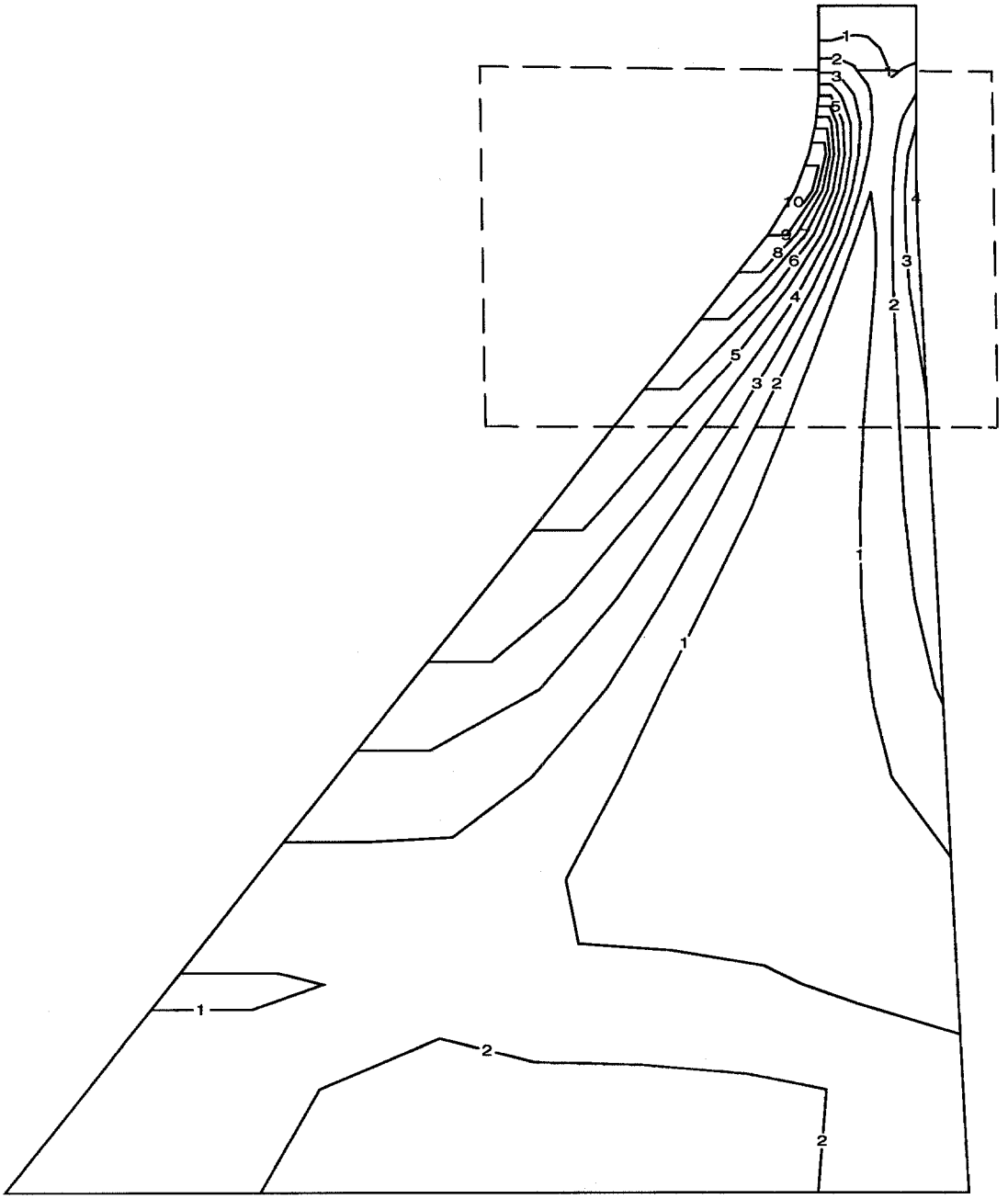

Figure 33c. Contours of maximum principal tensile stress (static plus dynamic). Stress vectors within the boxed region are shown in part d.

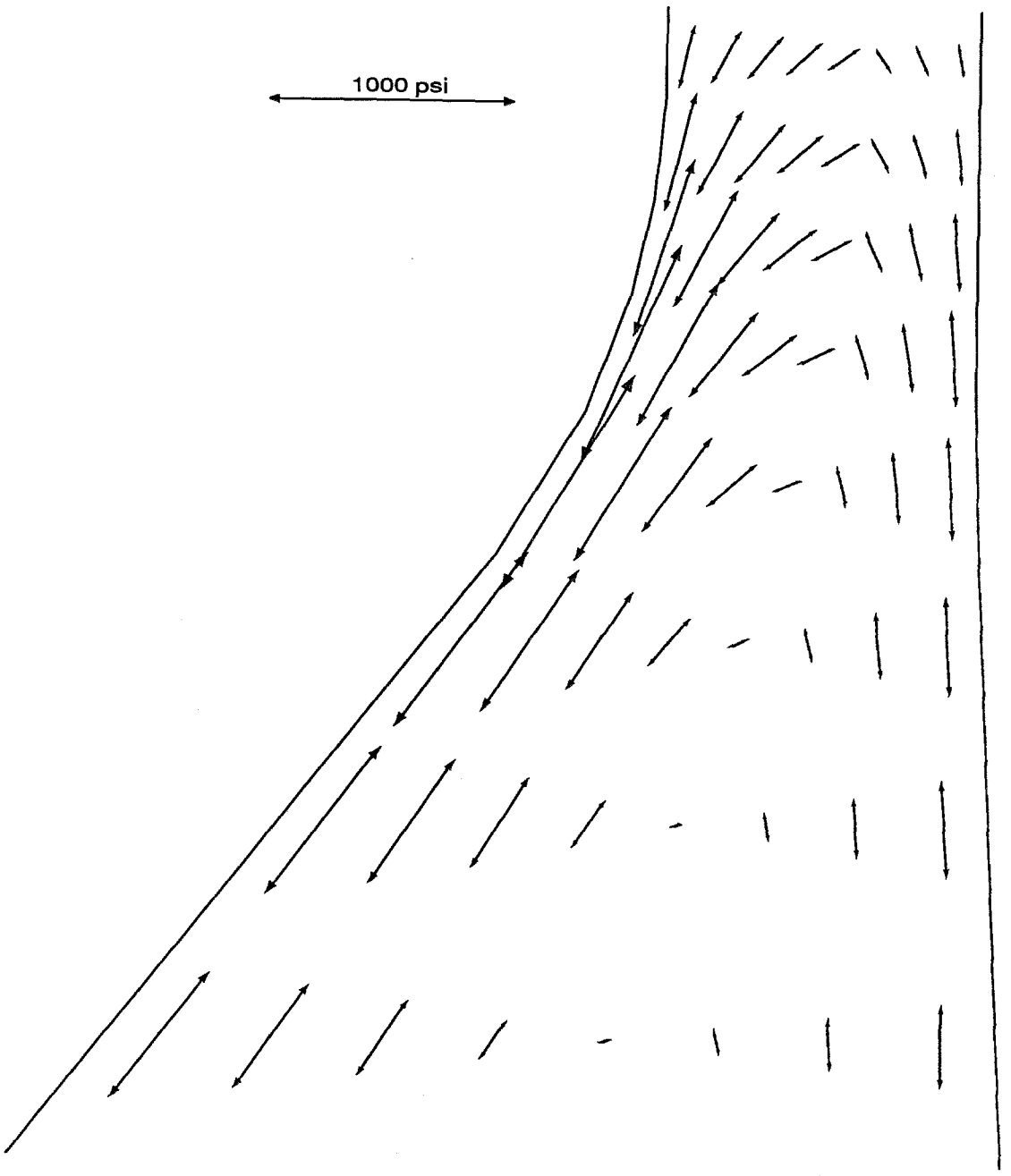

Figure 33d. Vectors of maximum principal tensile stress (static plus dynamic) in the neck region. See part c for region plotted.

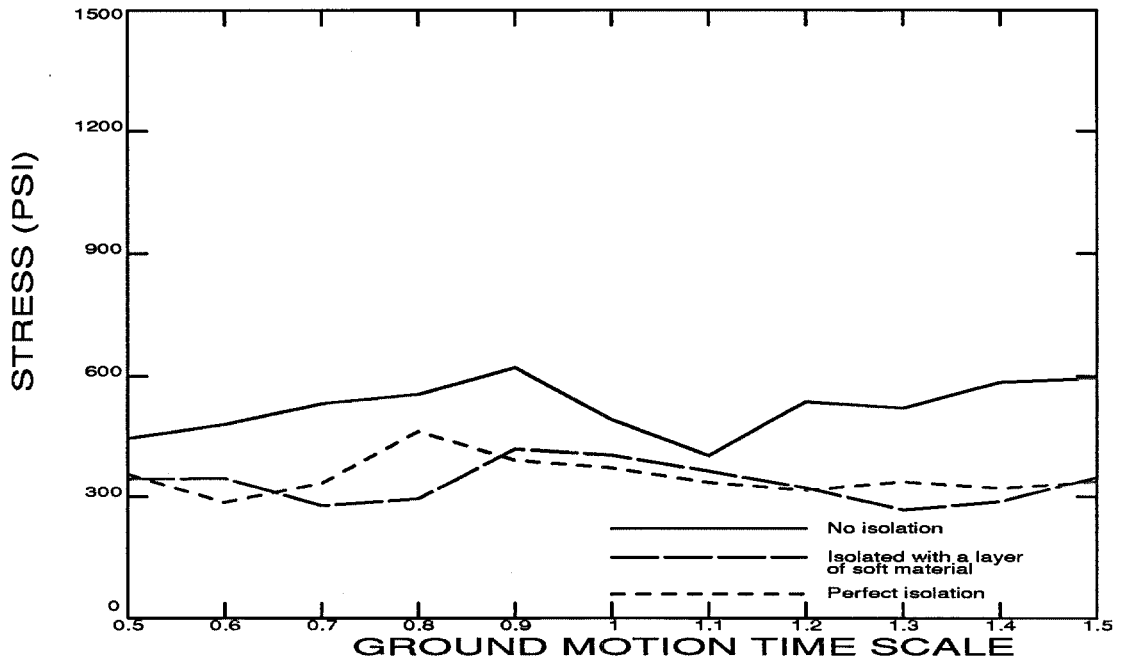

a. Upstream face

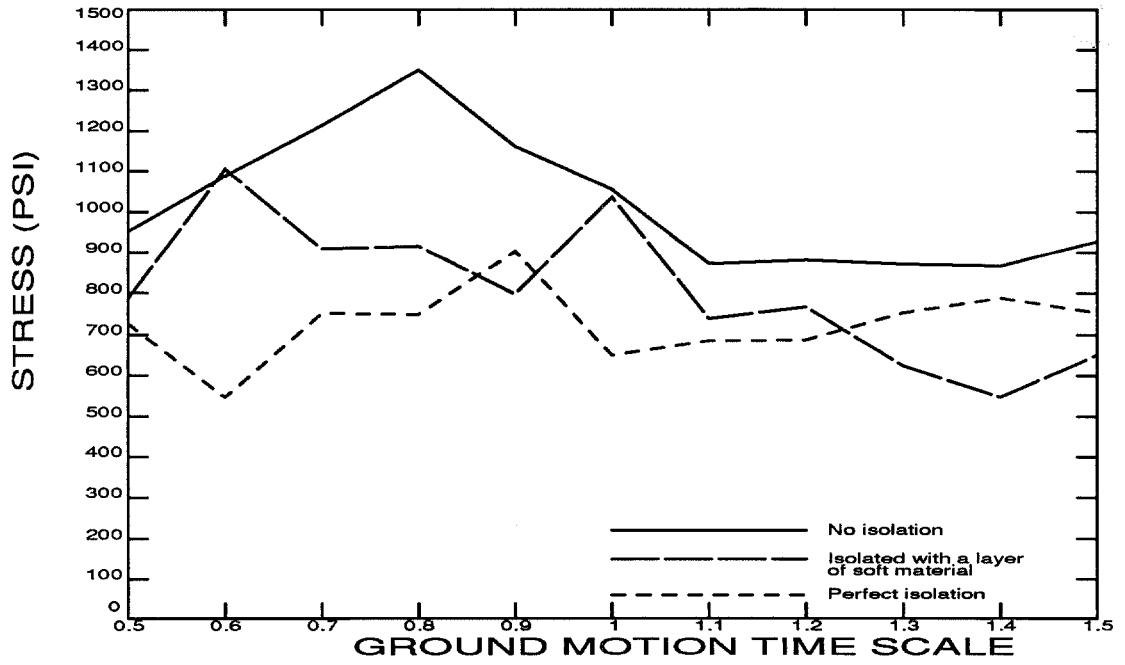

b. Downstream face

Figure 34. Maximum principal tensile stresses (static plus dynamic) as a function of ground motion time scale that occur at the faces of Pine Flat Dam with and without hydrodynamic isolation — full reservoir and keyed base.

CALIFORNIA INSTITUTE OF TECHNOLOGY

Reports Published

by

Earthquake Engineering Research Laboratory (EERL)*

Dynamics Laboratory (DYNL)

Disaster Research Center (DRC)

Soil Mechanics Laboratory (SML)

Note: Numbers in parenthesis are Accession Numbers assigned by the National Technical Information Service; these reports may be ordered from the National Technical Information Service, 5285 Port Royal Road, Springfield, Virginia, 22161. Accession Numbers should be quoted on orders for reports (PB — —). Reports without this information either have not been submitted to NTIS or the information was not available at the time of printing. An N/A in parenthesis indicates that the report is no longer available at Caltech.

1. Alford, J.L., G.W. Housner and R.R. Martel, "Spectrum Analysis of Strong-Motion Earthquake," 1951. (Revised August 1964). (N/A)
2. Housner, G.W., "Intensity of Ground Motion During Strong Earthquakes," 1952. (N/A)
3. Hudson, D.E., J.L. Alford and G.W. Housner, "Response of a Structure to an Explosive Generated Ground Shock," 1952. (N/A)
4. Housner, G.W., "Analysis of the Taft Accelerogram of the Earthquake of 21 July 1952." (N/A)
5. Housner, G.W., "A Dislocation Theory of Earthquakes," 1953. (N/A)
6. Caughey, T.K. and D.E. Hudson, "An Electric Analog Type Response Spectrum," 1954. (N/A)
7. Hudson, D.E. and G.W. Housner, "Vibration Tests of a Steel-Frame Building," 1954. (N/A)
8. Housner, G.W., "Earthquake Pressures on Fluid Containers," 1954. (N/A)
9. Hudson, D.E., "The Wilmot Survey Type Strong-Motion Earthquake Recorder," 1958. (N/A)
10. Hudson, D.E. and W.D. Iwan, "The Wilmot Survey Type Strong-Motion Earthquake Recorder, Part II," 1960. (N/A)
11. Caughey, T.K., D.E. Hudson and R.V. Powell, "The CIT Mark II Electric Analog Type Response Spectrum Analyzer for Earthquake Excitation Studies," 1960. (N/A)
12. Keightley, W.O., G.W. Housner and D.E. Hudson, "Vibration Tests of the Encino Dam Intake Tower," 1961. (N/A)
13. Merchant, H.C., "Mode Superposition Methods Applied to Linear Mechanical Systems Under Earthquake Type Excitation," 1961. (N/A)

---

* **To order directly by phone, the number is (703) 487–4650.**

14. Iwan, W.D., "The Dynamic Response of Bilinear Hysteretic Systems," 1961. (N/A)

15. Hudson, D.E., "A New Vibration Exciter for Dynamic Test of Full-Scale Structures," 1961. (N/A)

16. Hudson, D.E., "Synchronized Vibration Generators for Dynamic Tests of Full-Scale Structures," 1962. (N/A)

17. Jennings, P.C., "Velocity Spectra of the Mexican Earthquakes of 11 May and 19 May 1962," 1962. (N/A)

18. Jennings, P.C., "Response of Simple Yielding Structures to Earthquake Excitation," 1963. (N/A)

19. Keightley, W.O., "Vibration Tests of Structures," 1963. (N/A)

20. Caughey, T.K. and M.E.J. O'Kelly, "General Theory of Vibration of Damped Linear Dynamic Systems," 1963. (N/A)

21. O'Kelly, M.E.J., "Vibration of Viscously Damped Linear Dynamic Systems," 1964. (N/A)

22. Nielsen, N.N., "Dynamic Response of Multistory Buildings," 1964. (N/A)

23. Tso, W.K., "Dynamics of Thin-Walled Beams of Open Section," 1964. (N/A)

24. Keightley, W.O., "A Dynamic Investigation of Bouquet Canyon Dam," 1964. (N/A)

25. Malhotra, R.K., "Free and Forced Oscillations of a Class of Self-Excited Oscillators," 1964.

26. Hanson, R.D., "Post-Elastic Response of Mild Steel Structures," 1965.

27. Masri, S.F., "Analytical and Experimental Studies of Impact Dampers," 1965.

28. Hanson, R.D., "Static and Dynamic Tests of a Full-Scale Steel-Frame Structures," 1965.

29. Cronin, D.L., "Response of Linear, Viscous Damped Systems to Excitations Having Time-Varying Frequency," 1965.

30. Hu, P.Y.-F., "Analytical and Experimental Studies of Random Vibration," 1965.

31. Crede, C.E., "Research on Failure of Equipment when Subject to Vibration," 1965.

32. Lutes, L.D., "Numerical Response Characteristics of a Uniform Beam Carrying One Discrete Load," 1965. (N/A)

33. Rocke, R.D., "Transmission Matrices and Lumped Parameter Models for Continuous Systems," 1966. (N/A)

34. Brady, A.G., "Studies of Response to Earthquake Ground Motion," 1966. (N/A)

35. Atkinson, J.D., "Spectral Density of First Order Piecewise Linear Systems Excited by White Noise," 1967. (N/A)

36. Dickerson, J.R., "Stability of Parametrically Excited Differential Equations," 1967. (N/A)

37. Giberson, M.F., "The Response of Nonlinear Multi-Story Structures Subjected to Earthquake Excitation," 1967. (N/A)

38. Hallanger, L.W., "The Dynamic Stability of an Unbalanced Mass Exciter," 1967.

39. Husid, R., "Gravity Effects on the Earthquake Response of Yielding Structures," 1967. (N/A)

40. Kuroiwa, J.H., "Vibration Test of a Multistory Building," 1967. (N/A)

41. Lutes, L.D., "Stationary Random Response of Bilinear Hysteretic Systems," 1967.

42. Nigam, N.C., "Inelastic Interactions in the Dynamic Response of Structures," 1967.

43. Nigam, N.C. and P.C. Jennings, "Digital Calculation of Response Spectra from Strong-Motion Earthquake Records," 1968.

44. Spencer, R.A., "The Nonlinear Response of Some Multistory Reinforced and Prestressed Concrete Structures Subjected to Earthquake Excitation," 1968. (N/A)

45. Jennings, P.C., G.W. Housner and N.C. Tsai, "Simulated Earthquake Motions," 1968.

46. "Strong-Motion Instrumental Data on the Borrego Mountain Earthquake of 9 April 1968," (USGS and EERL Joint Report), 1968.

47. Peters, R.B., "Strong Motion Accelerograph Evaluation," 1969.

48. Heitner, K.L., "A Mathematical Model for Calculation of the Run-Up of Tsunamis," 1969.

49. Trifunac, M.D., "Investigation of Strong Earthquake Ground Motion," 1969. (N/A)

50. Tsai, N.C., "Influence of Local Geology on Earthquake Ground Motion," 1969. (N/A)

51. Trifunac, M.D., "Wind and Microtremor Induced Vibrations of a Twenty-Two Steel Frame Building," EERL 70–01, 1970.

52. Yang, I-M., "Stationary Random Response of Multidegree-of-Freedom Systems," DYNL–100, June 1970. (N/A)

53. Patula, E.J., "Equivalent Differential Equations for Non-linear Dynamic Systems," DYNL–101, June 1970.

54. Prelewicz, D.A., "Range of Validity of the Method of Averaging," DYNL–102, 1970.

55. Trifunac, M.D., "On the Statistics and Possible Triggering Mechanism of Earthquakes in Southern California," EERL 70–03, July 1970.

56. Heitner, K.L., "Additional Investigations on a Mathematical Model for Calculation of Run-Up of Tsunamis," July 1970.

57. Trifunac, M.D., "Ambient Vibration Tests of a Thirty-Nine Story Steel Frame Building," EERL 70–02, July 1970.

58. Trifunac, M.D. and D.E. Hudson, "Laboratory Evaluations and Instrument Corrections of Strong-Motion Accelerographs," EERL 70–04, August 1970. (N/A)

59. Trifunac, M.D., "Response Envelope Spectrum and Interpretation of Strong Earthquake Ground Motion," EERL 70–06, August 1970.

60. Keightley, W.O., "A Strong-Motion Accelerograph Array with Telephone Line Interconnections," EERL 70–05, September 1970.

61. Trifunac, M.D., "Low Frequency Digitization Errors and a New Method for Zero Baseline Correction of Strong-Motion Accelerograms," EERL 70–07, September 1970.

62. Vijayaraghavan, A., "Free and Forced Oscillations in a Class of Piecewise-Linear Dynamic Systems," DYNL–103, January 1971.

63. Jennings, P.C., R.B. Mathiesen and J.B. Hoerner, "Forced Vibrations of a 22–Story Steel Frame Building," EERL 71–01, February 1971. (N/A) (PB 205 161)

64. Jennings, P.C., "Engineering Features of the San Fernando Earthquake of February 9, 1971," EERL 71–02, June 1971. (PB 202 550)

65. Bielak, J., "Earthquake Response of Building-Foundation Systems," EERL 71–04, June 1971. (N/A) (PB 205 305)

66. Adu, R.A., "Response and Failure of Structures Under Stationary Random Excitation," EERL 71–03, June 1971. (N/A) (PB 205 304)

67. Skattum, K.S., "Dynamic Analysis of Coupled Shear Walls and Sandwich Beams," EERL 71–06, June 1971. (N/A) (PB 205 267)

68. Hoerner, J.B., "Model Coupling and Earthquake Response of Tall Buildings," EERL 71–07, June 1971. (N/A) (PB 207 635)

69. Stahl, K.J., "Dynamic Response of Circular Plates Subjected to Moving Massive Loads," DYNL–104, June 1971. (N/A)

70. Trifunac, M.D., F.E. Udwadia and A.G. Brady, "High Frequency Errors and Instrument Corrections of Strong-Motion Accelerograms," EERL 71–05, 1971. (PB 205 369)

71. Furuike, D.M., "Dynamic Response of Hysteretic Systems With Application to a System Containing Limited Slip," DYNL–105, September 1971. (N/A)

72. Hudson, D.E. (Editor), "Strong-Motion Instrumental Data on the San Fernando Earthquake of February 9, 1971," (Seismological Field Survey, NOAA, C.I.T. Joint Report), September 1971. (PB 204 198)

73. Jennings, P.C. and J. Bielak, "Dynamics of Building-Soil Interaction," EERL 72–01, April 1972. (PB 209 666)

74. Kim, B.-K., "Piecewise Linear Dynamic Systems with Time Delays," DYNL–106, April 1972.

75. Viano, D.C., "Wave Propagation in a Symmetrically Layered Elastic Plate," DYNL–107, May 1972.

76. Whitney, A.W., "On Insurance Settlements Incident to the 1906 San Francisco Fire," DRC 72–01, August 1972. (PB 213 256)

77. Udwadia, F.E., "Investigation of Earthquake and Microtremor Ground Motions," EERL 72–02, September 1972. (PB 212 853)

78. Wood, J.H., "Analysis of the Earthquake Response of a Nine-Story Steel Frame Building During the San Fernando Earthquake," EERL 72–04, October 1972. (PB 215 823)

79. Jennings, P.C., "Rapid Calculation of Selected Fourier Spectrum Ordinates," EERL 72–05, November 1972.

80. "Research Papers Submitted to Fifth World Conference on Earthquake Engineering, Rome, Italy, 25–29 June 1973," EERL 73–02, March 1973. (PB 220 431)

81. Udwadia, F.E. and M.D. Trifunac, "The Fourier Transform, Response Spectra and Their Relationship Through the Statistics of Oscillator Response," EERL 73–01, April 1973. (PB 220 458)

82. Housner, G.W., "Earthquake-Resistant Design of High-Rise Buildings," DRC 73–01, July 1973. (N/A)

83. "Earthquake and Insurance," Earthquake Research Affiliates Conference, 2–3 April, 1973, DRC 73–02, July 1973. (PB 223 033)

84. Wood, J.H., "Earthquake-Induced Soil Pressures on Structures," EERL 73–05, August 1973. (N/A)

85. Crouse, C.B., "Engineering Studies of the San Fernando Earthquake," EERL 73–04, March 1973. (N/A)

86. Irvine, H.M., "The Veracruz Earthquake of 28 August 1973," EERL 73–06, October 1973.

87. Iemura, H. and P.C. Jennings, "Hysteretic Response of a Nine-Story Reinforced Concrete Building During the San Fernando Earthquake," EERL 73–07, October 1973.

88. Trifunac, M.D. and V. Lee, "Routine Computer Processing of Strong-Motion Accelerograms," EERL 73–03, October 1973. (N/A) (PB 226 047/AS)

89. Moeller, T.L., "The Dynamics of a Spinning Elastic Disk with Massive Load," DYNL 73–01, October 1973.

90. Blevins, R.D., "Flow Induced Vibration of Bluff Structures," DYNL 74–01, February 1974.

91. Irvine, H.M., "Studies in the Statics and Dynamics of Simple Cable Systems," DYNL–108, January 1974.

92. Jephcott, D.K. and D.E. Hudson, "The Performance of Public School Plants During the San Fernando Earthquake," EERL 74–01, September 1974. (PB 240 000/AS)

93. Wong, H.L., "Dynamic Soil-Structure Interaction," EERL 75–01, May 1975. (N/A) (PB 247 233/AS)

94. Foutch, D.A., G.W. Housner and P.C. Jennings, "Dynamic Responses of Six Multistory Buildings During the San Fernando Earthquake," EERL 75–02, October 1975. (PB 248 144/AS)

95. Miller, R.K., "The Steady-State Response of Multidegree-of-Freedom Systems with a Spatially Localized Nonlinearity," EERL 75–03, October 1975. (PB 252 459/AS)

96. Abdel-Ghaffar, A.M., "Dynamic Analyses of Suspension Bridge Structures," EERL 76–01, May 1976. (PB 258 744/AS)

97. Foutch, D.A., "A Study of the Vibrational Characteristics of Two Multistory Buildings," EERL 76–03, September 1976. (PB 260 874/AS)

98. "Strong Motion Earthquake Accelerograms Index Volume," Earthquake Engineering Research Laboratory, EERL 76–02, August 1976. (PB 260 929/AS)

99. Spanos, P-T.D., "Linearization Techniques for Non-Linear Dynamical Systems," EERL 76–04, September 1976. (PB 266 083/AS)

100. Edwards, D.B., "Time Domain Analysis of Switching Regulators," DYNL 77–01, March 1977.

101. Abdel-Ghaffar, A.M., "Studies of the Effect of Differential Motions of Two Foundations upon the Response of the Superstructure of a Bridge," EERL 77–02, January 1977. (PB 271 095/AS)

102. Gates, N.C., "The Earthquake Response of Deteriorating Systems," EERL 77–03, March 1977. (PB 271 090/AS)

103. Daly, W., W. Judd and R. Meade, "Evaluation of Seismicity at U.S. Reservoirs," USCOLD, Committee on Earthquakes, May 1. (PB 270 036/AS)

104. Abdel-Ghaffer, A.M. and G.W. Housner, "An Analysis of the Dynamic Characteristics of a Suspension Bridge by Ambient Vibration Measurements," EERL 77–01, January 1977. (PB 275 063/AS)

105. Housner, G.W. and P.C. Jennings, "Earthquake Design Criteria for Structures," EERL 77–06, November 1977 (PB 276 502/AS)

106. Morrison, P., R. Maley, G. Brady and R. Porcella, "Earthquake Recordings on or Near Dams," USCOLD, Committee on Earthquakes, November 1977. (PB 285 867/AS)

107. Abdel-Ghaffar, A.M., "Engineering Data and Analyses of the Whittier, California Earthquake of January 1, 1976," EERL 77–05, November 1977. (PB 283 750/AS)

108. Beck, J.L., "Determining Models of Structures from Earthquake Records," EERL 78–01, June 1978 (PB 288 806/AS)

109. Psycharis, I., "The Salonica (Thessaloniki) Earthquake of June 20, 1978," EERL 78–03, October 1978. (PB 290 120/AS)

110. Abdel-Ghaffar, A.M. and R.F. Scott, "An Investigation of the Dynamic Characteristics of an Earth Dam," EERL 78–02, August 1978. (PB 288 878/AS)

111. Mason, A.B., Jr., "Some Observations on the Random Response of Linear and Nonlinear Dynamical Systems," EERL 79–01, January 1979. (PB 290 808/AS)

112. Helmberger, D.V. and P.C. Jennings (Organizers), "Strong Ground Motion: N.S.F. Seminar-Workshop," SL–EERL 79–02, February 1978.

113. Lee, D.M., P.C. Jennings and G.W. Housner, "A Selection of Important Strong Motion Earthquake Records," EERL 80–01, January 1980. (PB 80 169196)

114. McVerry, G.H., "Frequency Domain Identification of Structural Models from Earthquake Records," EERL 79–02, October 1979. (PB–80–194301)

115. Abdel-Ghaffar A.M., R.F.Scott and M.J.Craig, "Full-Scale Experimental Investigation of a Modern Earth Dam," EERL 80–02, February 1980. (PB–81–123788)

116. Rutenberg, A., P.C. Jennings and G.W. Housner, "The Response of Veterans Hospital Building 41 in the San Fernando Earthquake," EERL 80–03, May 1980. (PB–82–201377)

117. Haroun, M.A., "Dynamic Analyses of Liquid Storage Tanks," EERL 80–04, February 1980. (PB–81–123275)

118. Liu, W.K., "Development of Finite Element Procedures for Fluid-Structure Interaction," EERL 80–06, August 1980. (PB 184078)

119. Yoder, P.J., "A Strain-Space Plasticity Theory and Numerical Implementation," EERL 80–07, August 1980. (PB–82–201682)

120. Krousgrill, C.M., Jr., "A Linearization Technique for the Dynamic Response of Nonlinear Continua," EERL 80–08, September 1980. (PB–82–201823)

121. Cohen, M., "Silent Boundary Methods for Transient Wave Analysis," EERL 80–09, September 1980. (PB–82–201831)

122. Hall, S.A., "Vortex-Induced Vibrations of Structures," EERL 81–01, January 1981. (PB–82–201849)

123. Psycharis, I.N., "Dynamic Behavior of Rocking Structures Allowed to Uplift," EERL 81–02, August 1981. (PB–82–212945)

124. Shih, C.-F., "Failure of Liquid Storage Tanks Due to Earthquake Excitation," EERL 81–04, May 1981. (PB–82–215013)

125. Lin, A.N., "Experimental Observations of the Effect of Foundation Embedment on Structural Response," EERL 82–01, May 1982. (PB–84–163252)

126. Botelho, D.L.R., "An Empirical Model for Vortex-Induced Vibrations," EERL 82–02, August 1982. (PB–84–161157)

127. Ortiz, L.A., "Dynamic Centrifuge Testing of Cantilever Retaining Walls," SML 82–02, August 1982. (PB–84–162312)

128. Iwan, W.D. (Editor) "Proceedings of the U.S. National Workshop on Strong-Motion Earthquake Instrumentation, April 12–14, 1981, Santa Barbara, California," California Institute of Technology, Pasadena, California, 1981.

129. Rashed, A., "Dynamic Analysis of Fluid-Structure Systems, " EERL 82–03, July 1982. (PB–84–162916)

130. National Academy Press, "Earthquake Engineering Research—1982."

131. National Academy Press, "Earthquake Engineering Research—1982, Overview and Recommendations."

132. Jain, S.K., "Analytical Models for the Dynamics of Buildings," EERL 83–02, May 1983. (PB–84–161009)

133. Huang, M.-J., "Investigation of Local Geology Effects on Strong Earthquake Ground Motions," EERL 83–03, July 1983. (PB–84–161488)

134. McVerry, G.H. and J.L. Beck, "Structural Identification of JPL Building 180 Using Optimally Synchronized Earthquake Records." EERL 83–01, August 1983. (PB–84–162833)

135. Bardet, J.P., "Application of Plasticity Theory to Soil Behavior: A New Sand Model," SML 83–01, September 1983. (PB–84–162304)

136. Wilson, J.C., "Analysis of the Observed Earthquake Response of a Multiple Span Bridge," EERL 84–01, May 1984. (PB–85–240505/AS)

137. Hushmand, B., "Experimental Studies of Dynamic Response of Foundations," SML 83–02, November 1983. (PB–86–115383/A)

138. Cifuentes, A.O., "System Identification of Hysteretic Structures," EERL 84–04, 1984. (PB–240489/AS14)

139. Smith, K.S., "Stochastic Analysis of the Seismic Response of Secondary Systems," EERL 85–01, November 1984. (PB–85–240497/AS)

140. Maragakis, E., "A Model for the Rigid Body Motions of Skew Bridges," EERL 85–02, December 1984. (PB–85–248433/AS)

141. Jeong, G.D., "Cumulative Damage of Structures Subjected to Response Spectrum Consistent Random Process," EERL 85–03, January 1985. (PB–86–100807)

142. Chelvakumar, K., "A Simple Strain-Space Plasticity Model for Clays," EERL 85–05, 1985. (PB–87–234308/CC)

143. Pak, R.Y.S., "Dynamic Response of a Partially Embedded Bar Under Transverse Excitations," EERL 85–04, May 1985. (PB–87–232856/A06)

144. Tan, T.-S., "Two Phase Soil Study: A. Finite Strain Consolidation, B. Centrifuge Scaling Considerations," SML 85–01, August 1985. (PB–87–232864/CC)

145. Iwan, W.D., M.A. Moser and C.-Y. Peng, "Strong-Motion Earthquake Measurement Using a Digital Accelerograph," EERL 84–02, April 1984.

146. Beck, R.T. and J.L. Beck, "Comparison Between Transfer Function and Modal Minimization Methods for System Identification," EERL 85–06, November 1985. (PB–87–234688/A04)

147. Jones, N.P., "Flow-Induced Vibration of Long Structures," DYNL 86–01, May 1986. (PB–88–106646/A08)

148. Peek, R., "Analysis of Unanchored Liquid Storage Tanks Under Seismic Loads," EERL 86–01, April 1986. (PB–87–232872/A12)

149. Paparizos, L.G., "Some Observations on the Random Response of Hysteretic Systems," EERL 86–02. 1986. (PB–88235668/CC)

150. Moser, M.A., "The Response of Stick-Slip Systems to Random Seismic Excitation," EERL 86–03, September 1986. (PB–89–194427/AS)

151. Burridge, P.B., "Failure of Slopes," SML 87–01, March 1987. (PB–89–194401/AS)

152. Jayakumar, P., "Modeling and Identification in Structural Dynamics," EERL 87–01, May 1987. (PB–89–194146/AS)

153. Dowling, M.J., "Nonlinear Seismic Analysis of Arch Dams," EERL 87–03, September 1987. (PB–89–194443/AS)

154. Duron, Z.H., "Experimental and Finite Element Studies of a Large Arch Dam," EERL 87–02, September 1987. (PB–89–194435/AS)

155. Whirley, R.G., "Random Response of Nonlinear Continuous Systems," EERL 87–04, September 1987. (PB–89–194153/AS)

156. Peng, C.-Y., "Generalized Model Identification of Linear and Nonlinear Dynamic Systems," EERL 87–05, September 1987. (PB–89–194419/AS)

157. Levine, M.B., J.L. Beck, W.D. Iwan, P.C. Jennings and R. Relles, "Accelerograms Recorded at Caltech During the Whittier Narrows Earthquakes of October 1 and 4, 1987: A Preliminary Report," EERL 88–01, August 1988. (PB–

158. Nowak, P.S., "Effect of Nonuniform Seismic Input on Arch Dams," EERL 88–03, September 1988. (PB–89–194450/AS)

159. El-Aidi, B., "Nonlinear Earthquake Response of Concrete Gravity Dam Systems," EERL 88–02, August 1988. (PB–89–193124/AS)

160. Smith, P.W., Jr., "Considerations for the Design of Gas-Lubricated Slider Bearings," DYNL 89–01, January 1988. (PB–

161. Donlon, W.P., Jr., "Experimental Investigation of the Nonlinear Seismic Response of Concrete Gravity Dams," EERL 89–01, January 1989. (PB–

162. Jensen, H.A., "Dynamic Response of Structures with Uncertain Parameters," EERL 89–02, September 1989. (PB–

163. Thyagarajan, R.S., "Modeling and Analysis of Hysteretic Structural Behavior," EERL 89–03, October 1989. (PB–91–154195)

164. US–China Joint Project on Strong Ground Motion Measurements, "Digital Near Source Accelerograms Recorded by Instrumental Arrays in Tangshan, China," EERL 89–04. (PB–91–154112)

165. Tan, P., "Numerical Simulations of Two-Dimensional Saturated Granular Media," SML 90–02, October 1989. (PB–

166. Allard, M.A., "Soil Stress Field Around Driven Piles," SML 90–01, October 1989. (PB–

167. Hou, Z., "Nonstationary Response of Structures and Its Application to Earthquake Engineering," EERL 90–01, April 1990. (PB–

168. Levine, M., "Accelerogram Processing Using Reliability Bounds and Optimal Correction Methods," EERL 90–02, June 1990. (PB–

169. Papadimitriou, K., "Stochastic Characterization of Strong Ground Motion and Applications to Structural Response," EERL 90–03, October 1990. (PB–